Inaugural dissertation

for

obtaining the doctoral degree

of the

Combined Faculty of Mathematics, Engineering and Natural Sciences

of the

Ruprecht - Karls - University

Heidelberg

Presented by

M.sc. Sheldon Steyn

born in: Pretoria, South Africa

Oral examination: 28 February 2023

Investigating the role of BPLF1 in the EBV life cycle

Referees:

apl. Prof. Dr. Martin Müller

Prof. Dr. Dr. Henri-Jacques Delecluse

Table of Contents

Summary

The Epstein-Barr Virus (EBV) is a γ-herpesvirus that establishes a lifelong infection in human hosts. This infection can manifest into cancer. This affliction is attributed to the latent encoded EBV proteins. However, lytic proteins have recently been demonstrated to contribute to tumour development, with notable examples being tegument proteins BNRF1 and BPLF1. In my thesis, I studied BPLF1 in its full form to identify novel regions involved in the EBV life cycle and in carcinogenesis. These goals are achieved through expression in vitro expression studies and in the context of EBV virions that infect primary B cells ex vivo. I used co-immunoprecipitation in tandem with mass spectrometric analysis to identify novel host BPLF1 binding partner SENP6, a deSUMOylase responsible for maintaining genomic integrity. I proceeded to study the effects that BPLF1 has on SENP6 activity and the physiological consequences. I produced domain knockouts of the BPLF1 protein to map the region responsible for interaction and activity of BPLF1 on SENP6. I found that not only does BPLF1 bind to SENP6; it also effectively suppresses SENP6 activity. Downstream effects on SENP6 inhibition are the reduction of Centromeric Protein A (CENP-A) constituency at the centromeres, leading to improper chromosomal segregation during anaphase. This leads to the accumulation of genomic abnormalities such as increased rates of aneuploidy and polyploidy. I found this phenotype occurs independently from the catalytic region of BPLF1 and is mapped to the $BPLF1^{765\text{-}1327}$ stretch of amino acids. B cells exposed to virus particles devoid of BPLF1, showed reduced nuclear abnormalities when compared to virus particles containing BPLF1. I observed increased SUMO2/3 conjugation and loss of CENP-A at the centromeric regions in B cells exposed to virus particles possessing BPLF1 in contrast to virus devoid of BPLF1, showing BPLF1's interference in chromosomal stability.

Zusammenfasung

Das Epstein-Barr-Virus (EBV) ist ein γ-Herpesvirus, das zu einer lebenslangen Infektion im Menschen führt. Diese Infektion kann sich in Krebs manifestieren und wird den latenten EBV-Proteinen zugeschrieben. Es wurde jedoch kürzlich gezeigt, dass lytische Proteine zur Tumorentwicklung beitragen, wobei bemerkenswerte Beispiele die Tegumentproteine BNRF1 und BPLF1 sind. In dieser Doktorarbeit wurde das lytische Protein BPLF1 untersucht, um neue Regionen zu identifizieren, die am EBV-Lebenszyklus und an der Karzinogenese beteiligt sind. Dies wurde durch Expressionsstudien in vitro im Zusammenhang mit EBV-Virionen erreicht, die primäre B-Zellen ex vivo infizieren. Co-Immunpräzipitation zusammen mit massenspektrometrischer Analyse wurden angewendet, um den neuen BPLF1-Bindungspartner SENP6 zu identifizieren, SENP6 ist eine Desumoylase, die für die Aufrechterhaltung der genomischen Integrität verantwortlich ist. Ich habe folgend die Auswirkungen von BPLF1 auf die SENP6-Aktivität und die physiologischen Konsequenzen untersucht. Dazu wurden Domänen-Knockouts des BPLF1-Proteins angefertigt, um die Region zu identifizieren, die für die Interaktion und Aktivität zwischen BPLF1 und SENP6 verantwortlich ist. So konnte ich zeigen, dass BPLF1 nicht nur an SENP6 bindet, sondern auch, dass es auch effektiv die SENP6-Aktivität unterdrückt. Eine nachgeschaltete Wirkunge auf die SENP6-Hemmung ist die Verringerung der zentromeren Protein A (CENP-A)-Bestandteile an den Zentromeren, was zu einer unsachgemäßen chromosomalen Segregation während der Anaphase führt. Dies wiederum führt zu einer Akkumulation von genomischen Anomalien, wie einer erhöhten Raten von Aneuploidie und Polyploidie. Weiter konnte ich zeigen, dass dieser Phänotyp unabhängig von der katalytischen Region von BPLF1 auftritt und auf der Aminosäuresequenz $BPLF1^{765\text{-}1327}$ abgebildet wird. B-Zellen, die Viruspartikeln ohne BPLF1 ausgesetzt waren, zeigten im Vergleich zu Viruspartikeln, die

BPLF1 enthielten, weniger nukleäre Anomalien. Ich beobachtete eine erhöhte SUMO2/3-Konjugation und den Verlust von CENP-A in den zentromerischen Regionen in B-Zellen, die Viruspartikeln mit BPLF1 ausgesetzt waren, im Gegensatz zu Viren ohne BPLF1, was die Beeinträchtigung der chromosomalen Stabilität durch BPLF1 zeigte.

Acknowledgements

I would like to thank Prof. Henri-Jacques Delecluse for providing me with the opportunity to work in his world-class lab and for his dedication and guidance during my studies.

Also, a big thank you to Dr. Susanne Delecluse for her help and advice during some of the difficult periods that I endured.

A special thank you to Dr. Dwain van Zyl for his valuable mentorship, it was a great privilege to be working with you.

Thank you to all at F100 for their assistance and friendship which made my PhD a stimulating experience.

My heart goes out to my dear family for their endless love and support. I love you all.

1. Introduction

Epstein Barr Virus (EBV) was discovered through electron microscopy (EM) of lymphoblast sections derived from a Burkitt's lymphoma (BL), as the first known tumourigenic virus [1-3]. It asymptomatically infects mostly children with occasional precipitation into mononucleosis and has infected over 90 % of the global population with 3 million new cases each year [4, 5]. Viral particles are usually orally transmitted via the saliva and have distinct tropism for B cells and epithelial cells. EBV is known to rapidly transform naïve and memory B cells into immortal lymphoblastoid cell lines (LCLs) *in vitro* three days post infection and to establish lifelong latent infection in the memory B cell pool *in vivo*, where it is implicated in many human lymphoproliferative disorders [6, 7].

1.1. Phylogeny

EBV is a γ-herpesvirus (HV) of the family *Herpesviridae.* This family consists of 3 subfamilies, the *Alpha-*, *Beta-*, and *Gammaherpesvirinae*. The viral genomes of family members range from 125 to 230 kb in length with approximately 70 to 200 genes of differing base compositions and patterns of repeated sequences [8]. All 3 subfamilies possess a common subset of 40 genes, indicating common ancestry. DNA sequence analyses have been the principal approach for establishing phylogenetic relationships with further distinguishing of subfamilies along with occasional reassignments of several members between them. Mammalian HVs have members in each subfamily while all avian and reptilian HVs are in the *Alphaherpesvirinae*. Among the mammalian herperviruses, these lineages diverge into separate groups from the rest of the HVs. Piscine and amphibian HVs are in the *Alloherpesviridae* with the single known invertebrate HV belonging to another distinct family, the *Malacoherpesviridae* [9, 10]. All three of these families belong to the higher-level

taxon, *Herpesvirales*. Because of palaeontological histories, primate HVs form separate clades corresponding to new world or old-world lineages. Members of the *Gammaherpesvirinae* have relatively varied reproduction programmes when compared to other subfamilies and have 7 genera and 3 unassigned species. The *Lymphocryptovirus* genus, known for a predominant tropism for B cells, forms a distinct clade within the *Gammaherpesvirinae,* to which EBV (*Human gammaherpesvirus 4*) is a member species, along with its old world and new world primate infecting relatives [11].

1.2. EBV associated malignancies

Many human tumours, such as immunoblastic lymphoma in immunocompromised patients, Hodgkin's disease, gastric carcinoma (GC), and nasopharyngeal carcinoma (NPC) have been etiologically linked to EBV infection and particularly, the effects of latency programming and deregulated MYC [12]. A classic example of EBV associated cancer is BL, an aggressive non-Hodgkin lymphoma characterised by the translocation and constitutive activation of the MYC oncogene [13-15]. This form of EBV associated lymphoma has been linked to latency I program, while Hodgkin disease, T cell non-Hodgkin lymphoma, NPC, and gastric carcinoma are associated with latency II. In addition, hosts with suppressed or compromised immune systems can develop immunoblastic lymphomas associated with latency III programming [6]. Burkitt's and Hodgkin lymphoma, NPC, and GC constitute approximately 1 % of the global cancer burden with 200 000 new cases of EBV-associated cancers diagnosed every year [5].

1.2.1. Burkitt's Lymphoma

BL is rapidly growing lymphatic tumor derived from B lymphocytes at the germinal center, which is strongly associated with EBV infection. The tumor is characterised by dysregulation of the *c-myc* gene via chromosomal translocations [c-myc and IgH t(8;14)(q24;q32), IgK and

c-myc t(2;8)(p12;q24), or IgL and c-myc t(8;22)(q24;q11)] [16-18]. These translocations result in c-myc upregulation which promotes anti-apoptotic and pro-proliferative pathways [19].

BL is divided into three subtypes, endemic, sporadic, and immunodeficiency associated BL. Endemic BL is common in equatorial Africa. Serological studies of endemic BLs have identified them to be almost 100 % EBV-positive and to be caused by EBV [20]. In equatorial Africa, chronic malaria infections are considered a contributing environmental factor through extensively inducing B cell expansion, suppression of T cell immunity, accompanied with the increased EBV production, and genomic instability associated with increased expression of activation-induced cytidine deaminases [21].

1.2.2. *Hodgkin Lymphoma*

Hodgkin lymphoma (HL) consists of malignant lymphocytes forming multinucleated Reed-Sternberg cells (RSCs) in patients' lymph nodes [22-24]. There are two major types of HL, classical Hodgkin lymphoma (cHL) and nodular lymphocyte-predominant lymphoma (NLPHL). EBV has a stronger association to cHL, which consists mostly of B cell neoplasms originating from the GC. Histological classification has subdivided cHL into mixed-cellularity, nodular-sclerosis, lymphocyte-rich, and lymphocyte-depleted subtypes. EBV has been found to be associated with roughly 40 % of all cHL cases and most frequently with the mixed-cellularity subtype [25]. RSCs have a number of crippling mutations in the Ig genes due to somatic hypermutations during affinity maturation [26]. In order to prevent elimination by apoptosis, RSCs also have increased NFκB expression [27]. EBV is known to express an activated B cell receptor mimic (LMP2A) and an activator of NFκB (LMP1) in latency II [28].

1.2.3. Nasopharyngeal Carcinoma

Nasopharyngeal carcinoma associated with EBV is commonly found in South China, and Southeast Asia. Over 97 % of NPC incidents have been found to be EBV-positive with contributing factors alleged to be environmental factors such as diet and genetics. EBV associated with NPCs has been identified to be a unique strain variation. The rare T/NK lymphoma associated with EBV has been found to be restricted to Japan and Korea, coinciding very little with incidences of NPC. EBV associated gastric carcinoma (EBVaGC) accounts for 9 % of all gastric cancers. Host chromosomal CpG and EBV genome methylation are characteristic of this cancer with tumour suppressing genes silenced through methylation [29].

1.3. The EBV structure

The EBV structure consists of a toroid-shaped protein core, surrounded by the EBV genome encased in an icosahedral nucleocapsid of 162 capsomers. The capsid is covered by a tegument and enveloped by an outer member coated with glycoprotein spikes [30, 31].

1.3.1. The EBV genome

The EBV dsDNA genome is linear when packaged within the viral capsid. It encodes 80+ ORF's and is approximately 175 kb in length. The ORFs are mapped and classified by the digestion patterns of BamHI restriction enzyme, and which fragment they are found and the direction they extend. ORFs are divided into latent and lytic genes, which are further divided according to their temporal expression in these phases. These genes encode for proteins and non-translated RNA's such as EBV-*encoded* RNA (EBER)-1 and 2 [31]. The viral genome also encodes >49 mature micro-RNAs, 44 lie within intronic regions of the BamHI-A rightward transcripts (BART), and five within the BamHI-H rightward fragment 1 (BHRF1) [32, 33].

There are 0.5 kb long terminal repeats at the ends of the viral genome allowing for the circularization of the viral genome after infection, resulting in an episome persisting in the host cell maintained by the EBV nuclear antigen 1 (EBNA1) [34].

Viral genes expressed in latently infected cells are referred to as “EBV latent genes”. Examples of such latent genes are the six EBV nuclear antigens (EBNAs 1, 2, 3A, 3B, 3C, and -LP), and three latent membrane proteins (LMPs 1, 2A, and 2B). Of these proteins, EBNA1, 2, and 3C, and LMP1 are indispensable for EBV induced B cell transformation [35]. Genes expressed during productive replication cycle are called “EBV lytic genes”, examples of which are transcription factors (BZLF1), viral DNA polymerase (BALF5) and associated factors, viral glycoproteins (gp350/220 and gp110), and structural proteins (capsid and tegument proteins).

Selective pressures have resulted in EBV diverging into multiple variants and subvariants through its existence. Type 1 (type A) and type 2 (type B) were the first major variants discovered and are distinguished by the EBNA2 and EBNA3 gene sequences with 54 % amino acid similarity for EBNA2 [36]. The type 1 variant (e.g., B95-8, GD1, M81 and Akata) is the most prevalent EBV strain worldwide. The type 2 variant (e.g. AG876 and P3HR-1) is equally abundant as type 1 EBV in sub-Saharan Africa [37].

1.3.2. The EBV capsid

Capsids of herpesviruses have a triangulation number of T = 16 formed from 162 capsomers. These capsomers consist of 150 hexamers and 12 pentamers of the major capsid protein (BcLF1). On the outer surface of each hexon lies a small capsid protein (BFRF3). A heterotrimeric complex of $\alpha\beta_2$ (triplex complex, α – BORF1, β – BDLF1) is located between each 3 capsomers (consisting of 3 hexamers or 2 hexamers and 1 pentamer each) [38].

1.3.3. The EBV tegument

The viral tegument contains proteins of viral and cellular origin. It is located between the viral capsid and envelope. The tegument member proteins are multifunctional, aiding in the establishment of host infection and the progress of the virus life cycle. These activities include and are not limited to, gene transactivation, protein phosphorylation, immune evasion, suppressing of host protein synthesis, virion morphogenesis, and viral DNA packaging. Many of these functions are found conserved between homologues in other members of *Herpesviridae* [39].

1.3.3.1. BPLF1

The large tegument protein (LTP) BPLF1 is the largest known EBV transcript encoding 3150 amino acids [40]. It is known as a late lytic cycle protein that plays roles in early and late stages of infection. Studies into viral RNAs expressed during EBV replication have revealed the emergence of BPLF1 transcripts as early as 8 hours and reaching peak levels at 24 hours after viral lytic induction in Akata cells treated with α-human IgG [41]. Through the study of the homologue HSV UL36 LTP, BPLF1 is found to localize at the perinuclear cytoplasmic capsids, recruiting other tegument proteins such as BOLF1 to aid in the envelopment of the EB virion in the cytoplasm or plasma membrane [39]. Studies using virus devoid of BPLF1 showed compromised ability to transform infected B cells, with a reduction of both transformation percentage and speed of B cell transformation, and tumour development *in vitro* and *in vivo* respectively [42]. The LTPs of other members of the *Herpesviridae* family are known to also possess a conserved deubiquitinating (DUB) activity at their N-terminal regions [43]. Studies have shown BPLF1 to have cysteine protease activity with a conserved Cys-His-Asp catalytic triad, which allows BPLF1 and its homologues to deconjugate ubiquitin (Ub) and ubiquitin-like (UbL) peptide chains from substrate proteins. For BPLF1, the catalytic

triad is located in the first 200 amino acid N-terminal region and is deactivated upon mutation of its cysteine residue to alanine [43].

BPLF1 has been reported to be involved in the linkage of the viral capsid to the outer tegument. Cryo-EM studies have revealed that the tegument proteins, BSRF1 and BBRF1 form a complex that connects to the gH/gL, and gB proteins of the golgi membrane. This provides a region of adherence for BPLF1 coated viral capsids to bind to engage in secondary envelopment with this membrane [44]. Studies of BPLF1 homologues have shown them to mediate retrograde trafficking of viral capsids by recruiting host motor proteins [45].

Since the discovery of DUB activity in BPLF1, several targets have been discovered through the construction of a functional truncated form of the protein ($BPLF1^{1-246}$). Co-Immunoprecipitation (Co-IP) experiments identified EBV ribonucleotide reductase subunit RR2 as a direct interaction partner of BPLF1. BPLF1 was subsequently shown to hydrolyse K48- and K63-linked Ub chains of the RR1 subunit, thus abolishing its activity. This was shown to increase the conversion rate of NTPs to dNTPs, possibly to facilitate viral replication [46].

The second set of targets of BPLF1 DUB activity was found to be members of the Toll like Receptor (TLR) signalling pathway [47]. The first line of defence against pathogens of the host encompasses an assortment of non-specific strategies, such as physical barriers, complement, and inflammation. Host cells respond by initiating responses to pattern recognition receptors (PRRs) recognizing pathogen associated pattern molecular patterns (PAMPs). Examples of PRRs consist of membrane bound TLRs and RIG-I receptors (RLRs). Upon recognition of viral components, TLRs send a cascade of signals to initiate the production of type I interferons and pro-inflammatory cytokines to disrupt viral effects as

the adaptive response develops [48]. Several species of TLRs are known, with all possessing a single-pass membrane spanning receptor expressed in different cell types and different locales in the cell. EBV has been shown to activate the pathways of TLRs 2, 3, 7, and 9, with reports of receptor mRNA expression being suppressed during lytic and latent infection of B cells as a way for the virus to counter immune surveillance [47]. Aside from TLR 3, Recognition of PAMPs by TLRs universally results in dimerization and recruitment adaptor protein MyD88, leading to IL-1 receptor-associated kinase-1 (IRAK-1) phosphorylation and subsequent activation of tumour necrosis factor-associated factor 6 (TRAF6). Through linking of K64 polyubiquitin chains, TRAF6 polyubiquitinates itself and NEMO of the IκB kinase (IKK) complex. This results in phosphorylation and K48 ubiquitination of the inhibitor of NF-κB, IκBα. Upon ubiquination, IκBα is targeted for proteasomal degradation, permitting the translocation of NF-κB to the nucleus and initiating the transcription of pro-inflammatory cytokine genes [49]. As a result, ubiquitin conjugation and deconjugation tightly modulates TLR signalling pathways. Viral DUB BPLF1 has been shown to inhibit MyD88- and TRIF-dependent pathways through deconjugation of K63- and/or K48-linked Ub chains from intermediate members of these signalling pathways. These members include K63-Ub-TRAF6, K63-Ub-NEMO, and K48-Ub-IκBα (Figure 1). This form of inhibition has been suggested to serve the purposes of suppressing immune surveillance during infection and viral egress during productive life cycle [47, 50].

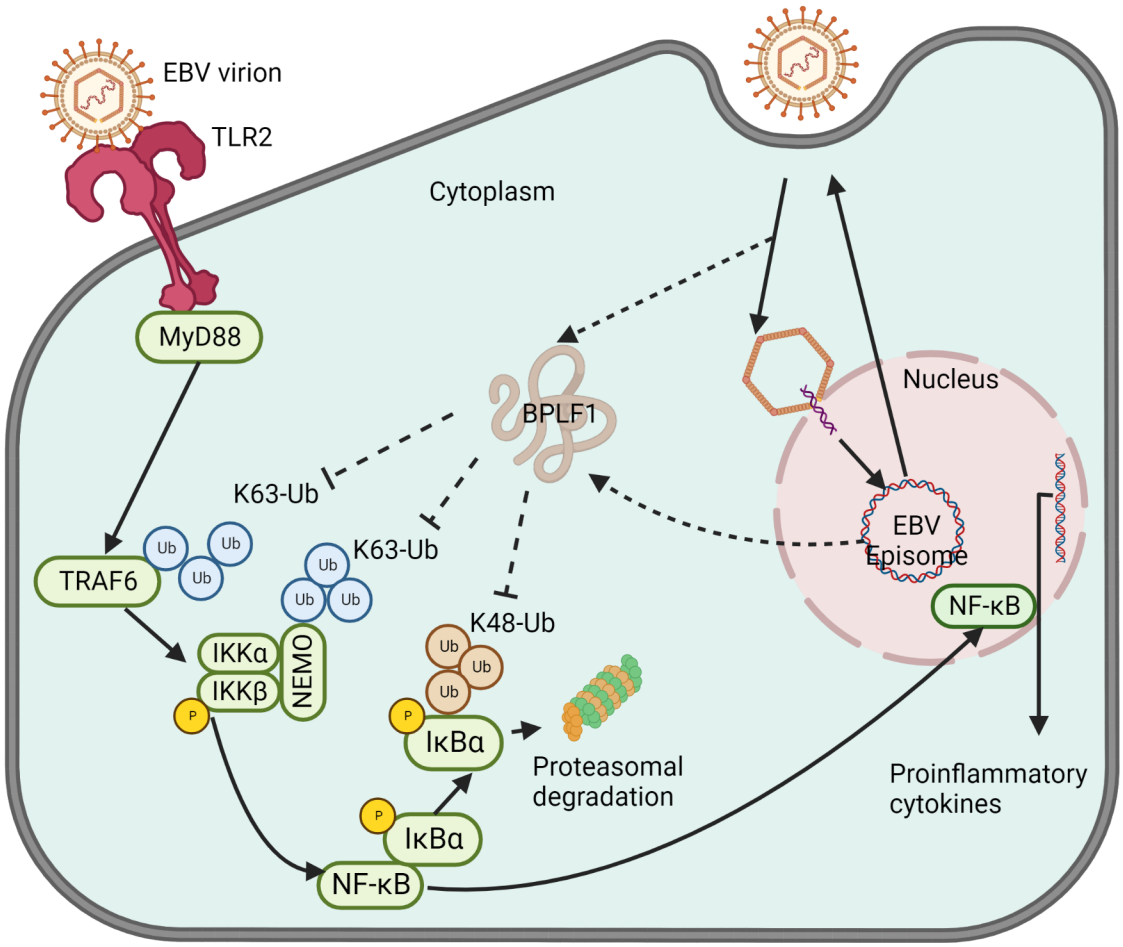

Figure 1: BPLF1 deubiquitinase activity interferes with TLR signalling of the innate immune surveillance. Incoming EBV virions shed the outer envelope to allow the capsid to target to the cytoplasm. Uncoating results in the release of BPLF1, which has deubiquitinase activity. TRAF6, NEMO, and IκBα need to be ubiquitinated TLR signal transduction. These components are targeted for deubiquitination by BPLF1, thus sequestering NF-κB functioning, allowing the virus to infect and exit the host cell.

BPLF1 was identified to inhibit type-I IFN responses in cells by promoting a tri-molecular complex with 14-3-3 and TRIM25. RIG-I is a cytosolic PRR ubiquitinated at Lys-63 by 14-3-3:TRIM25 in order to perform its signalling. The catalytic terminal domain of BPLF1 has been shown to promote autoubiquitination of TRIM25 and consequently, reduce its capacity to ubiquitinate RIG-I (Figure 2). As a result, IFNβ response is hampered in cells expressing the catalytic terminal domain of BPLF1. This effect is not due to altered intrinsic catalytic activity

of TRIM25 but rather due to diversion of ubiquitination. It has been suggested that association of BPLF1 with TRIM25 promotes release of RIG-I prematurely, but the exact mechanism has yet to be fully characterized [51].

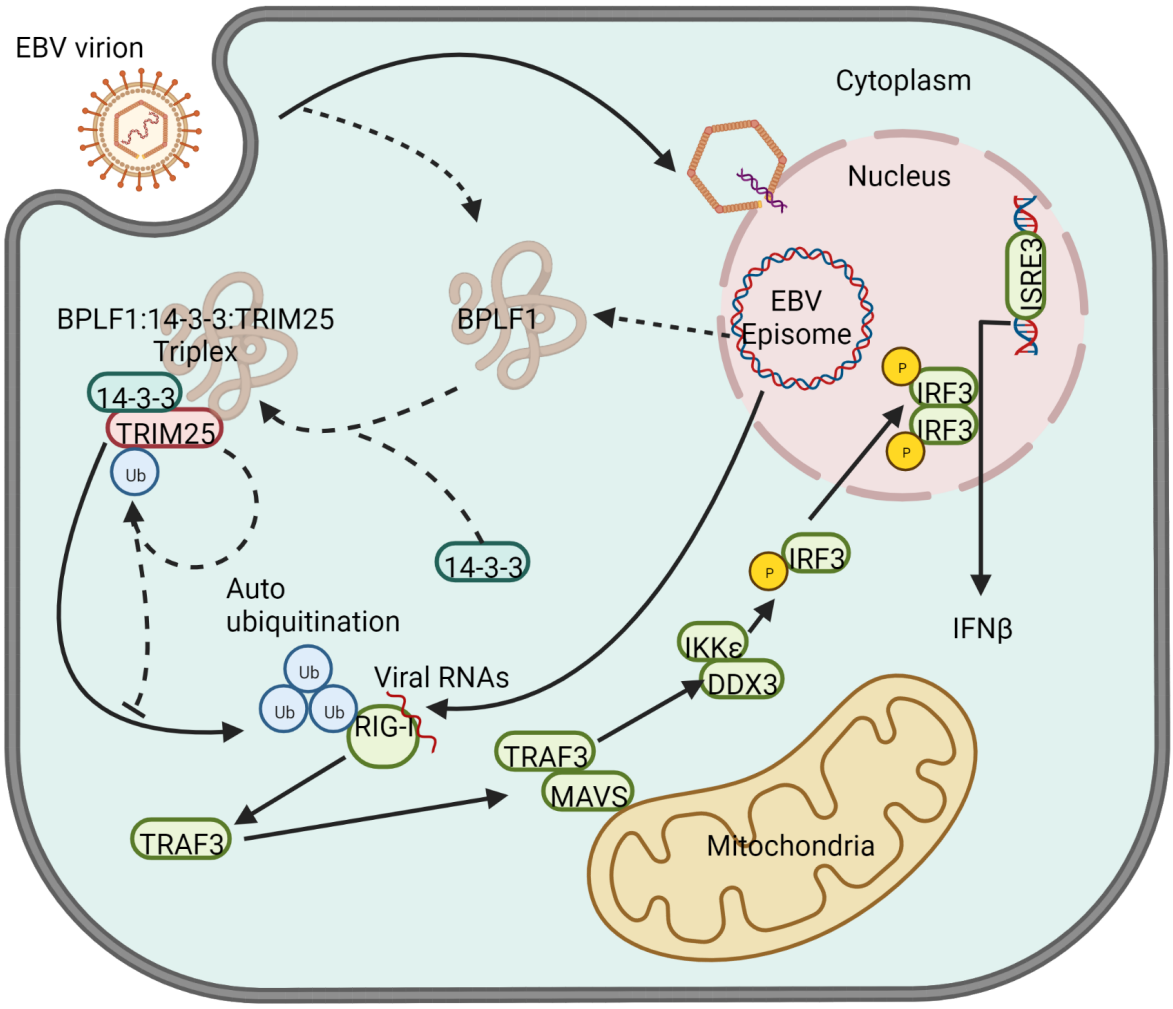

Figure 2: BPLF1 interferes with anti-viral RIG-I signalling. Upon entering the cell, BPLF1 recruits scaffold protein 14-3-3 to form a tri-molecular complex with ubiquitin ligase TRIM25, inducing autoubiquitination of TRIM25. Ubiquitinated TRIM25 is consequently unable to bind and ubiquitinate RIG-I, preventing signal transduction.

EBV and other herpesvirus infections can initiate host DDR, where repair proteins can be exploited for viral genome replication [52, 53]. EBV proteins can interact with several members of the translesion synthesis (TLS) pathway. The TLS pathway permits replication events to bypass DNA lesions such as pyrimidine dimers caused by UV exposure. When TLS is

activated, E4 ligase, and Rad18 is recruited to DNA damage sites where it ubiquitinates cellular processivity factor, PCNA, at Lys-164 mediating polymerase switching [54]. Polymerase eta (Pol η) is a TLS polymerase that interacts with PCNA via the PCNA interacting peptide (PIP) domain and the ubiquitin-binding zinc finger (UBZ) domain on Pol η with the monoubiquitinated PCNA [55]. This polymerase has a flexible catalytic site that allows for bulky DNA lesions to pass through without stalling. BPLF1 has been shown to interact with, stabilize, and deubiquitinate PCNA. This prevents Pol η from translocating to host genomic DNA lesions [56]. This coupled with the ability of Pol η to bind EBV DNA, suggests that it is recruited to prevent stalling during viral DNA replication [57].

Cullin ring ligases (CRLs) consist of multi-subunit ubiquitin E3 ligases. Each complex is composed of a cullin scaffold, RING finger protein (RBX1/RBX2), and a substrate adaptor. For the complex to assemble, a UbL residue NEDD8 must be conjugated to a conserved lysine residue. This process is called neddylation and induces conformational changes at the C-terminal RBX1-binding domain, promoting transfer of ubiquitin. CAND1 is the adaptor that binds to unneddylated cullin-RBX1 complexes, regulating complex assembly. BPLF1 has been shown to bind cullins and deconjugate NEDD8 via the conserved cysteine protease motif at the N-terminus, sequestering the activity of CRLs (Figure 3) [58, 59]. This subsequently results in the accumulation of CLR substrates such as the DNA licensing factor CDT1 that causes DNA re-replication. These events increase the rates of DNA damage and promote DNA-damage responses. This, along with the accumulation of CRL substrates that regulate DNA synthesis and cell cycle progression, causes stalling of the cell cycle in S-phase [59, 60]. The productive cycle of EBV occurs in an S-phase-like cellular environment and activates ATM (ataxia telangiectasia mutated) and Chk2-dependent DNA damage responses [52]. To exert its activity on its nuclear targets, BPLF1 possesses at least one caspase-1 cleavage site

(Asp_{216}) downstream of the N-terminal catalytic domain. Although the catalytic fragment is not known to have a nuclear localization signal, it has been proposed to be small enough (<40 kDa) to freely diffuse through the nuclear pores (Figure 3) [61]. Caspase-1 activity is triggered by the inflammasome, which is assembled in response to cytosolic components recognising bacterial or viral components [62].

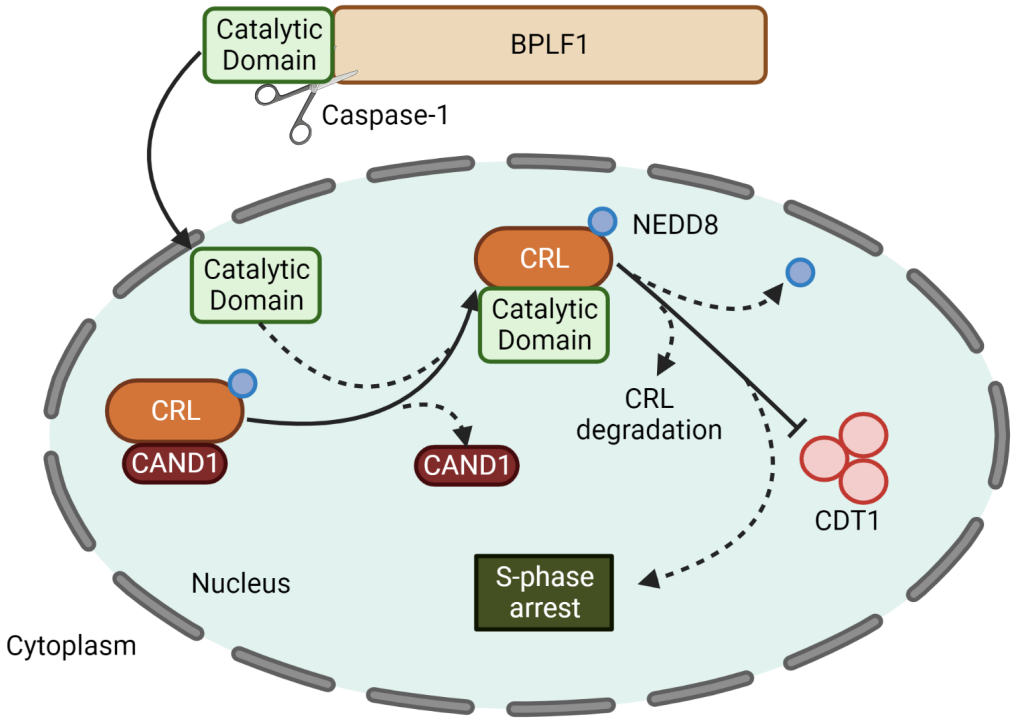

Figure 3: Caspase-1 cleaved BPLF1 catalytic fragment diffuses into the nucleus to displace CAND1 and bind CRL for deneddylation. Upon deneddylation, CRLs are degraded, resulting in the accumulation of CRL substrates such as the DNA licensing factor CDT1. The resulting increase in DNA damage results in DDR and subsequent stalling of cell cycle in the S-phase.

Autophagy is a process by which cells recycle their components and plays a vital defensive role for clearing out intracellular pathogens such as viruses. This process is performed in the cell's effort to regulate homeostasis in response to its microenvironment [63]. Autophagy results in the formation of double membrane enveloped vesicles called autophagosomes

with cellular components contained therein. Degradation of these components results from the fusion of the autophagosome with lysosomes. These steps can serve as initiators of innate and adaptive immune responses through controlling intracellular viral particles [64]. Genetic elements associated with autophagy are called *ATG* (autophagy related genes). Autophagosome nucleation and membrane assembly are mediated by the ULK1/2 protein complex consisting of ATG13, RB1CC1/FIP200, and ATG101, which facilitates MTOR signalling. This complex also contains BECN1/Beclin 1-PIK3C3/VPS34 consisting of the class III phosphatidylinositol 3-kinase PIK3C3/VPS34 and its regulatory proteins PIK3R4/VPS15, BECN1, and ATG14 [65]. Selective autophagy is targeted toward the recycling of organelles and protein aggregates and is initiated by the engagement of autophagic receptors such as OPTN (optineurin), CALCOC2/NDP52, SQSTM1/p62, BNIP3-BNIP3L/NIX factor or NBR1 [66]. Interactions of these receptors with their targets are mediated through ubiquitin, or LGALS (galectin) tags, to phagophore-anchored LC3 molecules via LC3-interacting regions (LIRs). Ubiquitin modification of core and regulatory components regulates selective autophagy [67].

Viruses have been demonstrated to exploit or to escape autophagic processing [68]. EBV is known to potentiate the formation of autophagosomes within virus-infected cells. Latent infection programming oversees the accumulation of EBNA1 in autophagosomes, which are subject to lysosomal processing for loading onto MHC-II molecules in B cells [69]. EBNA1 latent protein has been shown to resist autophagic clearance, and LMP1 has been demonstrated to upregulate autophagy to promote its turnover and reduce toxicity. Latent protein BHRF1 mimics BCL2, which is an inhibitor of autophagy and an anti-apoptotic protein [70]. EBV lytic activation in B cells has been correlated with enhanced autophagy in early lytic phase, followed by reduced autophagy in late lytic phase. Purified virus containing LC3

molecules coupled with the stabilization of autophagic membranes during EBV replication indicates that selective autophagic membrane markers are recruited by the EB virion to promote envelopment of capsids. BPLF1 has been demonstrated to inhibit selective autophagy through interactions with components of the vesicular trafficking and autophagy, such as autophagy receptor SQSTM1/p62. This effect has been countered by overexpressing SQSTM1/p62 [E209A, K420R] mutant that doesn't require ubiquitination for cargo loading [71].

1.4. The EBV Infection and Life Cycle

Much like its relatives in the *Herpesviridae*, EBV's life cycle consists of lytic and latent programming that have differentially regulated gene expression profiles. Infection is mediated by interactions between viral glycoproteins and cell receptors. Putative infection routes within the host involve the EB virion entering the epithelium of the Waldeyer tonsillar ring in the oropharynx and initiating the viral lytic cycle. Newly lytically produced virions then exit the epithelial cells and infect circulating B cells in the underlying lymphoid tissues [72]. Primary EBV infection is occasionally accompanied by fever, sore throat, lymphadenopathy, and splenomegaly in adolescents and young adults, resulting in lytic induced cell death. A more frequent occurrence is the passage of EBV into latency programming accompanied with a highly regulated gene expression profile. Infected naïve B cells are then transformed into activated lymphoblasts through latency III programming where EBNAs 3A, B, and C suppress EBV growth, allowing the cell to establish within the germinal centre of lymphoid follicles as latency II. The infected cell then exits the germinal centre as a resting memory B cell followed by transition into latency 0 programming where all viral protein expression is inhibited. When resting memory B cells divide, EBNA1 is expressed and thus latency I is established. These cells migrate back to the tonsil, where plasma-cell differentiation

occasionally triggers lytic reactivation, causing the release of viral particles back into the saliva to infect new hosts (Figure 4) [6, 7, 73].

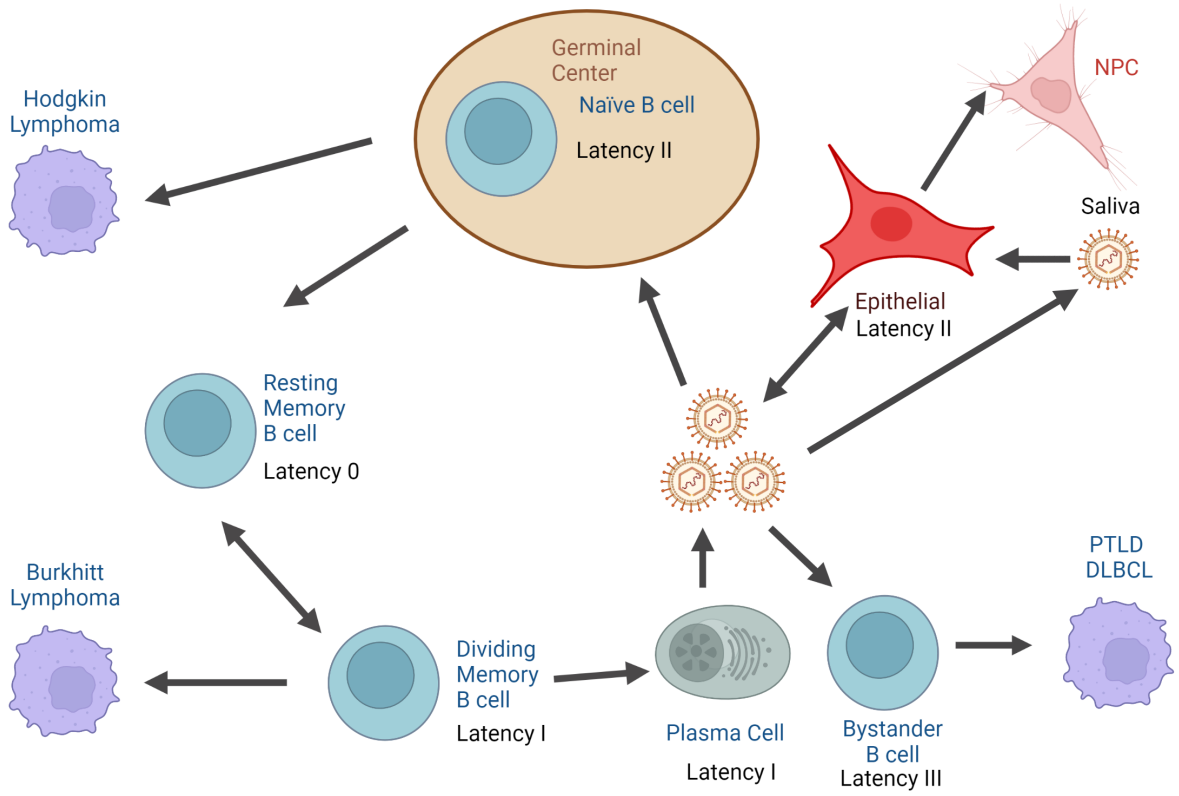

Figure 4: Schematic depicting the EBV life cycle, and the human malignancies associated with each latency phase. EBV is introduced through saliva particles from an infected host to a new host, where it enters via the epithelia of the oropharynx. Infection of epithelial cells may result in latency II programming leading to the potential development of carcinomas. Viral particles shed by the epithelial cells at the basolateral surfaces can enter the tonsillar region and blood and infect naïve B cells. These germinal centre cells will carry the EBV episome and express latency II encoded genes to provide survival signalling with potential of developing into Hodgkin lymphoma. These B cells exit the germinal center to become resting memory B cells where all latency genes are supressed as latency 0. As these resting memory B cells divide in response to growth stimuli, latency I programming comes into effect with the potential for B cells to develop into Burkitt's lymphoma. Memory B cells that differentiate into plasma cells in the tonsils occasionally become lytic, releasing virus back into the saliva to either infect new hosts or if the host is immunocompromised, infect bystander B cells with the potential of developing post-transplant lymphoproliferative disorder (PTLD) or diffuse large B cell lymphoma (BLBCL).

1.4.1. Binding and fusion with host cells

Herpesviruses have evolved the ability to utilize the mechanics of the host membrane component trafficking for localization, protein synthesis, and lipid envelopment processes [74]. The primary purpose of cell endocytosis is the internalization of macromolecules or particulates, such as nutrients or morphogenic compounds, from the surrounding medium for intracellular trafficking [75, 76]. EBV makes use of its glycoproteins to mediate attachment and fusion of the viral envelope with the cellular membrane. This then allows for the internalisation and release of the herpesviral capsids into the cytoplasm [77-79].

EBV interacts with resting primary B cells via the viral gp350 binding to B cell complement receptor 2 (CR2/CD21) [80]. In addition, complement receptor 1 (CR1/CD35) has also been identified to interact with gp350. Once EBV binds to the surface of the target cell, a cascade of interactions between EBV gp42 (BZLF2) and human leukocyte antigen (HLA) class II of B cells, triggers membrane fusion. Conformational changes to the structure of gp42 occur to facilitate the binding of its flexible 44-61 and 67-81 amino acid regions to gH/gL (BXLF2/BKRF2) during fusion [81]. After binding, a hydrophobic pocket of gp42 widens to possibly allow for interactions with gH/gL and gB or another receptor [82]. This then permits the embedding of the hydrophobic loops into the B cell membrane to induce fusion [83]. After fusion, the binding of CD21 triggers the formation of a CD21-CD19-CD81 complex, which is capped with the EBV, Ig superfamily members, tetraspannins, and integrins [84-86]. Binding of gp350 to CD21 induces interleukin-6 through activation of NF-κB. However, this induction has little effect on virus entry and doesn't immediately initiate lytic replication [87]. Entry of the virus into the B cells is accompanied by the release of the capsid, viral tegument proteins, and virally encoded RNAs into the cytoplasm. The tegument then serves to repress host cellular responses to viral infection and the viral RNAs encode for several

transactivators such as BZLF1 or serve to suppress host responses via miRNA mediated silencing of host genes [88, 89].

EBV attachment to epithelial cells is mediated by different receptors, as CD21 is expressed at low levels in epithelial cells in culture and in the tonsil. Recently, ephrin receptor A2 (EPHA2) has been identified to be essential for viral entry into epithelial cells via interaction with gH/gL [90]. Integrins have also been identified as possible candidates for EBV-host interactions. The EBV gH/gL also possesses an integrin KGD binding domain. The host epithelial integrins αυβ5, αυβ6, and αυβ8 serve as receptors for this KGD domain [90, 91]. BMRF2 also interacts with the α3β1, α5β1, and αυβ1 integrins of polarized oropharyngeal epithelial cells [92]. These interactions result in small conformational changes in gH/gL, allowing for binding to gB (gp110) and the fusing of the virus and cell plasma membranes [91]. Ultimately, EBV gH/gL is considered a fusion regulatory protein that is required for entry into both B cells and epithelial cells. The transcytosis machinery of membrane bound IgA receptor on the epithelial cells can also be exploited by α-gp350 polymeric IgA bound EBV particles, providing an alternative path of infection [93]. In addition, infection of epithelial cells has been demonstrated to occur via transfer from memory B cell surfaces to the basolateral surface of epithelial cells. To form a virological synapse between B cells and epithelial cells, EBV initiates this transfer via activation of CD21. The transfer is then facilitated by CD11b of memory B cells interacting with heparan sulphate moieties of CD44v4 and LEEP-CAM on epithelial cells. For transfer infection, EBV gH and gp110 have been shown to be essential while gp42 was not [94].

1.4.2. Transition into latency

Once the viral envelope is shed and the capsid is released into the cytosol, the linear genomic DNA of EBV is then targeted to the nucleus of the cell. Once in the nucleus, it circularizes and initiates a transient prelatent phase where it expresses a restricted set of latent and lytic genes. Latent genes such as EBNAs, LMPs, ncRNAs, and miRNAs, are expressed to promote B cell survival and proliferation, which results in the activation of quiescent B cells into B lymphoblasts. During activation, lytic genes such as viral Bcl-2 proteins (encoded from the *BHRF1* and *BALF1* genes), are also expressed to prevent endogenous stress and immediate activation-induced apoptosis of the B lymphocytes [95]. DNA damage response (DDR) is also potentially hindered by lytic gene expression during this phase [96]. Prelatency lasts for about 1 to 2 weeks after infection and no new viral particles are produced. In this phase, the viral genome undergoes extensive epigenetic modifications [95]. These modifications efficiently silence EBV lytic gene expression via CpG methylation, transitioning from infection to latency. Latency associated genes are spared from transcriptional repression as the promotors of the EBNAs change after methylation events [97].

B lymphocytes can be infected with EBV *in vitro* at efficiencies of >50 % and in a few days, immortalization is established in a subpopulation called lymphoblastoid cell lines (LCLs). These LCLs contain an extra-chromosomal episome of the viral genome maintained by EBNA1 [98]. Latently infected cells are known to express nine latent proteins and several non-coding RNAs controlled by the gene transactivator EBNA2 [99]. Latent genes encoded in these cells can function as oncogenes. For example, latent membrane protein 1 (LMP1) mimics activated CD40, initiating B cell activation and proliferation [100]. The transformative ability of EBV is suppressed *in vivo* by $CD8^+$ T lymphocytes acting on cells carrying latent

proteins [101]. When this immune surveillance is compromised, such as in cases of HIV infection or when immunosuppressive drugs are administered, lymphomas can develop [102].

1.4.3. Lytic reactivation

Reactivation of EBV from latency to lytic programming has been demonstrated *in vitro* and *in vivo*. In tissue culture, HDAC, protein kinase C agonists, DNA methyltransferase inhibitors, anti-immunoglobulin, and transforming growth factor beta can be used to reactivate EBV lytic cycle [12, 103-106]. Cellular events, such as terminal cell differentiation, can also contribute to lytic reactivation through disruption of latency [107, 108]. Signalling cascades produced by these exogenous signals trigger the expression of the transactivator of lytic genes, BZLF1 (also known as ZEBRA, Zta, EB1, or Z) and BMRF1 (also known as Rta, or R) [109]. The molecular switch BZLF1 is a member of the family of AP-1 transcription factors. When the lytic cycle is initiated, BZLF1 binds to viral and cellular promoters to induce gene expression, leading to the *de novo* synthesis of virions [12]. During the lytic cycle, the EBV genome is linearized and replicated by seven viral proteins BZLF1 (lytic transactivator which binds to oriLyt), BALF5 (DNA polymerase), BMRF1 (DNA processivity factor), BALF2 (ssDNA binding protein), BBLF4 (helicase), BSLF1 (primase), and BBLF2/3 (helicase-primase-associated proteins) [110, 111].

Capsid assembly relies on the transport of all capsid proteins to the site of assembly within the nucleoplasm [112]. The minor capsid protein (BORF1) contains a nuclear localisation signal (NLS) which allows it to enter the nucleus by itself where it facilitates nuclear entry of capsid proteins BDLF1 and MCP for capsid assembly at the PML-NBs [113]. The newly synthesized viral genomes are packaged into capsids in the nucleoplasm and bud through

the inner nuclear membrane into the perinuclear space to acquire the primary envelope which is lost through the fusion with the outer nuclear membrane, resulting in the release of the nucleocapsids into the cytoplasm. After release the capsids take up various tegument proteins and the secondary envelope via budding into organelles such as vesicles containing markers from both the cis-Golgi network and the trans-Golgi network [114, 115]. Within these vesicles EBV associates with small Rab GTPases (Rab8a, Rab10, and Rab11a) to coordinate intracellular trafficking to the cell plasma membrane, which is largely dependent on the microtubule-mediated cellular secretory pathway [116, 117].

2. Aims and Objectives

Since B cells exposed to EBV VLPs have demonstrated viral structural proteins to be involved in the development of nuclear abnormalities [118], it was decided that screening of additional proteins would identify targets that have not been discussed in literature. It is known that at least one of these structural proteins, BNRF1, is a major component responsible for these abnormalities and has been recently discovered to be involved in disrupting the cohesion complexes SMC5/6 [119]. In our study, preliminary screening of tegument proteins identified BPLF1 to have potentiating effects on genetic instability.

BPLF1 is the largest known EBV encoded transcript. Until now, less than 10 % of the protein length has been attributed to a function in the EBV life cycle. The current literature making use of full-length BPLF1 is scant with only one group making little use of a full-length expression construct in 2014 [47]. In effort to expand our knowledge involving this tegument protein, three aims were proposed:

I. Determine the role of BPLF1 during B cell infection.

II. Study the impact of BPLF1 on the cell genetic stability upon infection.

III. Identify the molecular mechanism that links BPLF1 to genetic instability.

3. Results

3.1. Nuclear abnormalities after BPLF1 transfection

3.1.1. Tegument Screening identifies BPLF1 as an inducer of Nuclear abnormalities

A full length BPLF1 expression plasmid (B1283) was generated from PCR amplification of the M81 BPLF1 open reading frame (ORF) from the M81 BACmid construct (B110) and its subsequent insertion into pRK5 expression vector through restriction digestion. To identify cells expressing BPLF1, I introduced a 3xFlag-tag (DYKDHDGDYKDHDIDYKDDDDK) to the start of the ORF through overlap PCR. This tagged plasmid was used in the proceeding nuclear abnormality studies. As the major tegument protein BNRF1 can induce genomic instability along with M81/ΔBNRF1 virus particles [118, 119], additional tegument proteins were considered for investigation. My first set of experiments consisted of transfection and transient expression of a panel of tegument proteins in HEK293 cells. The large tegument protein (BPLF1), major tegument protein (BNRF1), inner tegument protein (BOLF1), tegument protein BRRF2, tegument protein BLRF2, serine/threonine kinase (BGLF4), thymidine kinase (BXLF1), tegument protein BKRF4, and encapsidation chaperone protein (BGLF3) were studied alongside BNRF1 and Flag only control. I collected the cells 72 hours after transfection and used 4',6-diamidino-2-phenylindole (DAPI) to stain for DNA and α-Flag antibody to identify cells expressing tegument protein. To my surprise, BPLF1 expressing cells showed noticeably larger nuclei and increased multinuclearity when compared to control cells (Figure 5). As expected, BNRF1 expressing cells had noticeable increased nuclear abnormalities and BOLF1 showed slightly increased nuclear abnormalities.

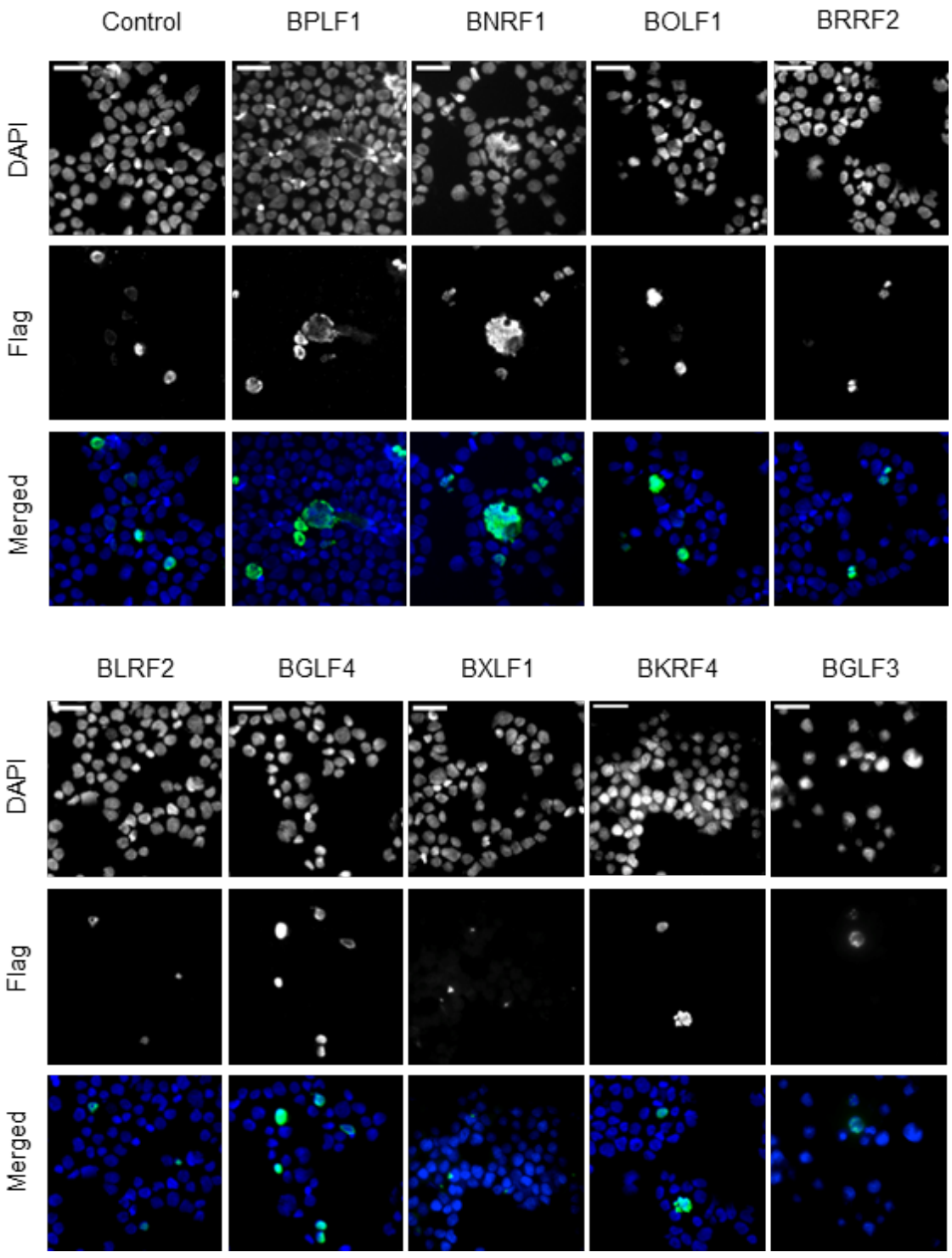

Figure 5: Screening tegument proteins for ability to induce nuclear abnormalities. HEK293 cells were transfected with Flag-Tagged tegument and were analysed 72 hours post transfection. a Percentage of interphase cells with nuclei greater than the average of the control (n=100). b Percentage of interphase cells with multiple nuclei (n=100). c Representative immunofluorescent microscopy images for each tegument transfection experiment. Scale bars represent 30 μm.

I subsequently decided to generate replicate data to make empirical measurements and comparisons of the treatments. I repeated all transfection experiments to make a total of 5 independent replicates. I decided to compare two phenotypes associated with nuclear abnormalities, rates of nuclear enlargement and multinuclearity in Flag positive cells. These phenotypes were used as indicators for genomic instability, which is one of the hallmarks of cancer. In Figure 5, BPLF1 and BNRF1 expressing cells had shown noticeable increases in rates of nuclear enlargement. I performed these measurements using the threshold tool in ImageJ software using the auto threshold settings to identify and demarcate nuclear regions using the DAPI signal. The mean nuclear sizes for the control treatments were used as a cut-off for each replicate. Any cell nuclear measurement greater than this threshold, was subsequently counted as enlarged. I proceeded to quantify the number of Flag-positive cells and calculated the percentage of cells with enlarged nuclei in Figure 6a. I also counted the number of nuclei in each Flag-positive cell and calculated the percentage of Flag-positive cells that were multinucleated in Figure 6b. For the 5 replicates, the mean rates of nuclear enlargement were 1.198 % for control cells, 18.49 % for BPLF1 expressing cells, 14.11 % for BNRF1 expressing cells, and 7.798 % for BOLF1 expressing cells. For the 5 replicates, the mean rates of multinuclearity were 2.458 % for control cells, 20.03 % for BPLF1 expressing cells, 10.83 % for BNRF1 expressing cells, and 8.756 % for BOLF1 expressing cells. As depicted in Figure 5, when compared to the control treatment BPLF1 showed the strongest set of changes in phenotypes for all proteins in the tegument panel for both enlarged nuclei and multinuclearity.

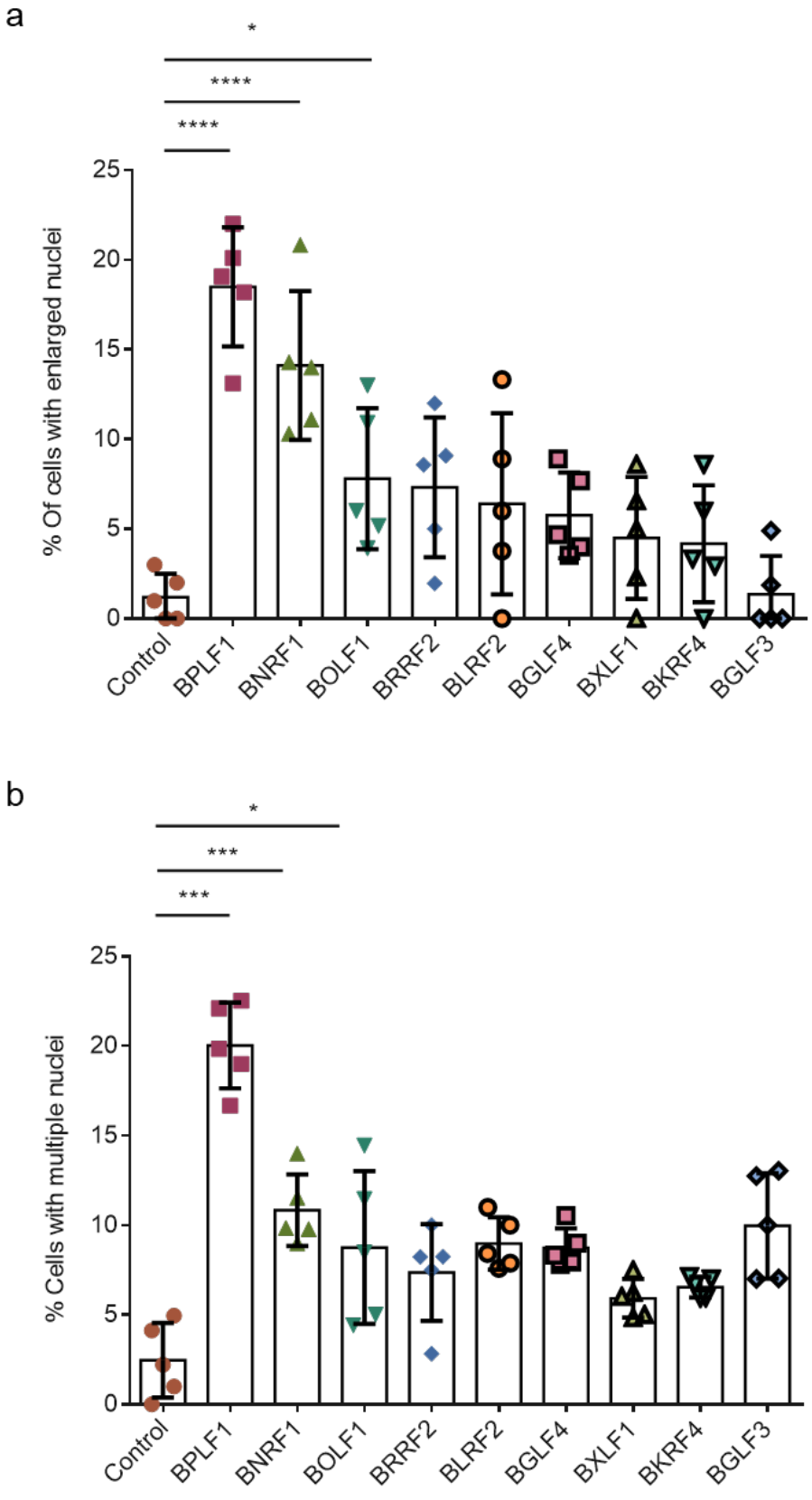

Figure 6: The tegument protein BPLF1 induces genomic abnormalities. HEK293 cells were transfected with a panel of tegument proteins. After 72 hours cells were collected and stained for Flag and DAPI. a Percentage of cells possessing enlarged nuclei. b Percentage of cells with multiple nuclei. (n = 5).

3.1.2. BPLF1 is associated with mitotic abnormalities

The next question to be addressed was how BPLF1 causes the accumulation of genetic material in the host cells. To achieve this, I aimed to test BPLF1 expression for effects on centriole and chromosomal counts in HEK293 cells as they are members of the cell's mitotic machinery. A normal interphase cell nucleus consists of 23 chromosome pairs with each pair possessing 2 centromeres to make a total of 46 centromeres. To measure cellular ploidy, I performed immunofluorescence staining using antibody specific for Centromeric Protein A (CENP-A), a member of the inner kinetochore and a marker for centromeric regions. HEK293 cells transfected with expression plasmids for BPLF1 and mCerulean were stained for CENP-A and compared in Figure 7. Cells expressing BPLF1 showed significant rates of aneuploidy and polyploidy when compared to control cells, which correlates with increased nuclear enlargement and multiple nuclei observed in Figure 9. This is an important finding as many EBV associated cancers such as gastric carcinomas, nasopharyngeal carcinomas, and post-transplant lymphoproliferative disorders are afflicted with increased rates of aneuploidy and chromosomal defects such as translocations and deletions [120-123].

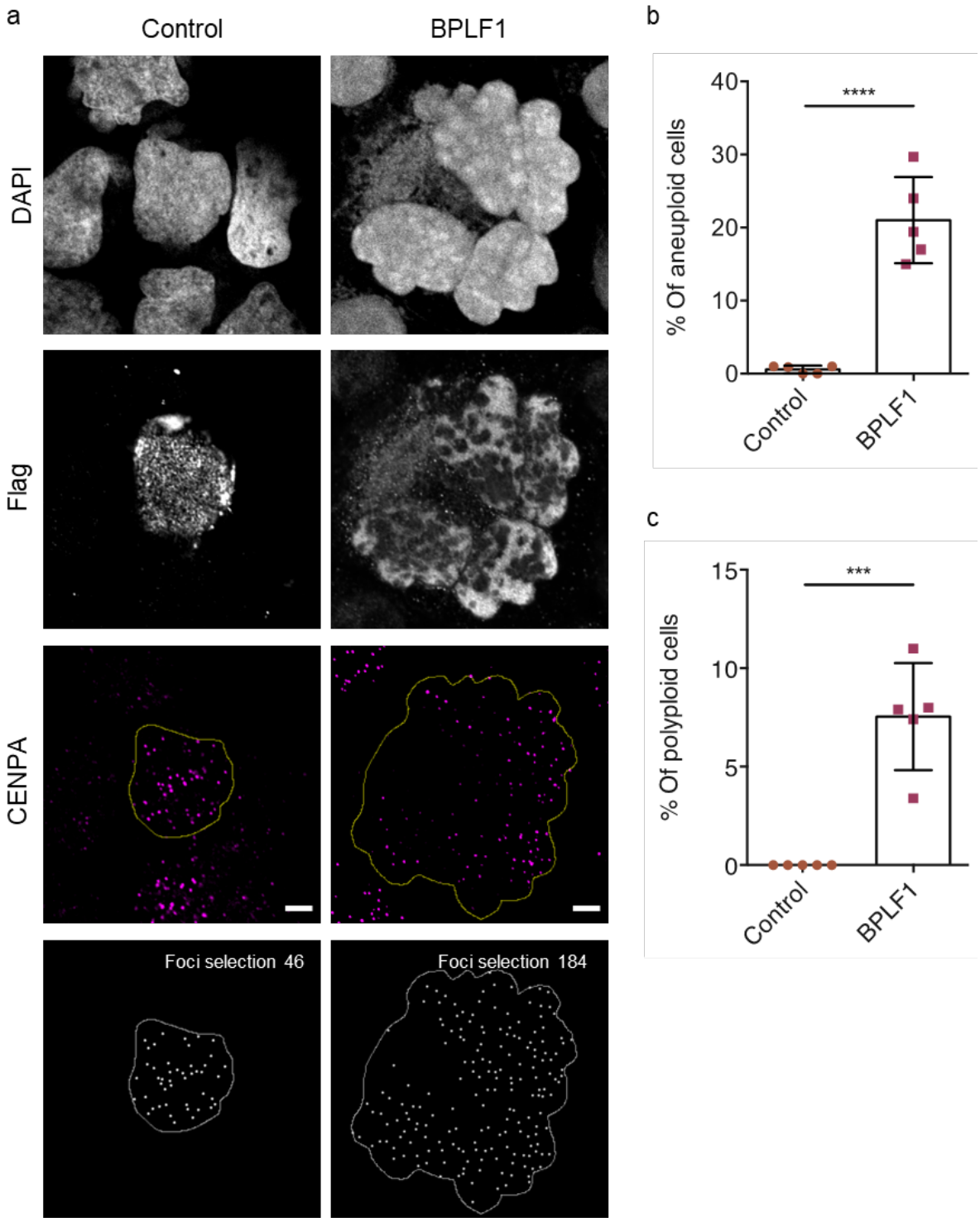

Figure 7: BPLF1 increases rates of aneuploidy. HEK293 cells were transfected with plasmids expressing Flag-BPLF1 or Flag-mCerulean as a control. Cells were collected 72 hours after transfection and stained for Flag, DAPI, and CENP-A. a Representative control Flag-mCerulean expressing cells. b Scatter plot for percentage of Flag positive cells with aneuploid nuclei (foci > 46). c Representative Flag-BPLF1 expressing cell. Nuclear regions are demarcated by yellow lines using DAPI signals and have their internal CENP-A foci marked with grey dots. Scale bars represent 5 µm. d Scatter plot of the percentage of Flag positive cells with polyploid nuclei (foci ≥ 92). c+d Each dot represents an individual biological replicate experiment of 50 cells (n=5). Error bars represent standard deviation. Unpaired student t-tests were performed. $^{****}p < 0.0001$, $^{***}p < 0.001$.

Next, I investigated effects of BPLF1 expression on the cell centrosomes. In healthy cells, centrosomes occur in pairs, with each centrosome possessing a mother and daughter centriole which provide scaffolds for the attachment of mitotic spindles. Mitotic abnormalities can lead to the overduplication of centrosomes which is achieved through mitotic slippage when cells revert from the S to G1 phase. This results in polyploid cells possessing greater than 2 centrosomes. Centrosomal abnormalities can be subdivided into 2 categories, centriole amplification, and centriole overduplication. Centriole amplification occurs when daughter centriole numbers are greater than the mother centrioles and centriole overduplication occurs when mother and daughter centriole numbers remain equal while the centrosome count is greater than 2. The antibody CEP170 targets for the mother centriole while the α-Centrin-2 antibody targets the Centrin-2 protein of both the mother and daughter centrioles. As depicted in Figure 8, Flag positive cells stained for CEP170 or Centrin-2 were compared for Control and BPLF1 expression. I performed these experiments in 5 independent replicates. Cells with >4 centrioles were counted as abnormal with BPLF1 cells having on average of 30 % versus control cells with an average of 7.58 % (Figure 8c) and cells with >2 centrosomes were counted as abnormal with BPLF1 cells having an average of 21.95 % versus control cells having an average of 3.634 % (Figure 8d). Cells expressing BPLF1 accumulated abnormal amounts of both mother and daughter centrioles indicating increased rates of mitotic abnormalities. This result, coupled with the increase in aneuploidy (Figure 7) and nuclear abnormalities (Figure 6) clearly indicates a strong deleterious effect of BPLF1 on the mitotic machinery of host cells. This effect leads to abnormal mitotic events, which lead to the accumulation of multiple nuclei and components of the mitotic machinery, and consequently to the accumulation of genomic abnormalities.

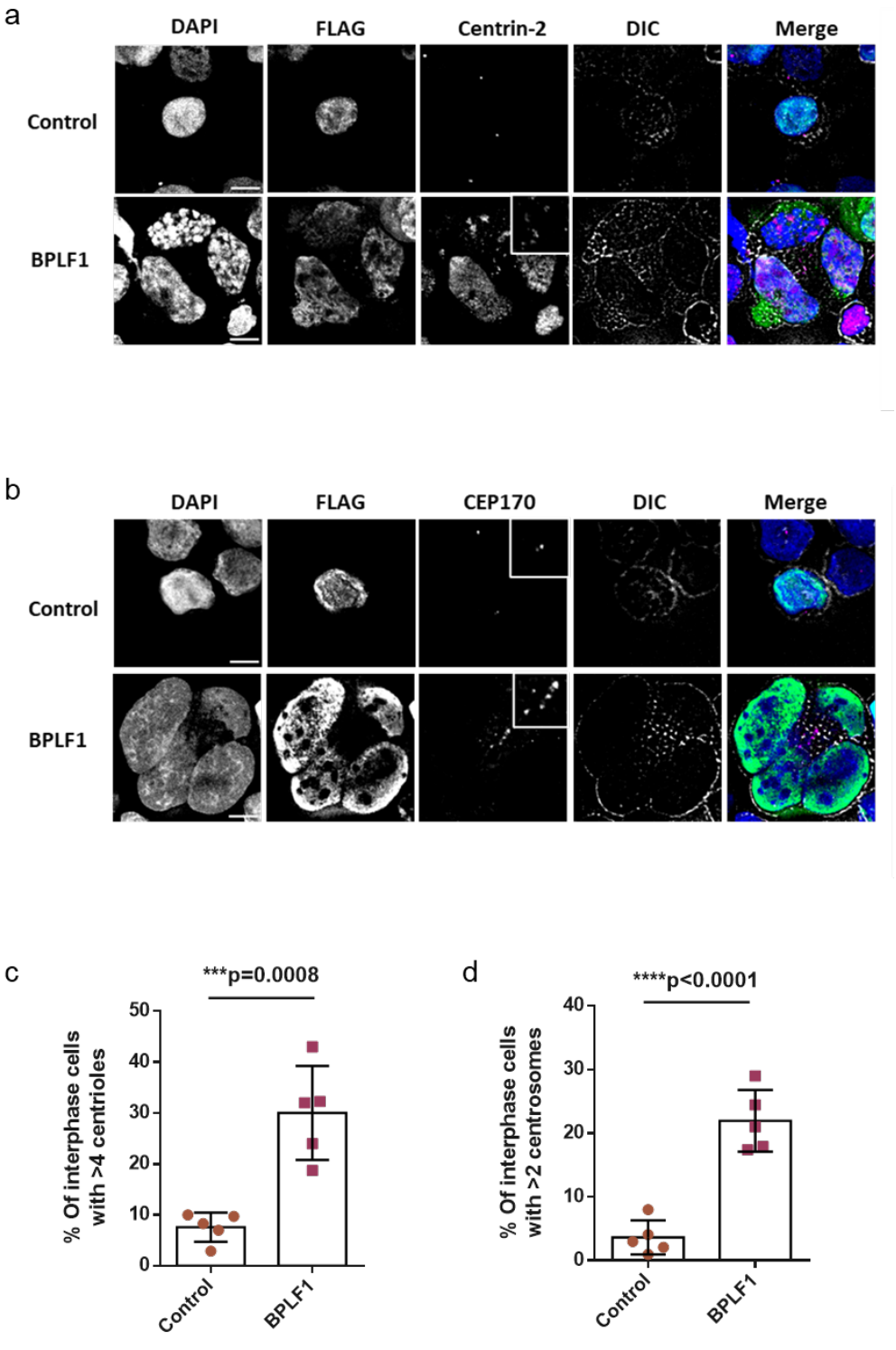

Figure 8: Centrosomal abnormalities occur when BPLF1 is expressed. a Interphase cells showing normal centriole counts for control treatment and abnormal centriole amplification for BPLF1 treatment. b Interphase cells showing normal centrosomal counts for control treatment and abnormal centrosome counts for BPLF1 treatment. c Dot plot shows that the number of interphase cells with abnormal centriole counts increases under BPLF1 expression when compared to control expression (n = 5). d Dot shows cells with abnormal centrosome counts increases (n = 5). Each value was calculated from at least 100 flag positive cells and results were plotted and compared using Paired-T tests. ***P < 0.001, ****P < 0.0001.

Since BPLF1 showed a significant phenotype leading to genomic instability I decided to investigate the regions of BPLF1 that contribute to this effect. Nuclear enlargement has previously been attributed to the N-terminal catalytic region consisting of the first 325 amino acids. This effect was abrogated upon mutation of the Cys-61 to Ala-61 [58, 59]. I performed a site directed mutagenesis on the full-length Flag-BPLF1 expression plasmid to generate the catalytic mutant BPLF1^{C61A}. I then performed transfections for the screening of nuclear abnormalities using control, BPLF1, and BPLF1^{C61A} (Figure 9). It was evident that both the wild type and the catalytic mutant gave similar effects on rates of enlarged nuclei and multiple nuclei with control cells showing 2.94 % abnormally enlarged nuclei with 1.33 % showing multinuclearity on average, BPLF1 expressing cells showed a 19.56 % rate of enlarged nuclei with 14.90 % multinuclearity on average, while the cells expressing the catalytic mutant showed a 20.78 % rate of enlarged nuclei with a 16.80 % rate of multinuclearity on average. From these results, it is likely that a region external to the previously described BPLF1 deconjugase catalytic region is likely responsible for this phenotype in HEK293 cells as the catalytic mutant BPLF1^{C61A} did not lose the ability to induce the nuclear abnormalities when compared to wild type BPLF1. The next questions that I proceeded to address were, what are the interaction partners of BPLF1 that lead to these phenotypes and which regions of BPLF1 are responsible for these interactions?

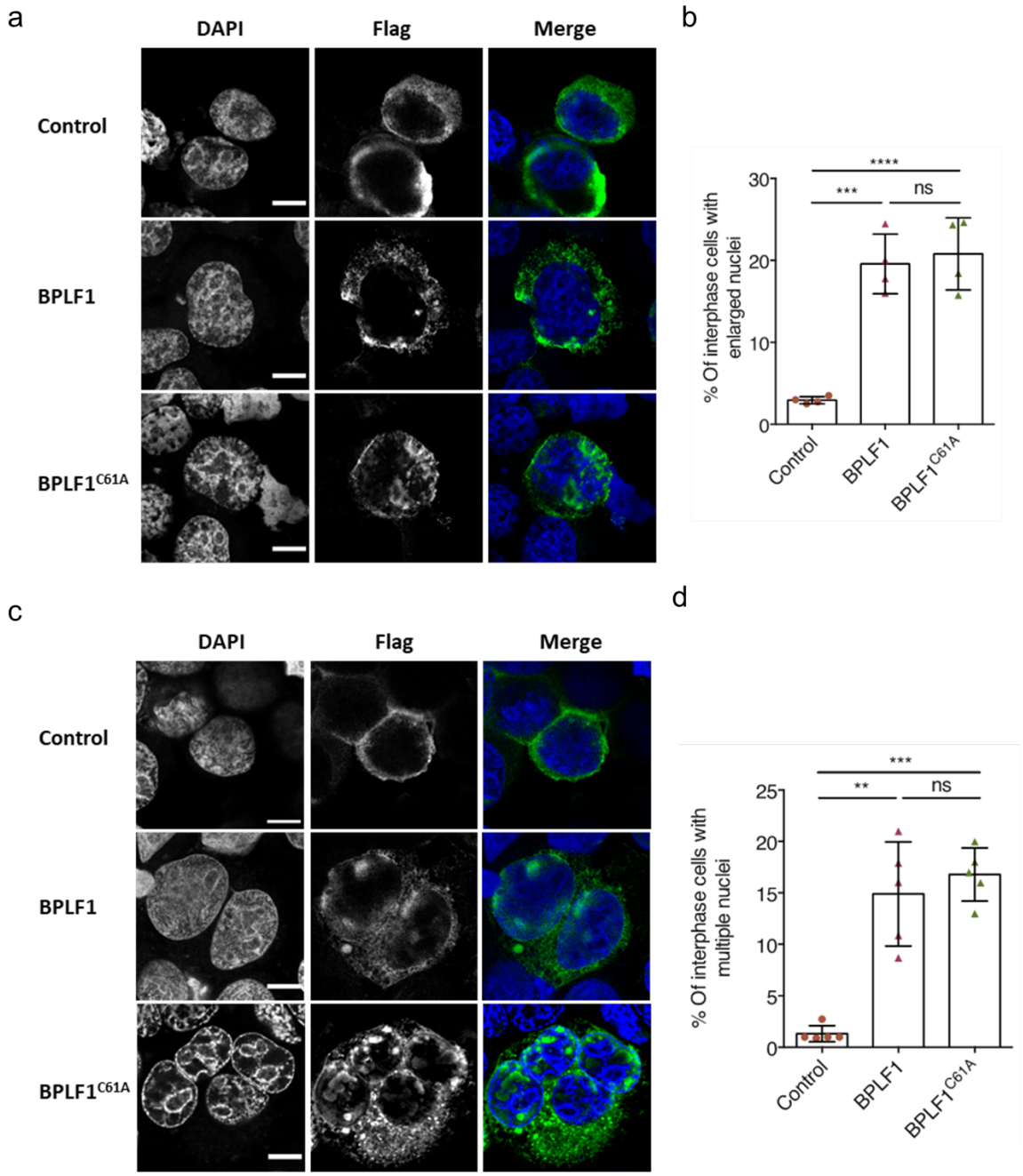

Figure 9: Comparing the abilities for BPLF1 and BPLF1^{C61A} to induce nuclear abnormalities. HEK293 cells expressing control, BPLF1, and BPLF1^{C61A} were collected 72 hours after transfection and stained for Flag and DAPI. a Percentage of interphase cells with nuclei greater than the average of the control (n=100). b Percentage of interphase cells with multiple nuclei (n=100). c Representative immunofluorescent microscopy images of cells. Scale bars represent 10 µm. Paired Ordinary one-way ANOVAs were performed. **P < 0.01, ***P < 0.001, ****P < 0.0001.

3.2. Identifying interaction partners of BPLF1

Understanding BPLF1 interactions is key to understanding the effects this protein has on the host and the ability for BPLF1 to induce genomic instability. To investigate this, I employed a label-free mass spectrometry (MS) approach. This procedure was repeated to make three independent immunoprecipitation-MS (IP-MS) experiments where Flag-BPLF1 or Flag-HA (negative control) were used as bait. Subsequent quantitative analysis using intensity-based absolute quantification (iBAQ) algorithm [124] identified 136 proteins that were at least twofold enriched in Flag-BPLF1 IPs when compared to the negative control. Of these interactors, several proteins previously identified as interaction partners of BPLF1 deconjugase domain (1-325 aa), were enriched in the pulldown. This includes Cul1, Cul3 [59, 61] and BAG6 [51, 125] which are involved in ubiquitin-dependent protein degradation. Of the endogenous HEK293 proteins that were identified to interact with BPLF1, the interactors that showed the highest levels of enrichment are listed in Table 1.

Table 1: Interaction partners of BPLF1 identified via Co-IP MS experiments. The top ten BPLF1 interactors from three independent pull-downs of Flag-BPLF1 and empty vector control expressing HEK293 cells.

Gene names	Protein names	Student's T-test Difference
UACA	Uveal autoantigen with coiled-coil domains and ankyrin repeats	7.85
RAVER1	Ribonucleoprotein PTB-binding 1	6.54
SENP6	Sentrin-specific protease 6	6.00
TIMM17B	Mitochondrial import inner membrane translocase subunit Tim17-B	5.89
FLOT1	Flotillin-1	5.59
BAG6;BAT3	Large proline-rich protein BAG6	5.33
GTPBP4	Nucleolar GTP-binding protein 1	4.78
PSMF1	Proteasome inhibitor PI31 subunit	4.78
NSUN4	5-methylcytosine rRNA methyltransferase NSUN4	4.16
SCML2	Sex comb on midleg-like protein 2	3.88

According to the Co-IP MS data, Sentrin-specific protease 6 (SENP6) was a protein of interest for study. SENP6 interaction with BPLF1 was confirmed through reciprocal Co-IPs. A reverse Co-IP pulldown of endogenous SENP6 for Flag-BPLF1 was performed in parallel (

Figure 10). This confirmed SENP6 as a novel interactor of BPLF1. SENP6 possesses SUMO1 and SUMO2/3 deconjugase activity and is widely regarded as a gatekeeper of genomic stability by orchestrating the deSUMOylation of several cellular targets including kinetochore proteins [53, 126-129].

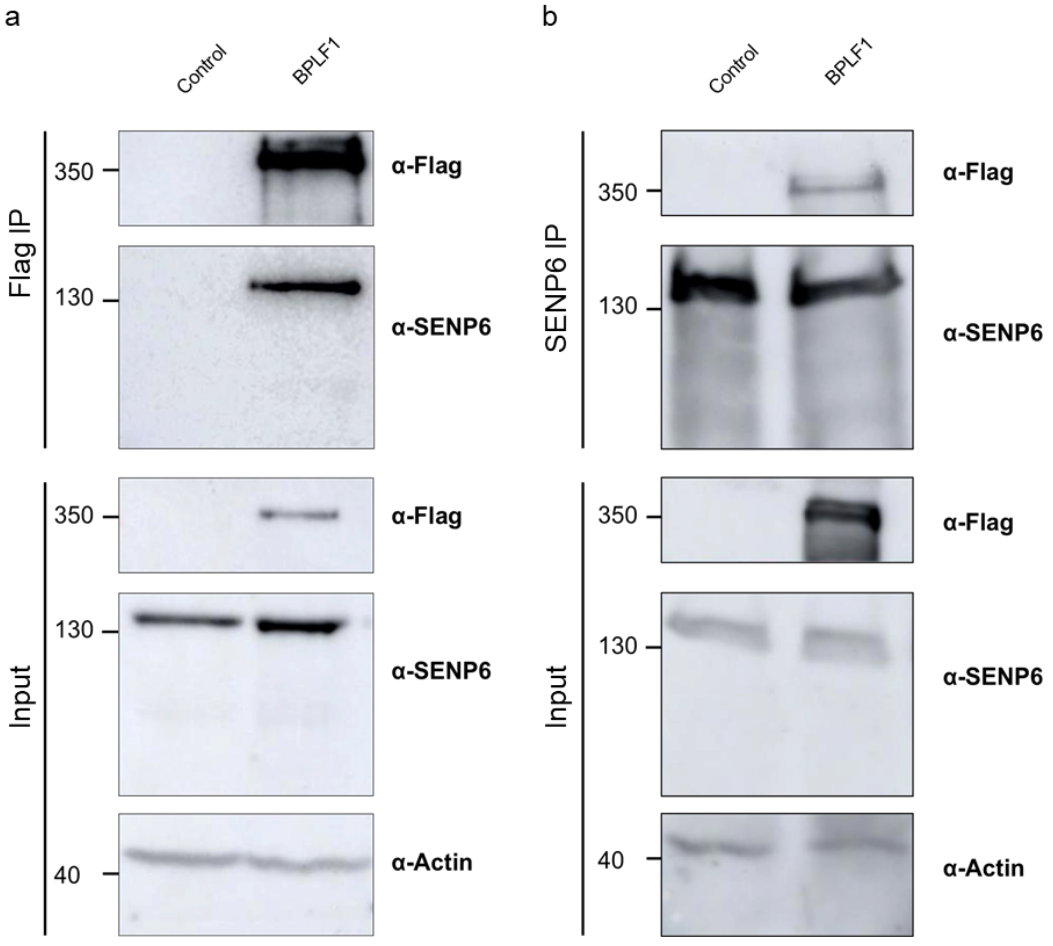

Figure 10: Western blots showing BPLF1 interaction with SENP6. a Co-IPs for Flag-HA (Control) or Flag-BPLF1 expressed in HEK293. b Reverse Co-IPs for endogenous SENP6 showing Flag-BPLF1 being pulled down with SENP6. Actin was used as a loading control for both western blots.

3.3. Design of truncated BPLF1 clones

To address the amino acid region of BPLF1 responsible for mediating SENP6 interaction, I submitted the full length M81 BPLF1 protein sequence, derived from the expression plasmid of Flag-BPLF1, to the pBLAST webserver to map known functions to the protein sequence [130]. Default settings were used to conduct this analysis, which allowed for conserved domains (CDs) to be identified via the built in CD-Search tool. Domain deletions were planned to leave functional domains intact while deleting amino acid regions in effort to preserve the overall structure. This was done under the assumption that structure is related to function [131-133]. Within the 3148 amino acid protein sequence submitted to the webserver, 6 CDs were identified (Table 2).

Table 2: CDs of BPLF1 identified by the CD-Search tool of pBlast. Herpes_teg_N (pfam04843) represents the N-terminal catalytic domain of BPLF1. PHA03247, is the HSV homologue of BPLF1, UL36 with domains conserved at both 391-649 and 2622-2952 aa regions of BPLF1. PRK07003 is a conserved architectural motif observed in DNA polymerase III subunit gamma/tau. Gag_spuma (pfam03276) represents the gag protein sequence motif conserved in primate Pan troglodytes foamy virus which is found to be involved in genome encapsidation [121]. Streccoc_I_II (NF033804) represents a family of LPXTG-anchored adhesins.

Name	Accession	Description	Interval	E-value
Herpes_teg_N	pfam04843	Herpesvirus tegument protein; N-terminal conserved region	45-221	1.70E-61
PHA03247	PHA03247	large tegument protein UL36; Provisional	2622-2952	4.10E-09
PHA03247	PHA03247	large tegument protein UL36; Provisional	391-649	5.51E-06
PRK07003	PRK07003	DNA polymerase III subunit gamma/tau	2872-3050	3.29E-04
Gag_spuma	pfam03276	Spumavirus gag protein	387-517	8.98E-04
Streccoc_I_II	NF033804	antigen I/II family LPXTG-anchored adhesin; Members of the antigen I/II family are adhesins …	397-522	6.63E-03

Taken together, these CDs span 3 distinct regions: 45-221 (176 aa), 387-649 (262 aa), and 2622-3050 (428 aa) on the BPLF1 protein sequence. A large uncharacterized region of 1973 amino acids (650 - 2621 aa) was submitted to the RaptorX webserver for tertiary structure prediction (Figure 11). RaptorX is a tertiary protein structure prediction site for proteins

without close homologues [134-139]. The resultant 3D model (Figure 11), showed two antiparallel domains, BPLF1$^{765\text{-}1327}$ (red) and BPLF1$^{1328\text{-}1976}$ (blue).

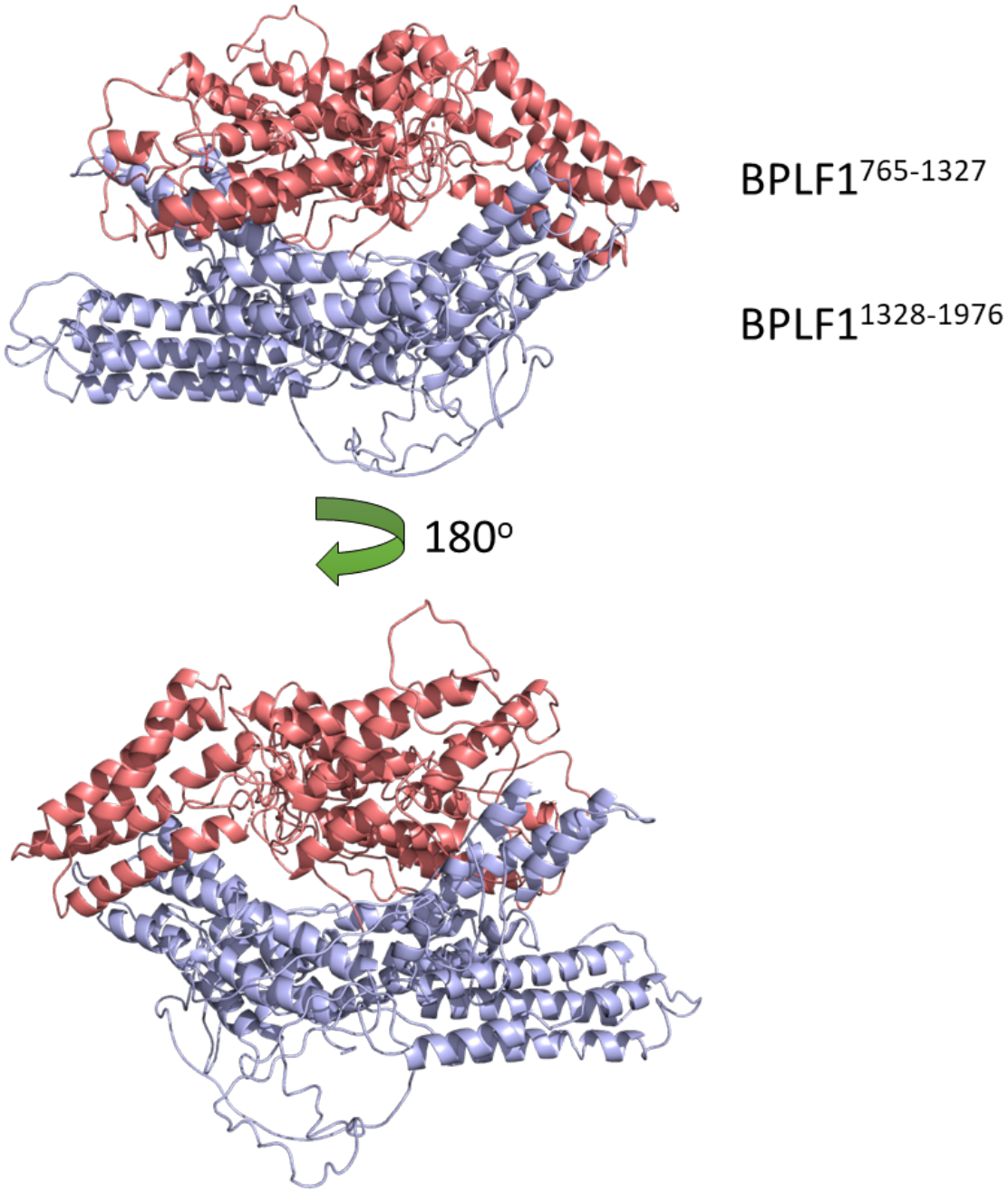

Figure 11: Predicted 3D structure of BPLF1$^{765\text{-}1976}$ obtained from the RaptorX webserver. The protein region was divided to preserve the secondary structure integrity. The two divided regions are coloured red (765-1327 aa) and blue (1328-1976 aa).

Information gathered from the predicted CDs in Table 2 and tertiary structure information in Figure 11, allowed for me to determine appropriate regions to delete while maintaining tertiary structural integrity and consequently, its biological functions in the remaining truncated peptides (Figure 12). The deletions were then planned for 6 sequential domains in BPLF1 (Figure 12b) along with a 3xFlag affinity tag at the N-terminal.

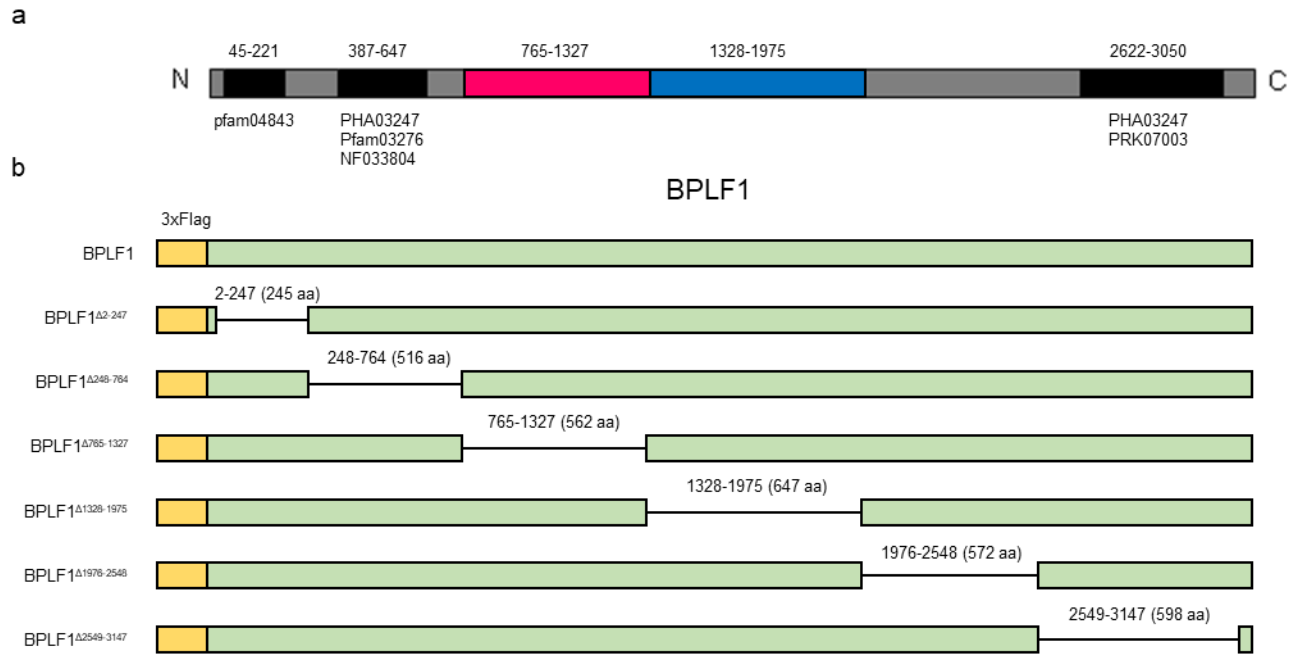

Figure 12: Schematic mapping out planned domain deletions based on bioinformatic analyses. a Full length BPLF1 sequence with conserved domains mapped in black and predicted fiber domains via RaptorX mapped in red and blue. b Planned BPLF1 domain deletion schematics showing amino acid regions to be deleted to generate the respective truncated mutants for use in expression studies.

3.4. BPLF1 domain studies

3.4.1. Generation of BPLF1 sub-clones

I performed domain deletion experiments on the tagged BPLF1 plasmid in accordance with the schematics in Figure 12b. After the cloning was performed, I used EcoRI restriction enzyme to screen for BPLF1$^{\Delta 2\text{-}247}$, BPLF1$^{\Delta 248\text{-}764}$, BPLF1$^{\Delta 765\text{-}1327}$, and BPLF1$^{\Delta 1328\text{-}1975}$ clones and

BamHI to screen for BPLF1$^{\Delta 1976\text{-}2548}$ and BPLF1$^{\Delta 2549\text{-}3147}$ clones. Both sets of restriction digests were conducted in parallel to Flag-BPLF1 to compare to wild type BPLF1 digestion patterns (Figure 13).

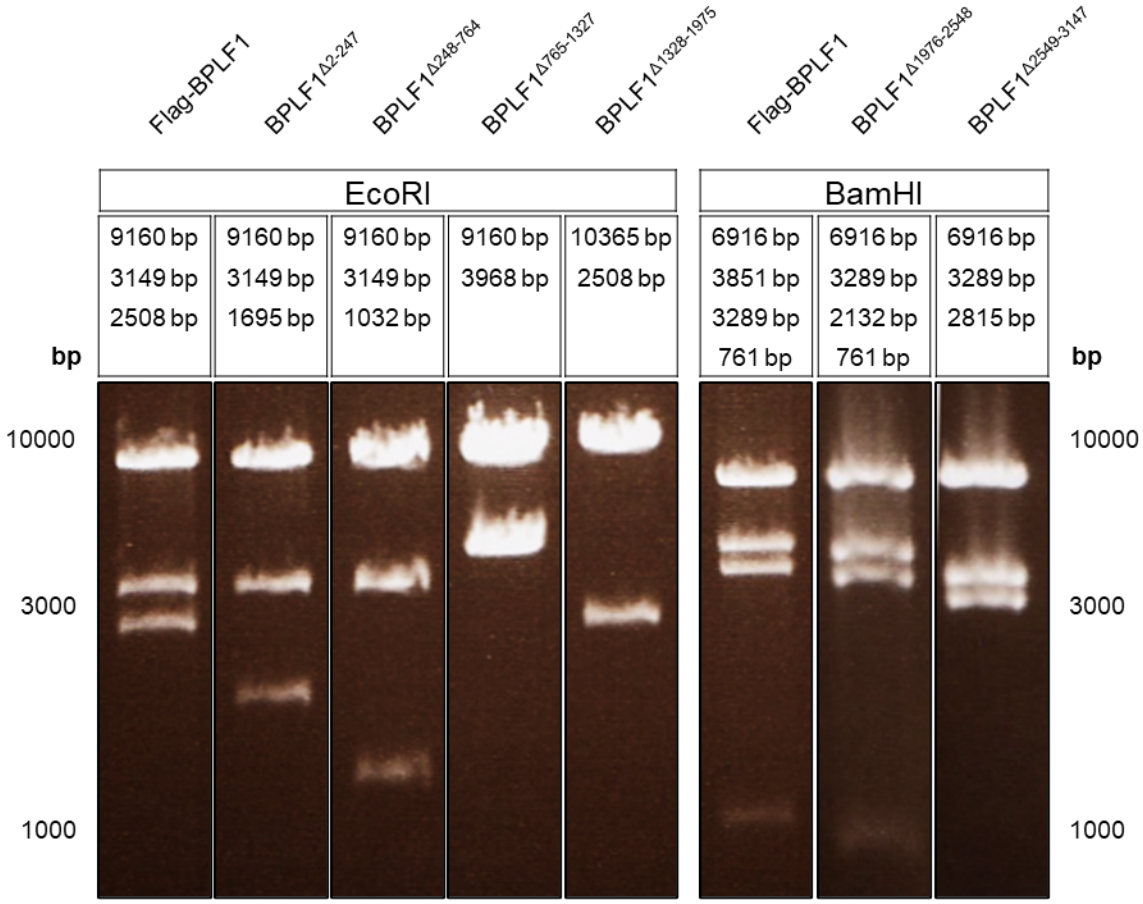

Figure 13: EcoRI and BamHI digestions of plasmids encoding truncated BPLF1 domain deletion mutants. Table above the gel image represents predicted digestion fragment sizes.

Next, I isolated and verified the plasmids from the cloning procedures via sequencing. In effort to verify expression and to normalize plasmid amounts according to the expression of the targeted protein, I transfected the plasmids into HEK293 cells for test expressions (Figure 14). The plasmid concentrations used for transient expression, were subsequently adjusted to normalize the BPLF1 protein signal for western blots.

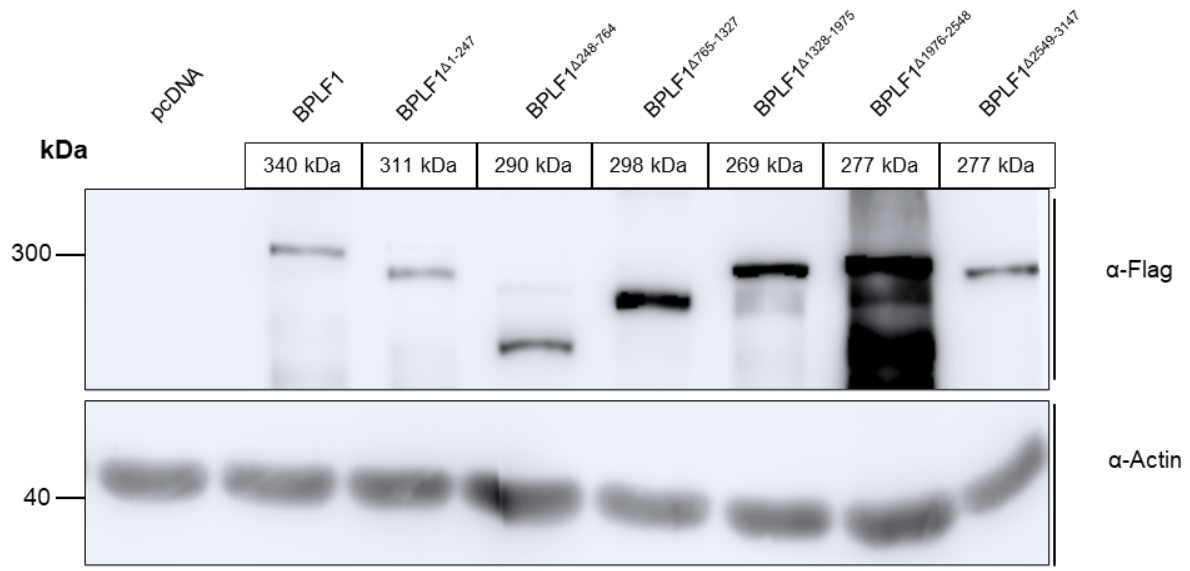

Figure 14: Expression of BPLF1 and domain knockout mutants. HEK293 cells (3.5E5 in 2 cm wells) transfected with a concentration of 3 µg for pcDNA and BPLF1$^{\Delta 765\text{-}1327}$, 2 µg for Flag-BPLF1 and BPLF1$^{\Delta 1\text{-}247}$, and 1 µg for BPLF1$^{\Delta 248\text{-}764}$, BPLF1$^{\Delta 1328\text{-}1975}$, BPLF1$^{\Delta 1976\text{-}2548}$, and BPLF1$^{\Delta 2549\text{-}3147}$. Actin was used as a loading control.

I performed Co-IP experiments to determine the SENP6 interacting region of BPLF1. HEK293 cells expressing each domain mutant were lysed 72 hours after transfection with expression plasmids of domain mutants and were bound to α-Flag affinity resin. I subsequently eluted bound protein complexes and electroblotted and probed them to generate the blot in Figure 15. BPLF1$^{\Delta 765\text{-}1327}$ showed almost complete loss of interaction with SENP6 while BPLF1$^{\Delta 1328\text{-}1975}$ showed slightly reduced SENP6 interaction. The next question that I had was, how SENP6 activity was being affected by BPLF1 interaction?

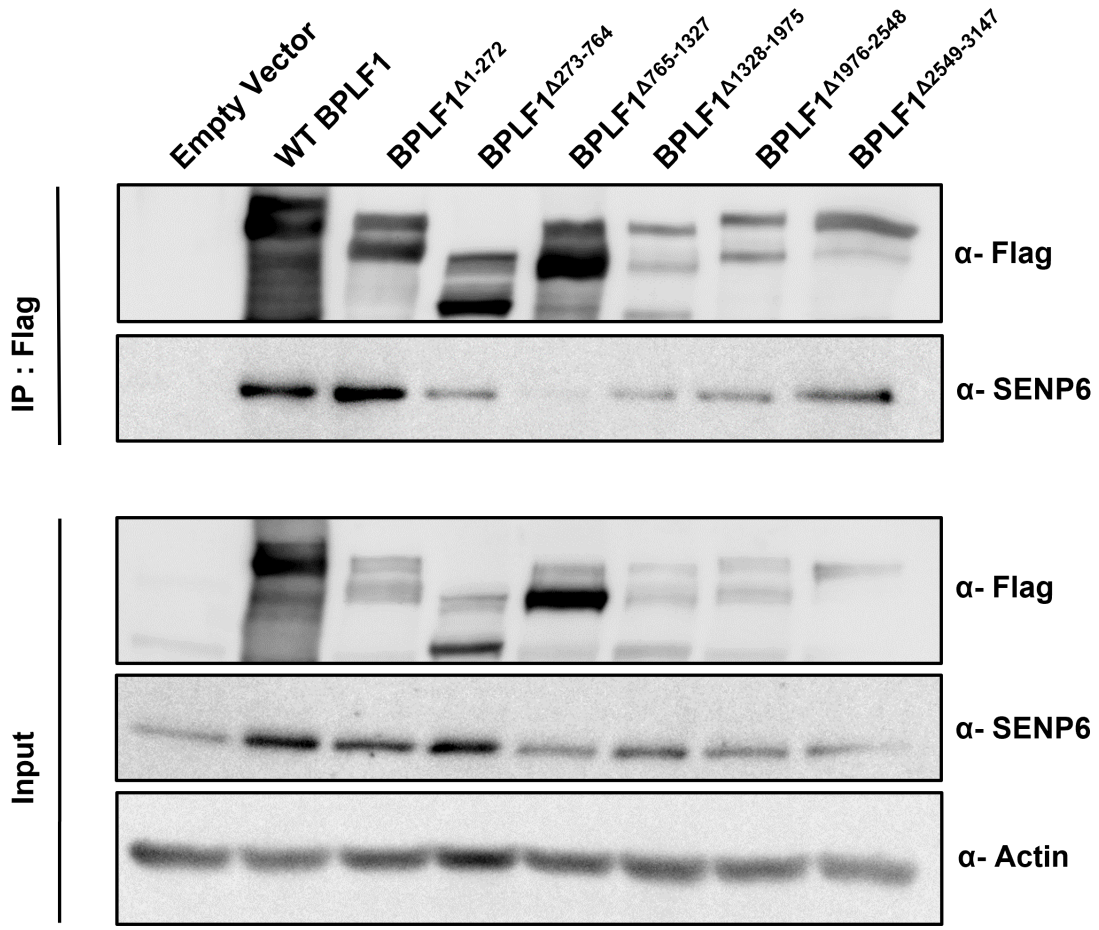

Figure 15: Co-IP pulldown of Flag-tagged domain knockout mutants. The sequential domain deletion mutants were pulled down by Flag affinity to detect the domain of BPLF1 responsible for endogenous SENP6 interaction.

3.4.2. BPLF1 effects on SENP6 activity

Since SENP6 shows preference for poly-SUMO2/3 chains I therefore decided to assay SENP6 activity via immunofluorescence and western blot for SUMO2/3. The catalytic mutant BPLF1^{C61A} that I generated in section 3.1.1, was transfected along with the wild type, control Flag-mCerulean, BPLF1$^{\Delta 765\text{-}1327}$ generated in section 3.4.1, and the BPLF1$^{765\text{-}1327}$ domain isolate. After 72 hours, I collected the cells and performed immunofluorescence stains for Flag, DAPI, and SUMO2/3 shown in Figure 16 and quantified SUMO2/3 nuclear foci for each Flag positive cell.

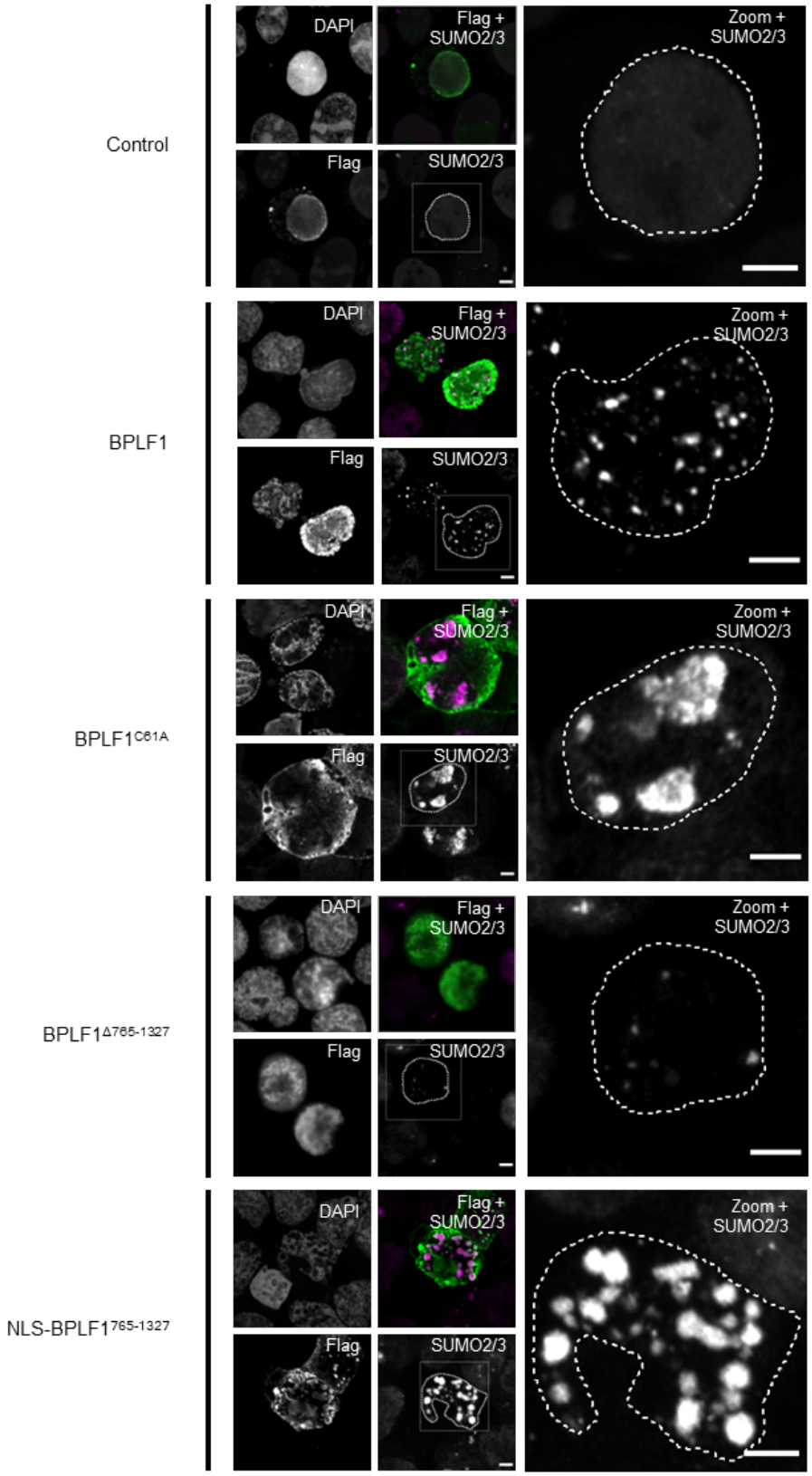

Figure 16: BPLF1 effectively attenuates SENP6 activity, resulting in uncontrolled poly-SUMOylation of SENP6 substrates. a-e HEK293 cells were transfected with expression plasmids for Flag-tagged mCerulean (Control), BPLF1, BPLF1^{C61A}, BPLF1$^{\Delta765-1327}$, and NLS-BPLF1$^{765-1327}$. After 48 hours of incubation, the cells were collected and fixed to glass slides. Subsequent immunostains for DAPI, Flag, and SUMO2/3 were performed and visualised via confocal microscope Zeiss LSM700. Nuclear regions were demarcated with dashed lines. Scale bars = 5 µm.

For 5 biological replicates, I quantified the SUMO2/3 foci of each Flag positive cell for 5 different conditions as shown in Figure 17. Control treated cells had a mean of 2.46 % Flag positive cells with increased SUMO2/3 foci numbers. BPLF1, BPLF1^{C61A}, and NLS-BPLF1$^{765\text{-}1327}$ expressing cells showed strong increase in SUMO2/3 foci when compared to the control treatment with BPLF1^{C61A} expression having the strongest effect with a mean of 75.95 % of cells with increased SUMO2/3 foci, and BPLF1 and NLS-BPLF1$^{765\text{-}1327}$ showing similarly strong effects of 74.45 % and 73.97 % respectively. This effect was partially reduced for the BPLF1 lacking the 765-1327 aa domain with 36.05 % of Flag-positive cells showing increased SUMO2/3 foci. This showed that not only the BPLF1 with the catalytically inert deubiquitinase domain (BPLF1^{C61A}) was able to replicate the effects of wild type BPLF1, but also the 765-1327 aa domain was primarily responsible for this effect implying that SENP6 activity is likely reduced by the BPLF1$^{765\text{-}1327}$ domain, resulting in the accumulation of poly-SUMO2/3 species within the host nuclei.

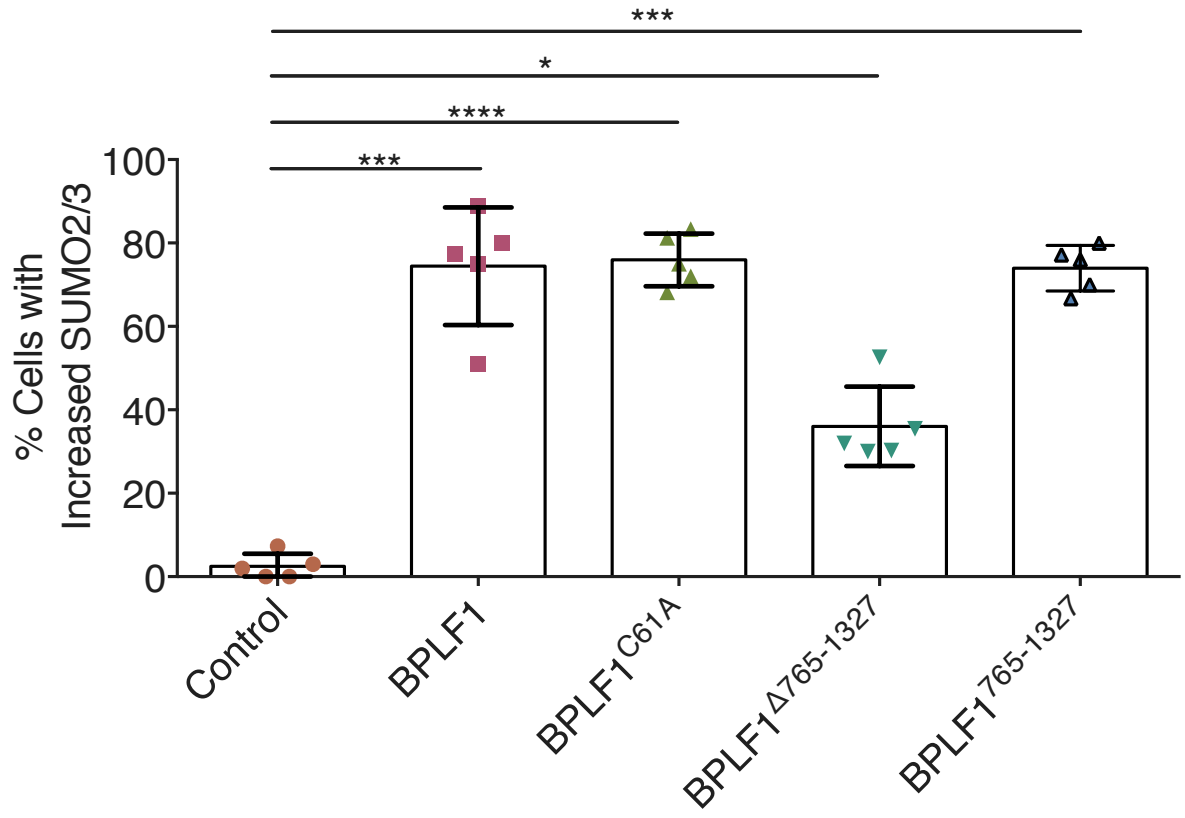

Figure 17: BPLF1 expression results in increased SUMO2/3 foci in cell nuclei. Error bars represent Standard Deviation. SUMO2/3 foci were quantified for each Flag-positive cell by counting foci numbers within nuclear regions. The mean number of SUMO2/3 foci of the control treatment for each replicate were used as separate threshold for their respective sets of replicate experiments (n = 100). Ordinary one-way ANOVA was performed with multiple comparisons. *P < 0.05, **P < 0.01, ***P < 0.001, ****P < 0.0001.

To further confirm this effect, I cloned a reporter expression plasmid with BPLF1 and mCerulean under separate promotors with the representative schematic shown in Figure 18. I subsequently transfected the reporter plasmid or the empty control plasmid into HEK293 cells. Expression of the mCerulean in the BPLF1 and control plasmid allowed for me to perform FACS assisted sorting of positively transfected cells. Additional staining using 7AAD allowed for me to discern between living and dead cells in the subsequent gating. I collected the sorted cells and blotted and probed the resultant lysates for SUMO2/3. The resultant blot (Figure 20) showed upregulation of SUMOylation of substrates of different molecular weights upon BPLF1 expression. When observing the immunofluorescence stains in Figure

16 and western blots for SUMO2/3 in Figure 20 I deduced that SENP6 activity was being inhibited through BPLF1 interaction, leading to uncontrolled poly-SUMOylation of various substrates within the host nucleus. I decided to investigate possible known SENP6 substrates that are associated with nuclear partitioning and chromatin maintenance.

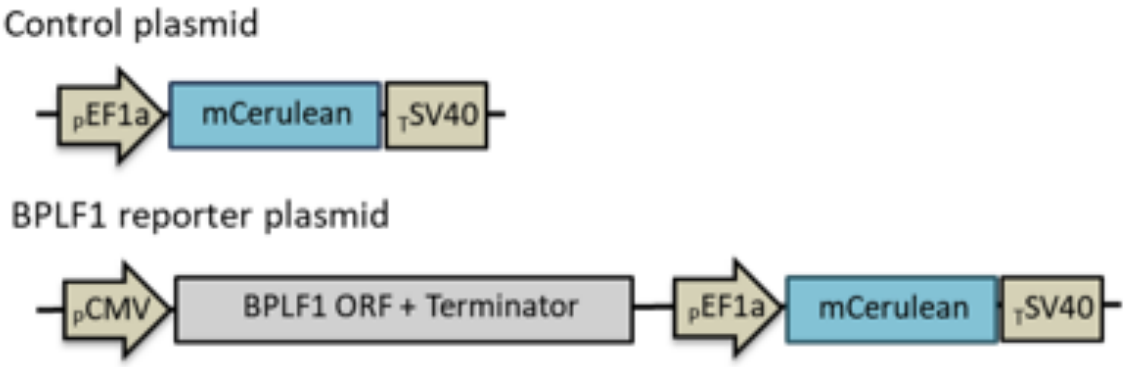

Figure 18: Schematics for reporter plasmid construction. Control plasmid was used as a template and BPLF1 ORF was amplified along with its promoter and terminator from the Flag-BPLF1 expression vector and inserted via restriction digestion and ligation.

Expression of the mCerulean in the BPLF1 and control plasmid allowed for me to perform FACS assisted sorting of positively transfected cells. Additional staining using 7AAD allowed for me to discern between living and dead cells in the subsequent gating. I collected the sorted cells and blotted and probed the resultant lysates for SUMO2/3. The resultant blot (Figure 20) showed upregulation of SUMOylation of substrates of different molecular weights upon BPLF1 expression. When observing the immunofluorescence stains in Figure 16 and western blots for SUMO2/3 in Figure 20, I deduced that SENP6 activity was being inhibited through BPLF1 interaction, leading to uncontrolled poly-SUMOylation of various substrates within the host nucleus. I decided to investigate downstream processes of SENP6 activity associated with nuclear partitioning and chromatin maintenance.

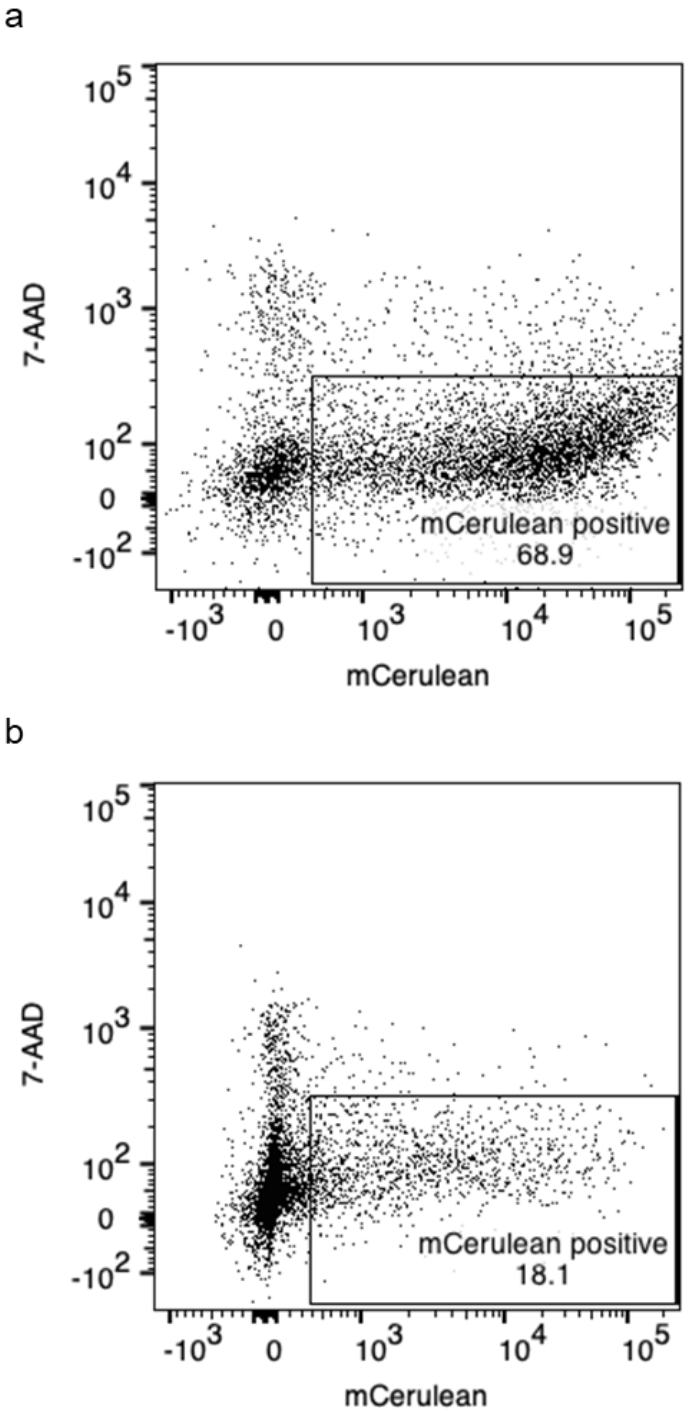

Figure 19: FACS sorting of HEK293 cells expressing mCerulean as a reporter for transfection and 7AAD as a stain for cell viability. FACS scatter plots showing gating for cells containing control plasmid and (c) BPLF1 reporter plasmid with percentage positive cells indicated.

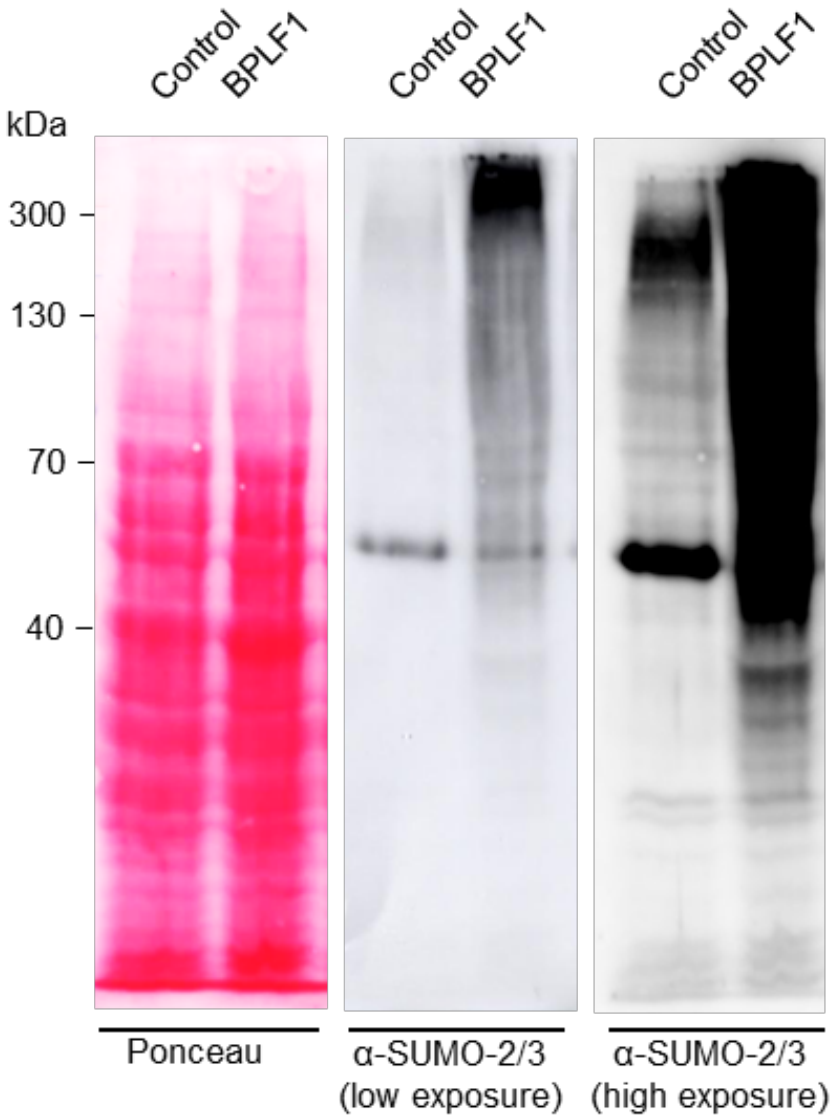

Figure 20: Western blot analysis for lysates of FACS sorted cells. Bradford assay of cell lysates was conducted and 50 µg of protein was loaded onto the SDS-PAGE gel. Ponceau was used as a loading control. Low and high exposure settings were 1 second and 10 seconds respectively.

3.4.3. CENP-A abundance is controlled by BPLF1

SENP6 has multiple known target substrates that are involved in the maintenance of nuclear integrity, such as Mis18BP1 [126, 129] and members of the Constitutive Centromeric Associated Network (CCAN) [127]. A notable example is the CENP-A protein of the inner kinetochore. Although it is not directly SUMOylated, it has been clearly shown to be highly influenced by SENP6 activity with any form of SENP6 disruption leading to the reduction of CENP-A protein at the centromeric regions of the host chromatin [127], and this has been observed to be accompanied by a deterioration of nuclear integrity [126, 129]. The mechanism by which this effect occurs has been shown to be partially because of uncontrolled poly-SUMOylation of Mis18BP1 leading to it being targeted for proteasomal degradation via RNF4 mediated ubiquitin ligation [126]. As CCAN members require deSUMOylation to remain at the centromeres they are displaced upon poly-SUMOylation and upon Mis18BP1 degradation, new CCAN member deposition at the centromeres is impaired, resulting in improper chromosome segregation during mitotic events [126, 129].

According to my experiments in Figure 21, transient BPLF1 expression resulted in increased rates of aneuploidy and polyploidy, which are determined through quantification of CENP-A foci. However, the individual CENP-A foci were observed have reduced signal intensities when compared with the control cells. Therefore, I repeated the expression experiments using the same U2OS cell line used in previous studies [126, 129]. U2OS cells have not been altered through viral transformation like HEK293 and HeLa cell lines, allowing for a more consistent baseline CENP-A MFI. I quantified fluorescence signals of 46 of the brightest CENP-A foci and calculated the mean fluorescence intensities (MFIs) for each cell nucleus (Figure 21). As seen in Figure 21b, the CENP-A foci MFIs were significantly reduced (55.21 %

of the control MFI) for Flag-BPLF1 expressing cells when compared with the control Flag-mCerulean expressing cells.

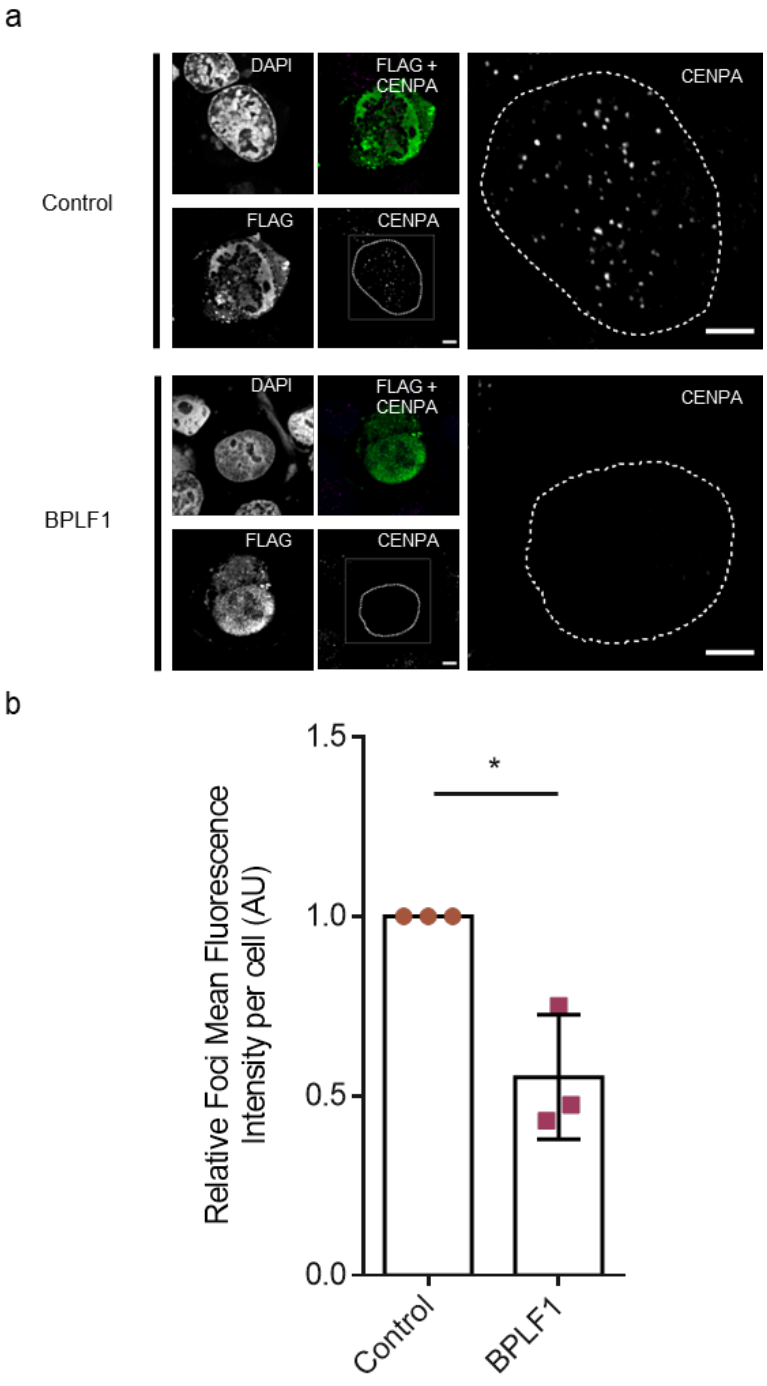

Figure 21: CENP-A foci signal is reduced upon BPLF1 expression. a U2OS cells were transfected with expression plasmids for Flag-mCerulean and Flag-BPLF1. After 72 hours the cells were collected and stained for Flag, DAPI, and CENP-A. Scale bars = 5 µm. d Scatter plots of the CENP-A MFI for interphase U2OS cells. The brightest 46 foci were measured for 15 Flag-positive cell nuclei. This was performed for 3 independent replicate experiments and the MFIs for each replicate were normalized to their respective control MFIs. Error bars represent Standard Deviation. Paired t-test was performed to compare treatment to control. *P < 0.05.

3.5. The role of BPLF1 in the context of the complete EBV virus

3.5.1. Construction of M81/ΔBPLF1 and M81/ΔBPLF1-Revertant BACs

The M81 variant of the EBV can spontaneously reactivate from latently infected LCL cells *in vitro* [140]. Our lab had constructed a bacterial artificial chromosome (BAC) containing the full EBV genomic sequence, which was stably transfected into HEK293 cells and selected for using a hygromycin B resistance gene. These stable cell lines, when co-transfected with BZLF1 expression plasmids can enter lytic replication and produce virus.

I constructed the BPLF1 knockout M81 BAC (M81/ΔBPLF1) within GS1783 bacterial cells. GS1783 cells transformed with M81 BAC DNA were cultured in LB-agar supplemented with kanamycin. Cassette exchange mutagenesis was performed to remove the BPLF1 gene sequence by transforming the GS bacteria containing the M81 BAC with an exchange plasmid possessing the ampicillin resistance gene (Figure 22). Homologous regions to the sequences flanking the BPLF1 gene on the BAC DNA, flanked the ampicillin gene. Bacterial recombinases within the GS cells dynamically rearrange, insert, or delete DNA sequences via homologous recombination. When cultured on LB-agar supplemented with kanamycin and ampicillin, BAC DNA containing both the kanamycin and ampicillin resistance genes can grow. BAC isolation via alkaline lysis method was performed on outgrowing colonies and verified through restriction endonuclease digestion and genomic sequencing.

Once stable HEK293 cells containing the M81/ΔBPLF1 were established, I isolated the BAC from the mammalian cells via plasmid rescue and electroporated the DNA into electrochemically competent DH10B cells. I isolated the BAC DNA from these cells via alkaline lysis and verified them via restriction digestion using restriction endonucleases and subjected the digests to agarose gel electrophoresis (Figure 23).

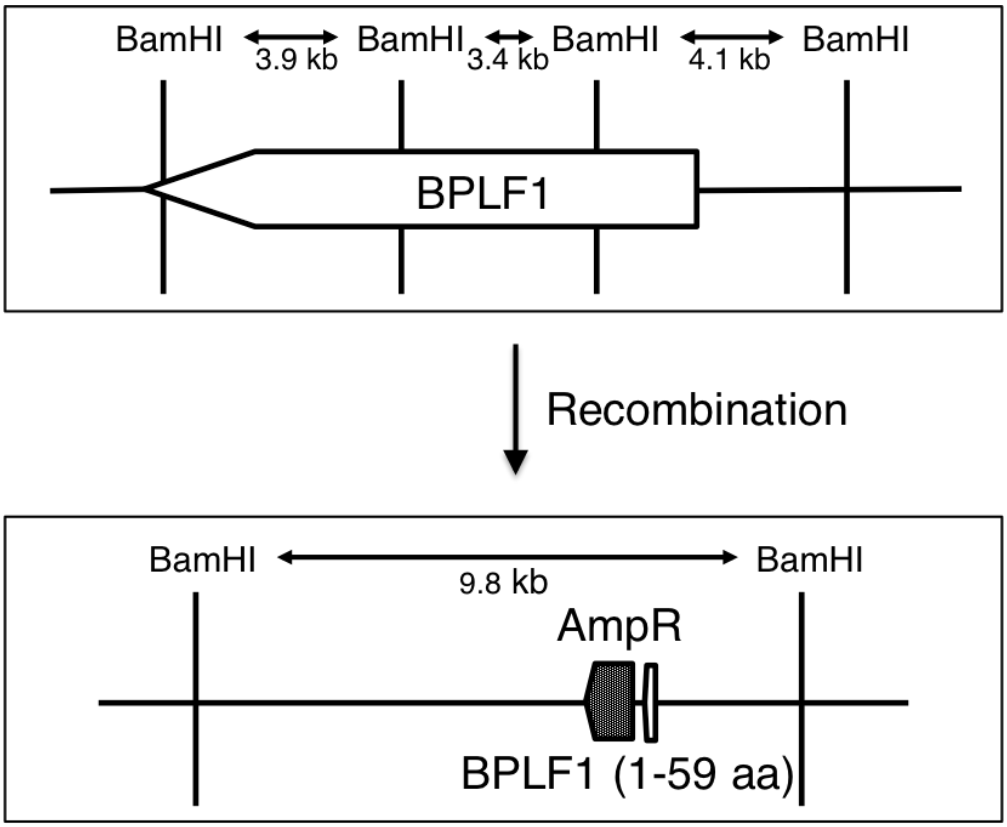

Figure 22: Cloning strategy for M81/ΔBPLF1 BAC. a Schematic showing the BPLF1 gene of the M81 BAC (top) and M81/ΔBPLF1 BAC (bottom), and the location of restriction sites targeted by BamHI restriction endonuclease before and after homologous recombination.

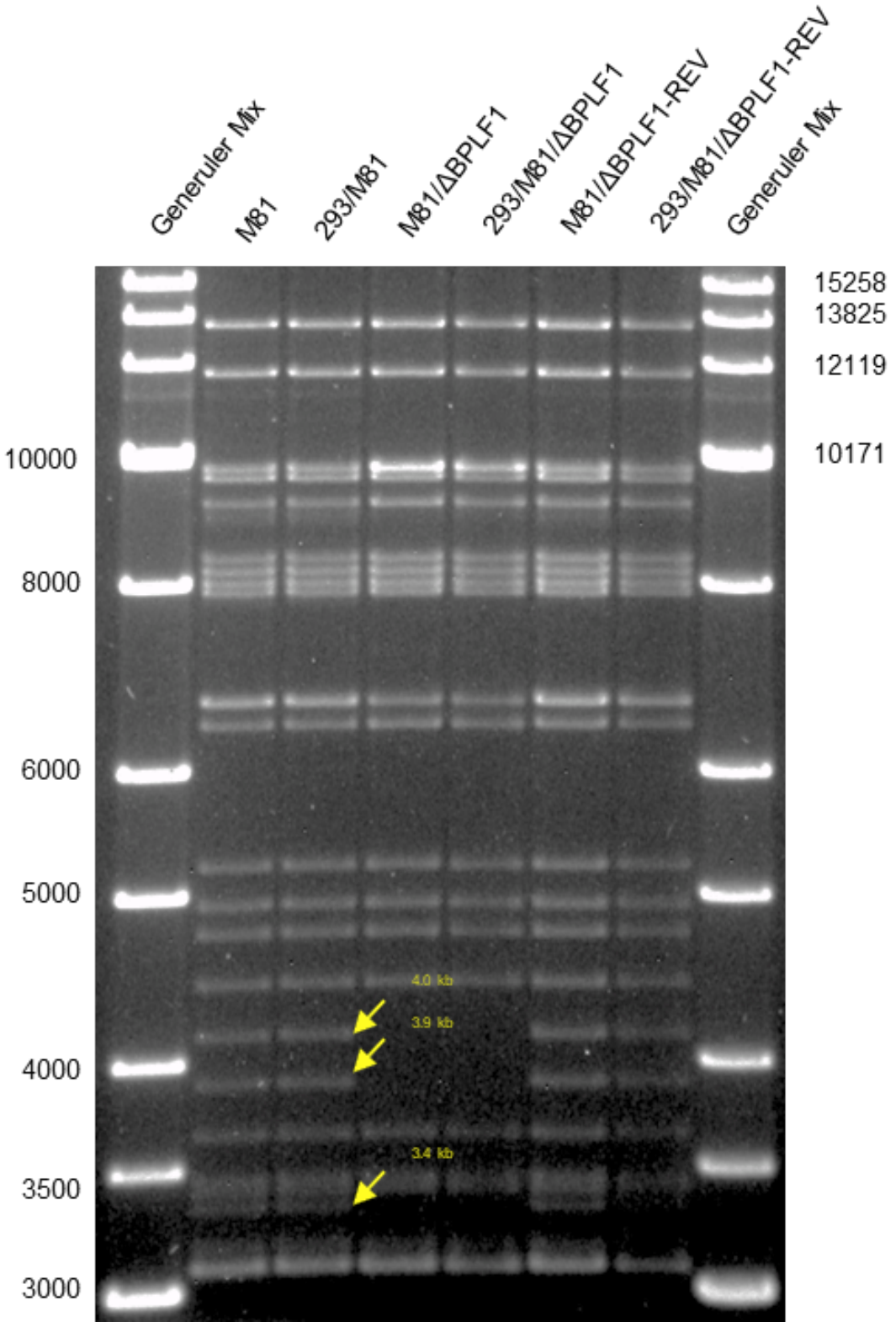

Figure 23: BamHI restriction digestion of wild-type (M81 WT), BPLF1 knock-out (M81/ΔBPLF1) and revertant (M81 Rev) genomes isolated from bacteria (*E. coli*) and mammalian producer cells (HEK293). Lane 1 - M81 BAC isolated from DH10B, 2 - Plasmid recovered from HEK293 cells, 3 - M81/ΔBPLF1 isolated from DH10B, 4 - M81/ΔBPLF1 recovered from HEK293 cells, 5 - M81/ΔBPLF1-REV isolated from DH10B, 6 - M81/ΔBPLF1-REV recovered from HEK293 cells DNA fragments that differ between knock-out and control genomes are emphasized with arrows.

3.5.2. Virus production and quantification

I co-transfected established producer cells (HEK293) with plasmids expressing BZLF1 (p509), gp110 (pRa), and BRLF1 (p2130). At 72 hours post-transfection, I collected and filtered the viral supernatants. I also collected the producer cells, and then fixed, and stained them for gp350. I quantified the supernatant via real-time qPCR (RT-qPCR) to quantify viral titers. In addition, I performed virus binding assays for virus like particles (VLPs) to determine the effective titer equivalent to M81 through the measurement of gp350 positive B cells via flow cytometry.

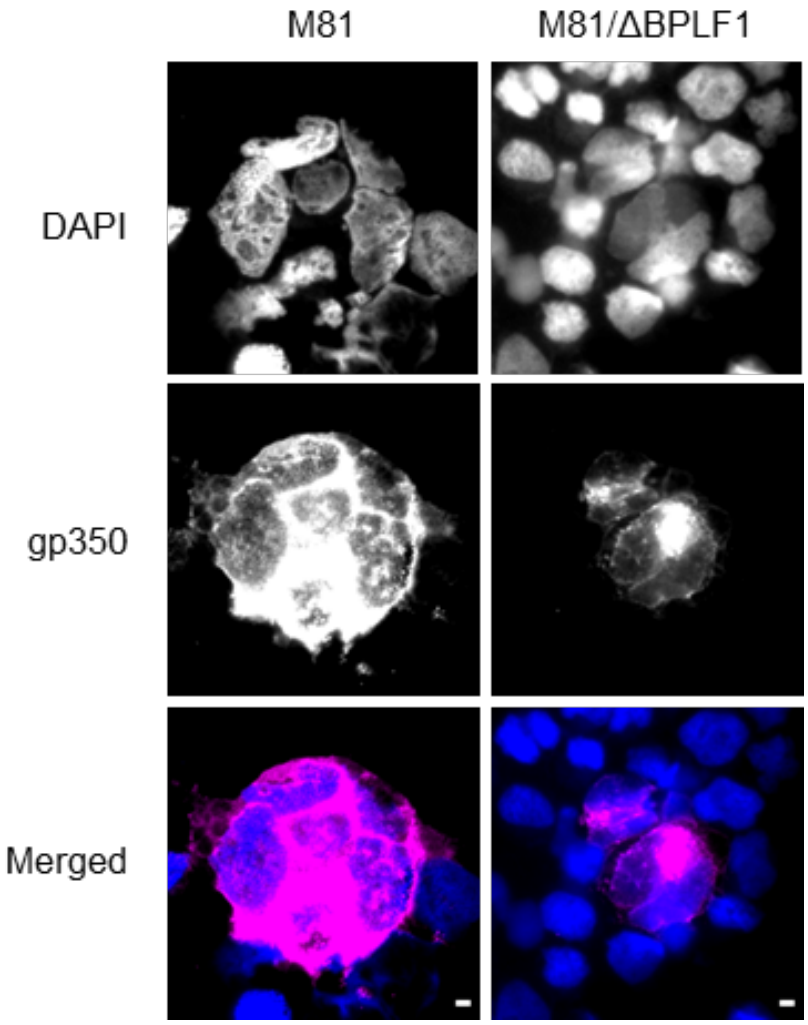

Figure 24: Viral producer cells stained for gp350 72 hours after induction. Producers induced to produce virus via transfection of BZLF1, BALF4, and BRRF1 were collected 72 hpi. Cells were fixed and stained for gp350 and DAPI. Scale bars = 5 µm.

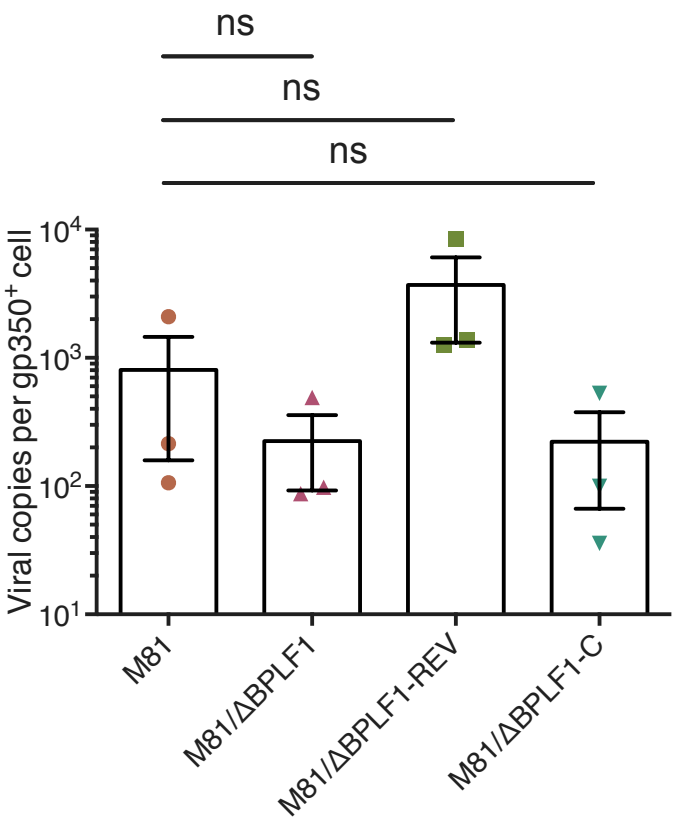

Figure 25: Viral yields for induced producer cell lines. Viral titres measured by RT-qPCR were divided by the percentage of gp350 positive cells and the number of cells seeded for induction. Error bars represent standard deviation.

3.5.3. BPLF1 and B cell infection

3.5.3.1. Infectivity studies

I isolated primary $CD20^+$ B cells from buffy coats obtained from 6 separate donors and subjected them to infectivity assays to test for the ability for M81/ΔBPLF1 to infect. I probed for EBNA2 expression as a marker, shown in Figure 26, for EBV infection as it is one of the earliest known proteins expressed after latent B-cell infection and is an important gene transactivator [141].

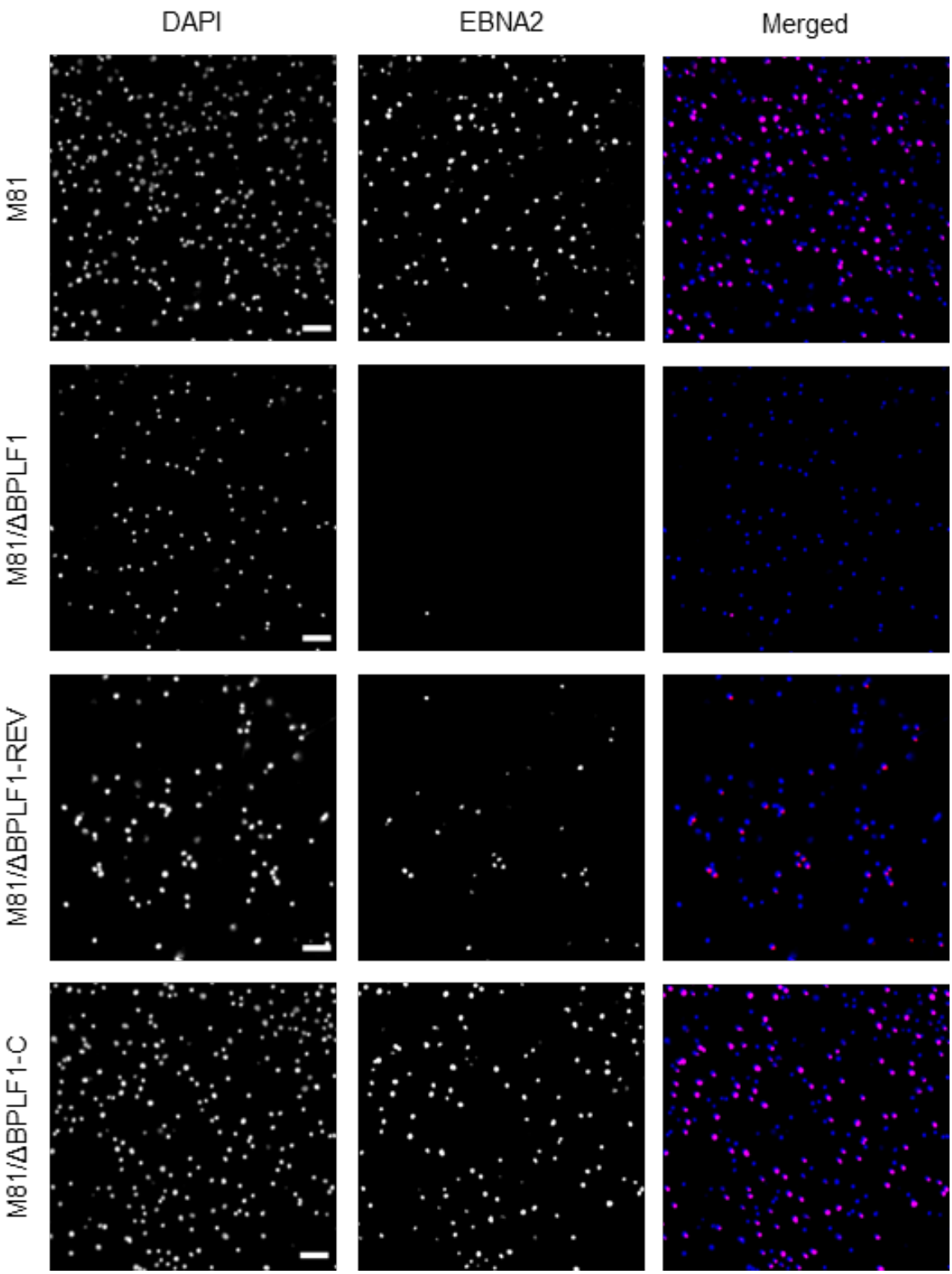

Figure 26: Primary B cells treated with viral supernatant at 30 MOI. Cells were collected at 3 dpi and tested for EBNA2 expression. Representative microscopy images of B cells stained for EBNA2 and DAPI. Scale bars = 50 µm.

As shown in Figure 27, M81 virus treatment at 30 MOI results in a mean B-cell infection rate of 42.75 %, while M81/ΔBPLF1 almost completely loses its ability to infect B cells with a 1.3% mean rate of infection. However, I was able to recapitulate infection upon complementation with BPLF1 to yield a mean rate of 41.72 % B cell infection while the revertant virus provided a mean rate of 39.02 % B cell infection.

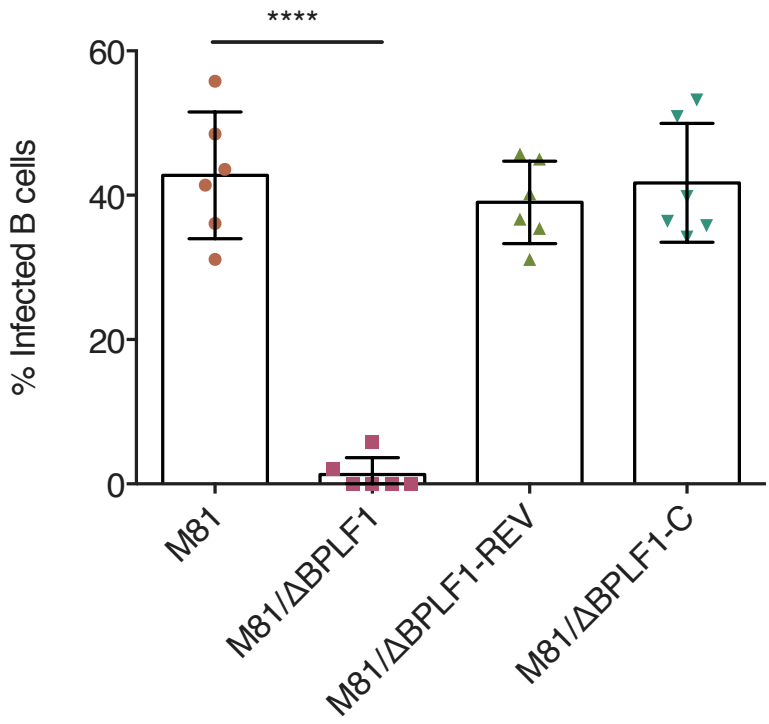

Figure 27: Infectivity assay of B cells exposed to different viruses at 30 MOI. Infected cells were determined by immunofluorescence staining for EBNA2. Error bars represent standard deviation. **** $p < 0.0001$.

3.5.3.2. A BPLF1-positive virus induces Nuclear abnormalities

BPLF1 was investigated for its ability to induce nuclear abnormalities when incorporated into virus particles infecting B cells. I isolated primary $CD20^+$ B cells from buffy coats of 5 separate donors and exposed them to different EBV virus particle treatments at 30 MOI and incubated them. Treated cell samples were collected at 3 dpi and stained for EBNA2 and DAPI and collected at 30 dpi and stained for gp350 and DAPI (Figure 28).

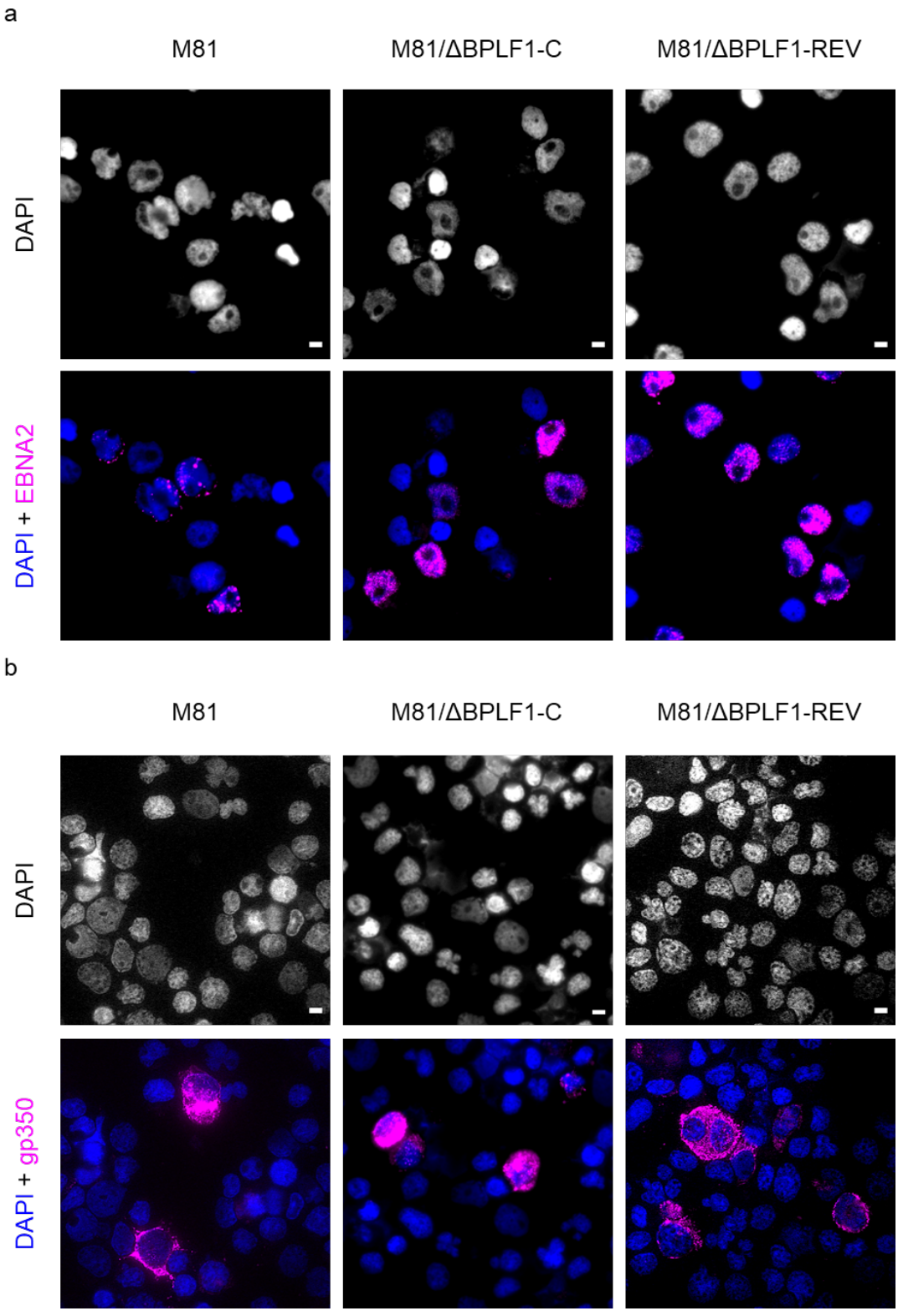

Figure 28: B cells infected with M81 experience increased rates of nuclear abnormalities over time. a Primary B cells were treated with M81, M81/ΔBPLF1-C, and M81/ΔBPLF1-REV. At 3 dpi cells were collected and stained for EBNA2 and DAPI, the remaining cell population was collected at 30 dpi and stained for gp350. b EBNA2 positive cell nuclei were measured for 3 dpi and gp350 positive cell nuclei for 30 dpi. Scale bars = 5 µm.

I used EBNA2 expression as a marker for infected cells at 3 dpi and gp350 expression as a marker for lytically reactivated EBV^+ LCLs at 30 dpi. This was performed to measure only the B cells expressing lytic proteins. The DAPI signal was used to demarcate the nuclei for measurements using ImageJ. Nuclear for 5 independent donors were measured at 3 dpi and at 30 dpi for each treatment shown in Figure 29. At 3 dpi, each treatment showed little difference in nuclear abnormalities with M81, M81/ΔBPLF1-C, and M81/ΔBPLF1-REV exhibiting averages of 6.72 %, 6.42 %, and 6.43 % rates of B cells with enlarged nuclei. However, as time progressed to 30 dpi these abnormalities were significantly higher in the M81 (15.19 %) and M81/ΔBPLF1-REV (11.38 %) when compared to the M81/ΔBPLF1-C (2.28 %) treated cells. This is likely due to the M81/ΔBPLF1-C possessing the protein in the virus during initial infection but lacking the BPLF1 ORF in the viral genome. This would in-turn, resulted in the loss of BPLF1 expression during lytic reactivation, thus likely reducing the accompanied toxic effects of BPLF1. These toxic effects likely resulted in the accumulation of nuclear abnormalities in the M81 and M81/ΔBPLF1-REV treated B cells.

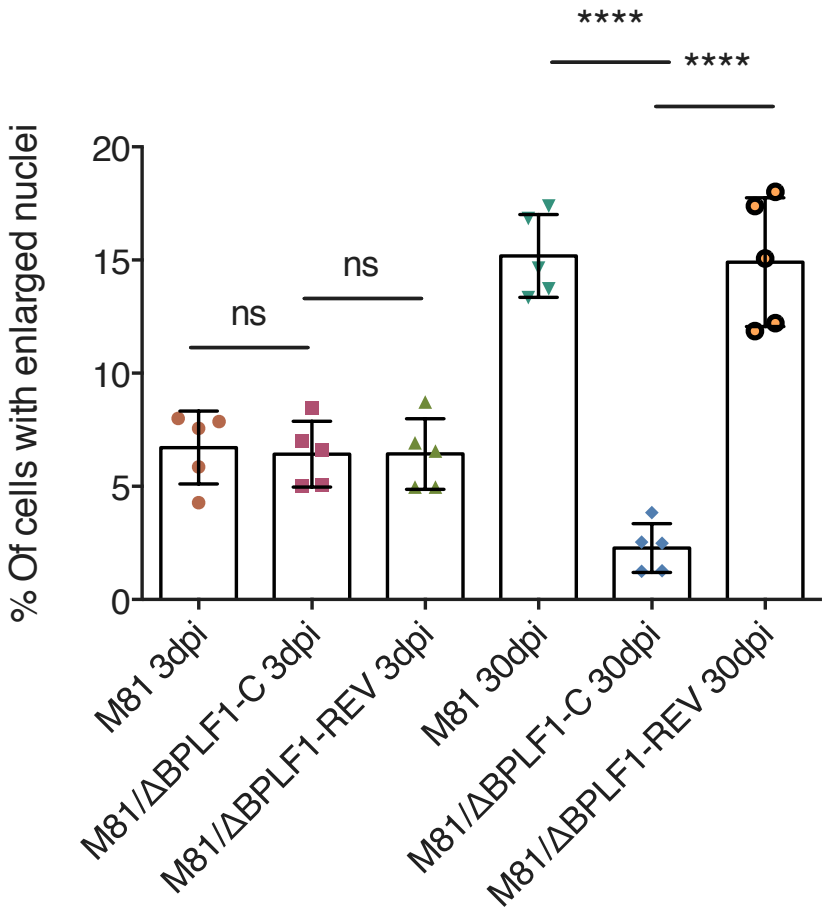

Figure 29: EBV BPLF1 containing virus particles induce nuclear abnormalities in B cells post infection. DAPI signal was used to demarcate the nuclear areas. Cell nuclei were measured and enlarged nuclei were quantified according to the crossing of control threshold determined by measuring respective 3 dpi nuclei. Error bars represent standard deviation. Ordinary one-way ANOVAs were performed. $^{****}p < 0.0001$.

To rule out latency programming effects, I treated LCLs established from BZLF1 and BRLF1 deficient virus with 50 MOI of M81, M81/ΔBPLF1, M81/ΔBPLF1-REV, and M81/ΔBPLF1-C virus supernatants. The M81/ΔZR generated LCLs lack the ability to enter lytic cycle and are in persistent latency infection. LCLs from 5 different donors that were transformed with M81/ΔZR served as 5 independent biological replicates in this study. After 5 days of incubation, the treated cells were collected and stained for DAPI showed in Figure 30.

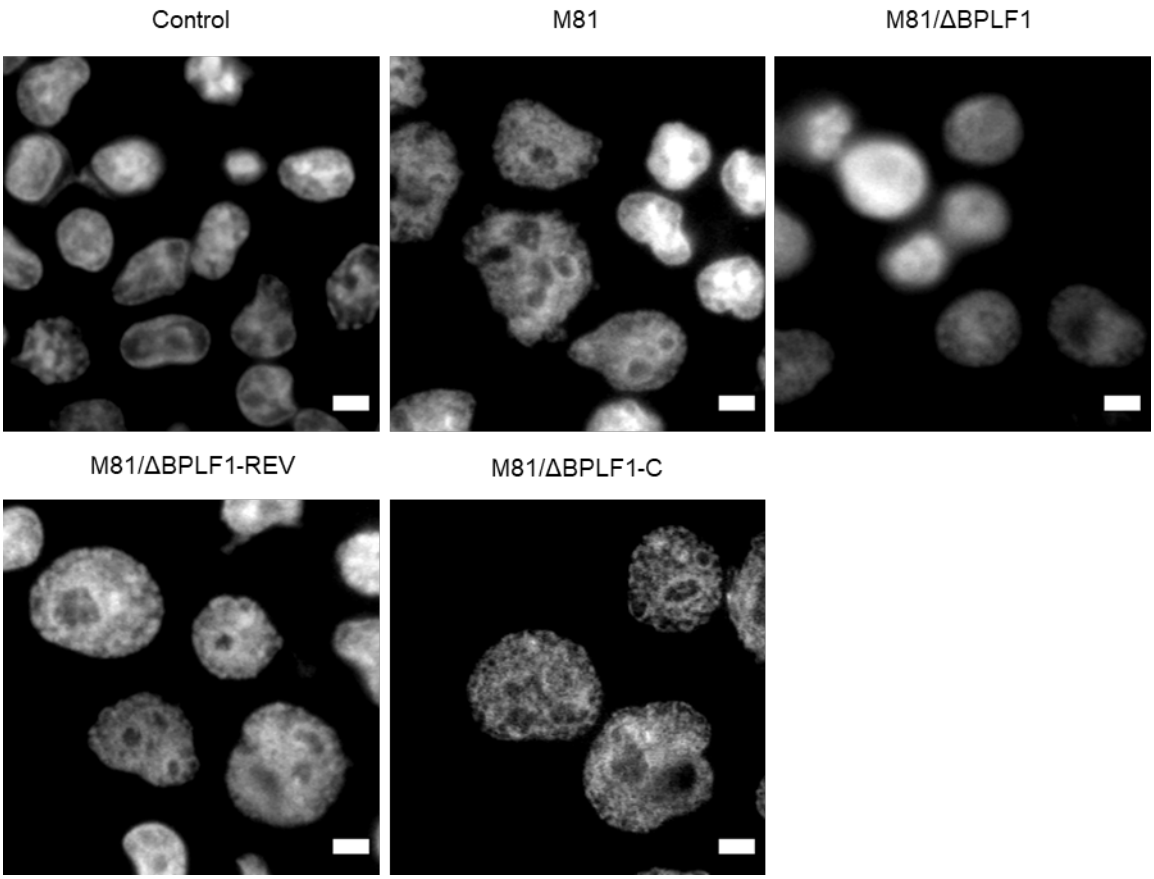

Figure 30: B cell exposure to virus particles containing BPLF1 leads to accumulation of nuclear abnormalities. LCLs, generated from ΔZR virus, were superinfected with M81, M81/ΔBPLF1, M81/ΔBPLF1-REV, and M81/ΔBPLF1-C at 50 MOI. After 5 days cells were collected and stained for DAPI. Scale bars = 5 μm.

Using DAPI as a nuclear marker, I used ImageJ to measure the nuclei of all the ΔZR LCLs for each treatment. As seen in Figure 31, there was a strongly significant increase in nuclear size in cells treated with M81, M81/ΔBPLF1-REV, and M81/ΔBPLF1-C compared to the control CD40L + IL4 treatment where M81/ΔBPLF1 treated cells showed no significant effect on nuclear size when compared to the control treatment. These data show BPLF1 exerting disruptive effects on the host nuclei upon exposure.

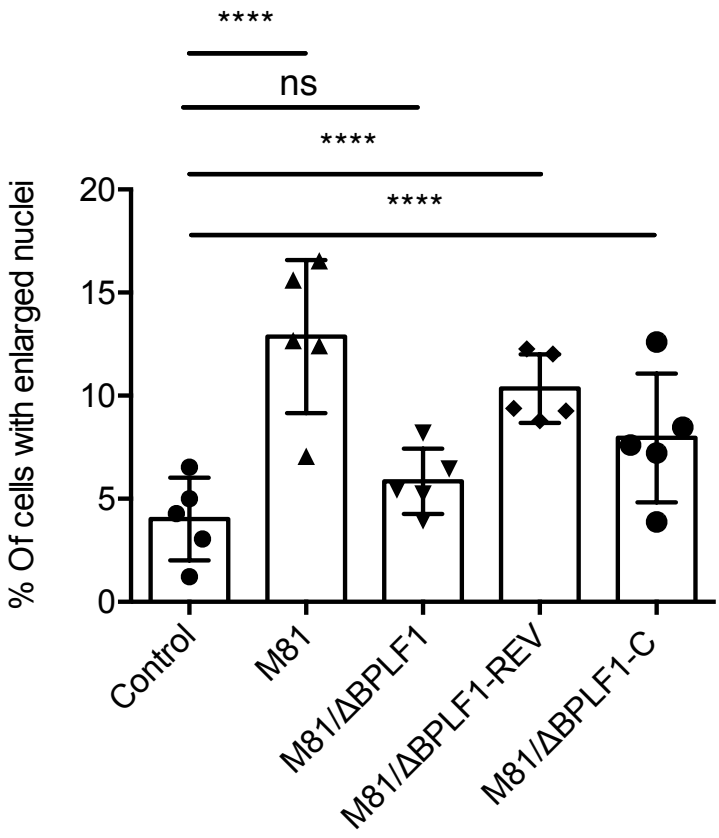

Figure 31: LCL superinfection using virus devoid of BPLF1 shows reduction in rates of nuclear abnormalities compared to wild type virus. Nuclear sizes were measured for over 200 cells for six biologically independent experiments (n = 6). Error bars represent standard deviation Logistical regressions were performed to compare the number of cells that surpass the nuclear size threshold. $^{****}p < 0.0001$.

3.5.3.3. Effects of EBV infection on SUMO2/3

To determine the effect that BPLF1 containing virus particles have on SENP6 activity. Primary B cells were infected with M81, M81/ΔBPLF1, M81/ΔBPLF1-REV, and M81/ΔBPLF1-C virus supernatants at 30 MOI with growth media supplemented with IL4 and CD40L supplemented growth media control. As seen in Figure 32, significant increases in SUMO2/3 foci were observed for M81, M81/ΔBPLF1-REV, and M81/ΔBPLF1-C in relation to the control as early as 1 hpi. This effect persisted for up to 48 hpi, signifying that BPLF1's effects on SENP6 occur prior to latency programming. This phenotype was not observed in M81/ΔBPLF1 treated B cells, implicating BPLF1 as a significant effector on SENP6 activity.

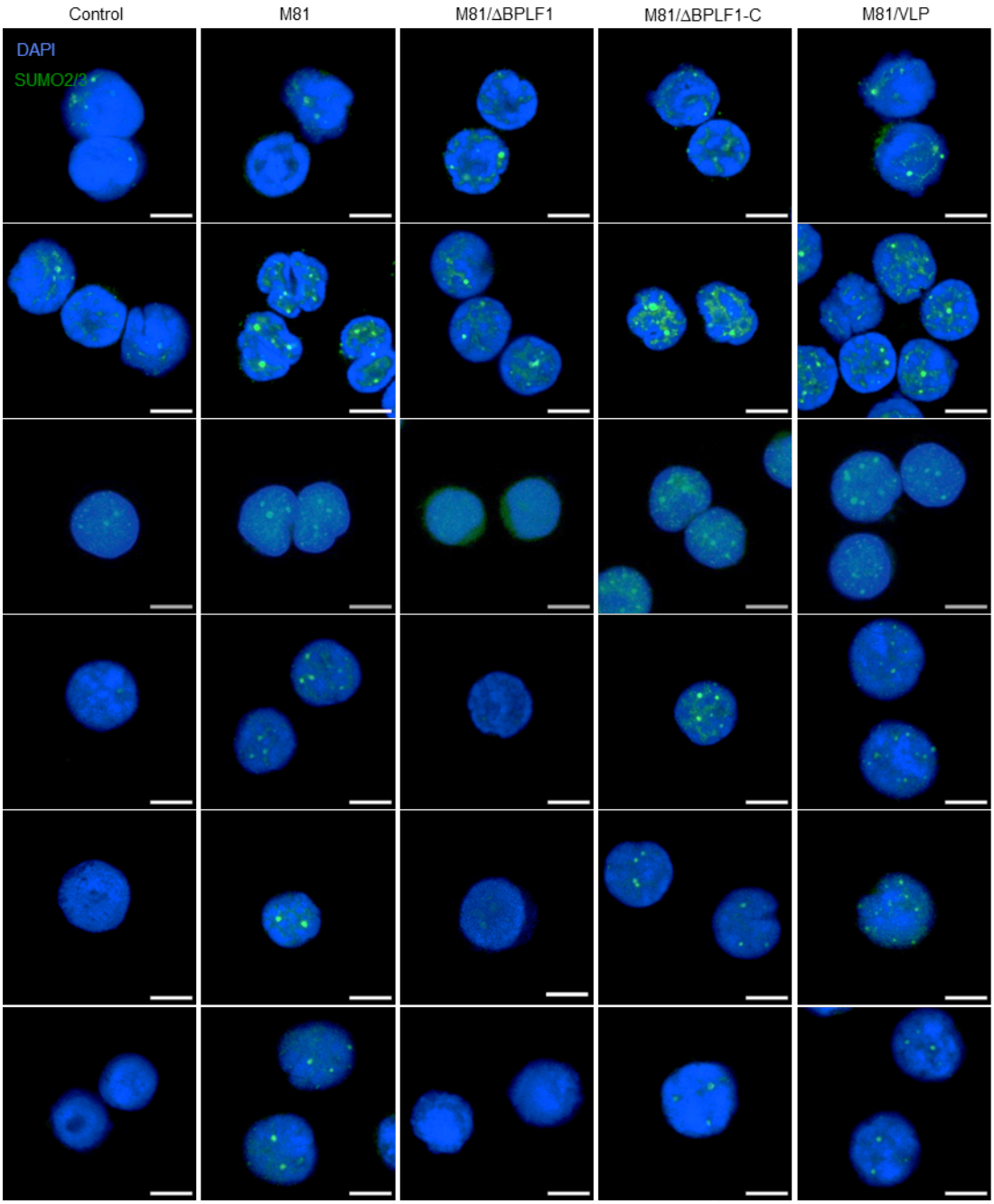

Figure 32: B cell exposure to virus particles containing BPLF1 leads to accumulation of nuclear SUMO2/3 foci. Representative images are from the 10 min, 1 hour, 6 hour, 12 hour, 24 hour, and 48 hour time points. For each time point cells were collected and stained for DAPI and SUMO2/3. Scale bars = 5 µm.

For quantitative analyses, the SUMO2/3 foci for over 50 cells were counted for each treatment and time point in this study and shown in Figure 33. A significant effect of SUMO2/3 foci increase was first observed at 1 hpi and persisted until 48 hpi. Using the same brightness threshold settings in ImageJ to count SUMO2/3 foci. At 10 min, the average foci counts were 1.74, 1.82, 2.67, 1.96, and 2.34 for control CD40L + IL4, M81, M81/ΔBPLF1, M81/ΔBPLF1-C, and M81/VLP treatments respectively. At 1 hpi, the average foci counts were 1.48, 2.97, 2.35, 2.92, and 2.6 for control CD40L + IL4, M81, M81/ΔBPLF1, M81/ΔBPLF1-C, and M81/VLP treatments respectively. At 6 hpi, the average foci counts were 2.22, 3.57, 1.67, 3.46, and 3.59 for control CD40L + IL4, M81, M81/ΔBPLF1, M81/ΔBPLF1-C, and M81/VLP treatments respectively. At 12 hpi, the average foci counts were 1.66, 3.46, 1, 3.3, and 3.8 for control CD40L + IL4, M81, M81/ΔBPLF1, M81/ΔBPLF1-C, and M81/VLP treatments respectively. At 24 hpi, the average foci counts were 1.04, 2.33, 1.04, 3.26, and 2.6 for control CD40L + IL4, M81, M81/ΔBPLF1, M81/ΔBPLF1-C, and M81/VLP treatments respectively. At 48 hpi, the average foci counts were 0.45, 2.1, 0.61, 2.26, and 1,57 for control CD40L + IL4, M81, M81/ΔBPLF1, M81/ΔBPLF1-C, and M81/VLP treatments respectively.

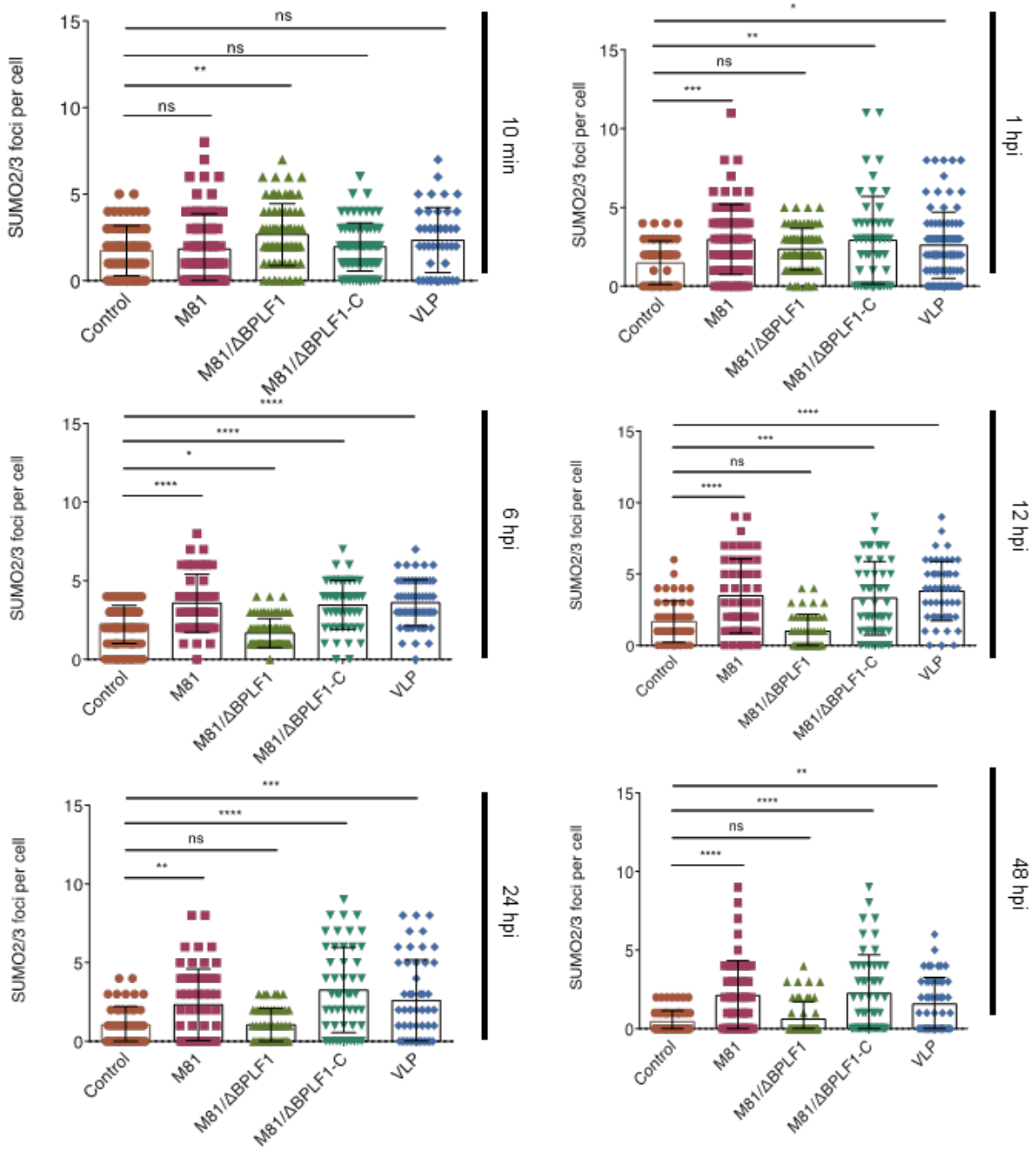

Figure 33: B cells infected with virus particles at 50 MOI show increased SUMO2/3 foci. SUMO2/3 foci numbers for over 50 B cells were counted for each viral treatment at 6 different time points. Error bars represent standard deviation. Results were grouped and compared via Two-way ANOVA. *P < 0.05, **P < 0.01, ***P < 0.001, ****P < 0.0001.

3.5.3.4. BPLF1 disorganizes CENP-A foci

Since SENP6 is known to play a part in maintaining the CCAN members at the centromeres, the increase rates of nuclear atypia could be attributed to EBV's effect on SENP6. It is known that SENP6 interference has been recently linked to the development of EBV related cancers [128] and it is suspected that centromere disturbance plays a role in the development of these abnormalities. This prompts the investigation into temporal changes in CENP-A fluorescence signal after EBV infection. B cells exposed to virus were collected at 0, 1, 2, and 3 dpi and were stained for CENP-A. Identical settings were used for CENP-A imaging to allow for comparisons of CENP-A foci between treatments. As seen in Figure 34, CENP-A foci signal is significantly reduced from 2 dpi for cells exposed to BPLF1 containing virus particles. This effect occurs after the increased SUMO2/3 levels, which is likely due to the CENP-A turnover time in B cells.

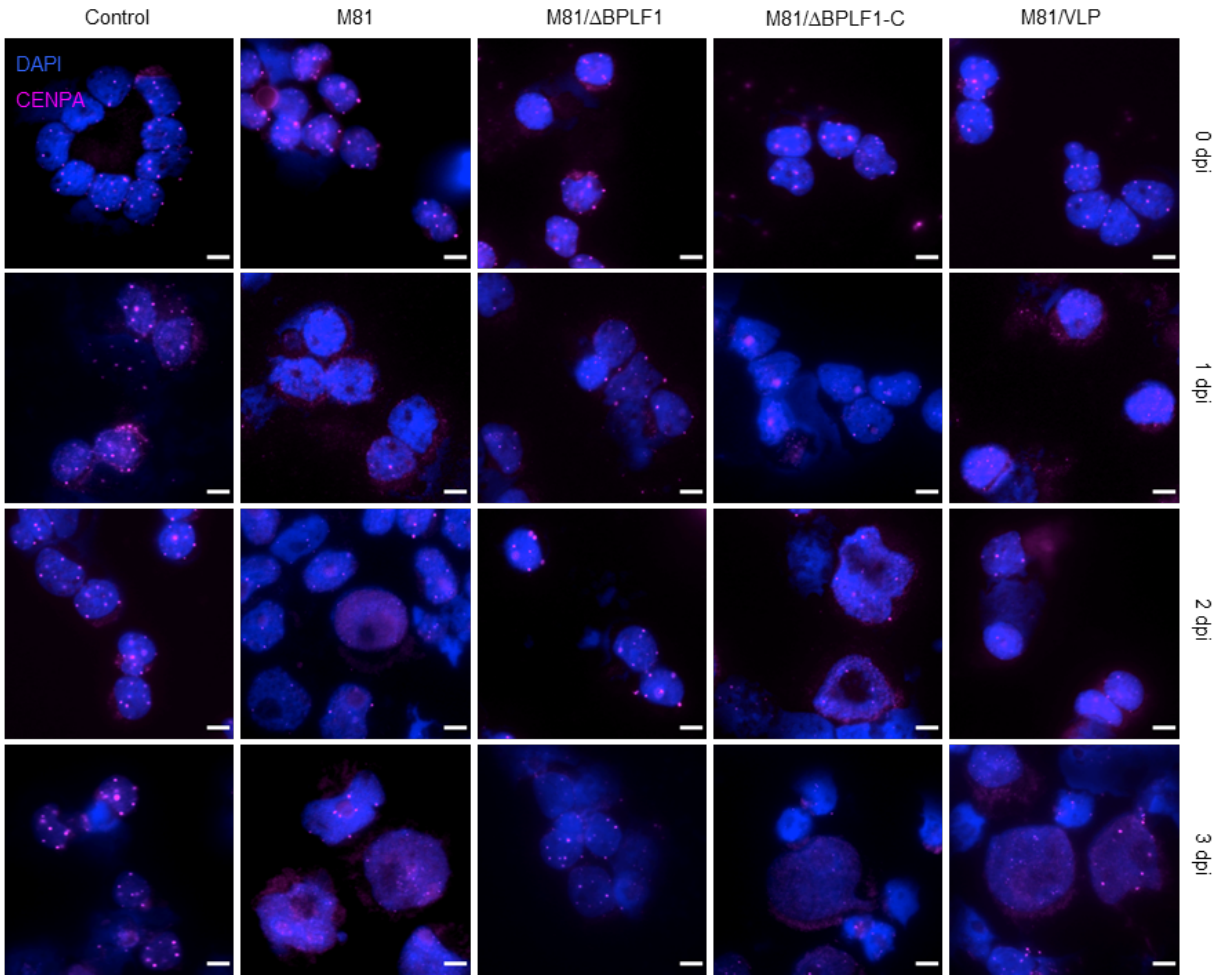

Figure 34: B cell exposed to virus particles containing BPLF1 have reduced CENP-A at the centromeres. Primary B cells were exposed to different virus treatments at 50 MOI or control (CD40L + IL4). Representative images are from time points 0 dpi, 1 dpi, 2 dpi, and 3 dpi. For each time point cells were collected and stained for DAPI and CENP-A. Scale bar = 5 µm.

The CENP-A MFI signal was measured for the 46 brightest foci of each B cell nucleus. These images were taken using the same settings to maintain fidelity in CENP-A brightness between samples. For each time point and treatment in Figure 35, 15 cells were measured. At 2 dpi, a significant difference in CENP-A MFI was apparent for M81, M81/ΔBPLF1-C, and M81/VLP treatments when compared to the control CD40L + IL4 treatment. This effect was greatest at 3 dpi where the MFI for B cells treated M81, M81/ΔBPLF1-C, and M81/VLP gave MFI values of 16594, 11213, and 13383 arbitrary units (AU) respectively while control CD40L + IL4 and BPLF1/ΔBPLF1 treated cells gave MFI values of 27359 and 24606 AU respectively. This shows that, in the context of the EBV infection of B cells, BPLF1 is a key player in the suppression of SENP6 activity, which is reflected in the rapid increase of SUMO2/3 levels (Figure 33) and consequently, reduced integrity of the inner kinetochore (Figure 35) resulting in the accumulation of genomic material (Figure 31 and Figure 29) over time.

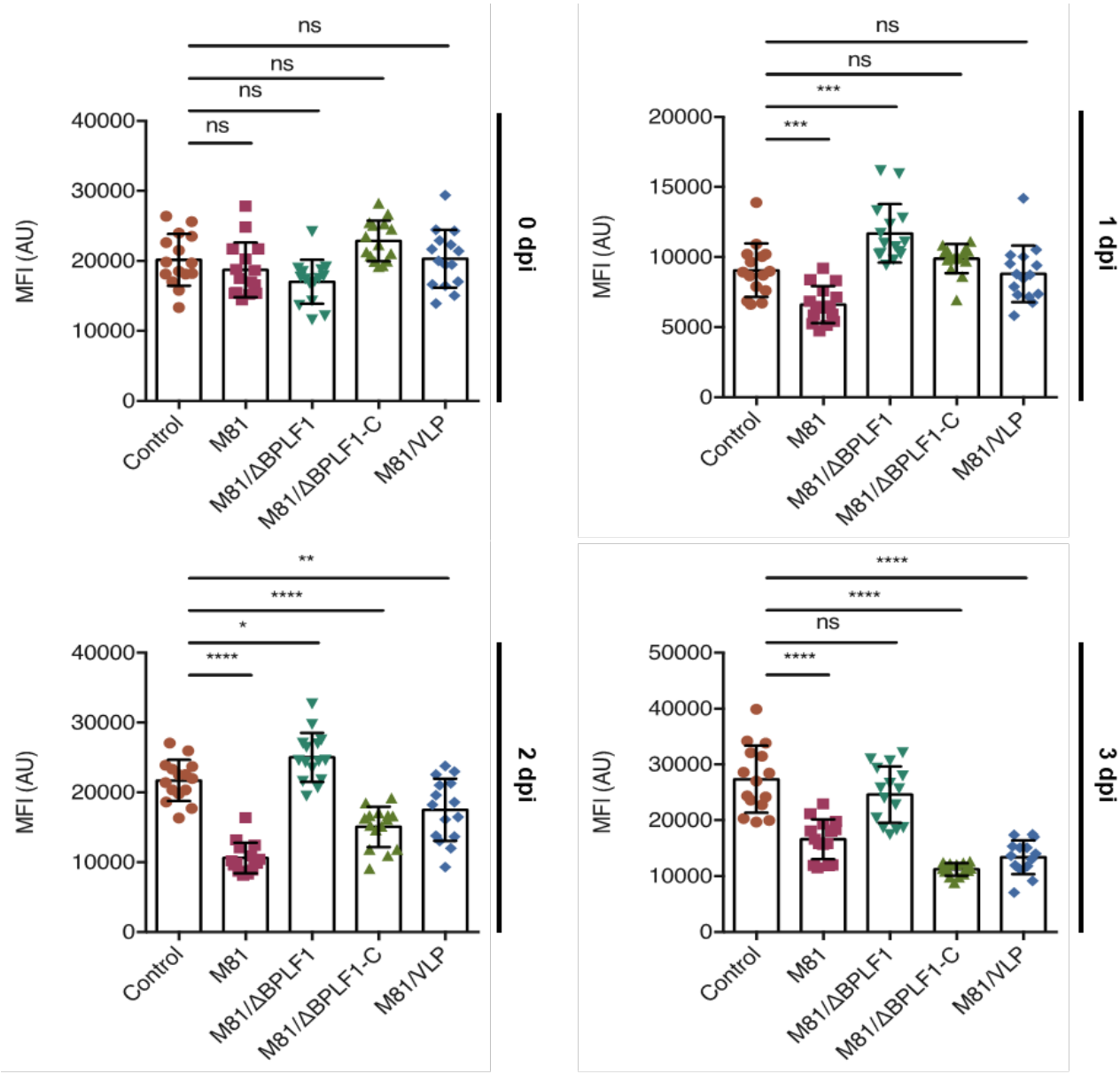

Figure 35: B cells exposed to EBV particles containing BPLF1 have reduced CENP-A signals at the centromeric regions over time. Error bars represent standard deviation. Results were grouped and compared via Two-way ANOVA. *P < 0.05, **P < 0.01, ***P < 0.001, ****P < 0.0001.

4. Discussion

Almost all biological processes within the cell are regulated by post-translational modifications (PTMs). These covalent modifications are reversable and serve to diversify proteins and maintain cellular homeostasis. The diverse array of biological processes that rely on PTMs of their constituents, underscores the degree to which PTM dysregulation is implicated in disease and cancer. The ubiquitin-like SUMO family of proteins have been discovered to be maintainers of genomic stability via cell cycle control and mediation of DNA damage response (DDR). Examples of proteins that serve as substrates for SUMO modification are the tumour suppressor p53 [142] and the oncoprotein MYC [143]. These, along with many other targets are implicated in the development of neoplastic disease [144-147], which include B cell lymphomas [148]. This form of modification is much akin to ubiquitin and NEDD8 modifications that have been previously described to be deconjugated by BPLF1. In this study, I used an unbiased approach to show the EBV large tegument protein BPLF1 as a newly described modulator of host cellular SUMOylation processes, by utilizing co-immunoprecipitation coupled with mass spectrometric analysis. Consequently, I found BPLF1 to be a disruptor of genomic stability in a similar manner as found in previous studies involving SENP6 depletion [126, 129].

Literature has shown EBV latency programming to be strongly implicated in oncogenesis. However, there is a growing body of research suggesting that productive infection, the lytic phase responsible for generating virions, plays an important role in the development of EBV-associated malignancies [146]. This is supported by the presence of high viral titres increasing the risk of NPC, GC and BL development [149-152], and that variants of EBV with more lytic activity being twice as likely to be found in EBV-associated malignancies when compared to non-malignant EBV-infected cells [153]. In a previous study from our lab, virion-

associated proteins in the form of particles devoid of viral DNA, were demonstrated to induce genetic abnormalities in B cells shortly after exposure [118]. The major tegument protein BNRF1 was identified to be a prime inducer of this phenotype through centriole overduplication. Recent studies have also linked BNRF1 to the degradation of the SMC5/6 cohesin complexes which are required for faithful chromosome segregation [119]. This helped to generate novel insights into BNRF1-expressing cells via live-cell imaging and positively identified irregular mitotic events. In this study, I show a suite of abnormalities induced by BPLF1, such as increased rates of abnormally enlarged nuclei, multinucleation, aneuploidy, polyploidy, and centriole overduplication. Many of these phenotypes were confirmed in B cells, where infection with M81 devoid of BPLF1 showed significantly reduced rates of genomic instability when compared to the wild-type virus infected B cells. These findings further highlight the role that BPLF1 plays in the genomic instability that is induced by EBV infection, implicating lytic proteins in cancer development.

The large tegument deNEDDylase BPLF1 and its homologues are the largest proteins known to be encoded by members of the *Herpesviridae*. These large proteins are difficult to manipulate and clone due to the enormous size of their coding sequences. Literature on BPLF1 largely involves the use of the N-terminal domain possessing deconjugase activity for ubiquitin and NEDD8 [43, 59]. These studies have implicated BPLF1 in various cellular processes ranging from DNA repair [56, 154], immune evasion [47, 51], and autophagy inhibition [71, 155]. In my study, the complete form of BPLF1 was made use of for the first time. I utilized an unbiased approach using proteomics to uncover over 100 cellular interactors of full-length BPLF1 with many of these interactors being completely unknown to literature as they only used the BPLF1 N-terminal domain as bait [51, 71]. Of these members, SENP6 was identified as a novel bona fide BPLF1 interactor which has been found to play a

pivotal role in the maintenance of the cellular SUMO landscape [126, 129]. SENP6 has been shown to deconjugate polymeric SUMO2/3 from many cellular targets involved in various aspects of cell biology, including protein networks involved in genomic stability and DNA damage response, showing SENP6 dysregulation may have broad impacts in EBV-associated diseases [126, 129, 156]. This is particularly important in the development of malignancies as the accumulation of genomic instabilities has been found to provide selective advantages through shorter cell cycles, or the ability of malignant cells to bypass intracellular or immunological controls [157]. Such genomic instabilities can arise because of base pair mutations, microsatellite instabilities, or changes in chromosome number or structures which is referred to as chromosomal instability (CIN) [158, 159]. CIN consists of incorrect chromosomal numbers or abnormal structures which has long been recognized to be a hallmark of cancer [160]. An estimated 60-80 % of human tumours have been found to harbour some form of CIN [161, 162], with increased rates in metastatic tumours and cancer relapses [163-165]. However, there is a debate on whether CIN is a cause or a result of cancer progression. Micronuclei formation as a result from CIN has been found to stimulate cGAS-STING, leading to chronic NF-κB activation. This has been shown to promote cellular migration and metastasis via the senescence-associated secretory phenotype [163]. Changes in cell karyotypes can confer fitness advantages to tumour cells. For instance, a study of pre-malignant peripheral blood samples from 151,202 UK bloodbank patients, found mosaic chromosomal alterations associated with CIN, to help drive early tumour clonal expansions [166]. Polyploid cancer cells have been suggested to gain survival benefits as the extra chromosome set helps to serve as a buffer against DNA damage and loss-of-function mutations [167], predisposing many cancers to metastasis, therapy resistance, and consequently, poorer prognoses [161, 168, 169]. Aneuploidy has been regarded as a crude

way to alter gene expression levels in pre-malignant cells. Over the course of time, the loss of genes such as tumour suppressors or the amplification of oncogenes, may lead to neoplastic development [170]. Of particular interest regarding CIN in tumour formation, is the Centromeric Protein E (CENP-E), which is considered as a mitotic checkpoint protein that regulates mitotic progression. The reduction of CENP-E in mice resulted in the development of aneuploid cells and consequently, late-life lymphomas and lung tumours [171].

In this study, I found that BPLF1 expression induces various molecular and morphological phenotypes previously described for SENP6 depleted cells [126, 129, 156, 172]. This includes the accumulation of SUMO2/3 foci in BPLF1-expressing cells and the formation of poly-SUMO2/3 conjugates of high molecular weights when compared to controls lacking BPLF1 expression. Consequently, SENP6 attenuation significantly disrupted CENP-A localization. SENP6 has been shown to promote centromeric deposition of CENP-A, as well as the other members of the CCAN, through deSUMOylating CENP-A loading factor Mis18BP1 [126, 173], preventing its targeting for proteasomal degradation by the SUMO-targeted RNF4 E3 ubiquitin ligase. Altogether, my data demonstrate both *in vivo* and *ex vivo*, that BPLF1 inhibits SENP6 activity. I demonstrated that the domain of BPLF1 responsible for SENP6 interaction (765 - 1327 aa), fused to the native NLS of BPLF1 (414 - 424 aa), induced the accumulation of SUMO2/3 foci in a similar manner to full-length BPLF1. In my expression studies, the aid of the NLS signal was due to SENP6 being identified to be localized within nucleus of the cell [126, 174], which suggests BPLF1 targeting to the nucleus is required to efficiently inhibit SENP6. Interestingly, I did not observe noticeable changes in SENP6 expression levels nor intracellular localization within BPLF1-expressing cells, suggesting that BPLF1 exerts some form of inhibition through direct contact. This is evidenced through

visualization of the BPLF1 binding domain of SENP6 (Uniprot ID: Q9GZR1, structure available on Alphafold) in

Figure 36. The experimentally determined catalytic region of SENP6 was in the amino acid region 630 – 1112. The BPLF1 binding domain of SENP6 was experimentally determined by our lab to be in the 449 – 629 aa region (unpublished data). As can be observed in

Figure 36, the BPLF1 binding domain is in close 3-dimensional proximity to the catalytic domain of SENP6 so it is highly probable that a form of steric hindrance occurs.

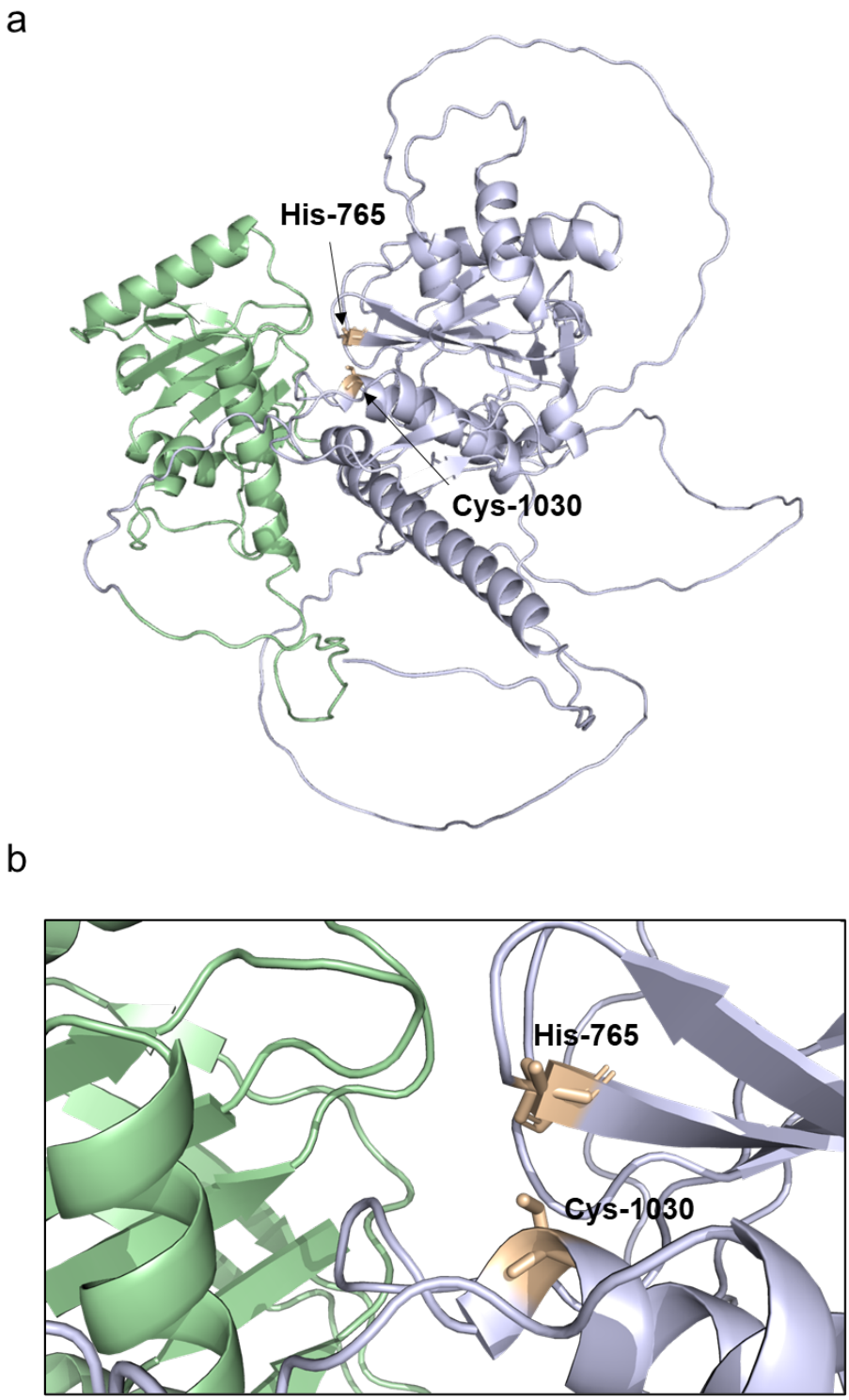

Figure 36: SENP6$^{449\text{-}1112}$ tertiary structure. a Full BPLF1 binding region (aa 449 - 629) coloured green, catalytic domains (aa 630 – 1112) coloured blue and active residues Cys-1030 and His-765 coloured yellow. b Zoomed in to focus on active residues of the catalytic domain. (Uniprot ID: Q9GZR1, structure available on Alphafold [175, 176], visualised via PyMol v2.5 [177])

Viruses have evolved a plethora of mechanisms to hijack cellular pathways, evade host immune recognition, establish infection, and successfully replicate. All members of the human herpesviruses have been found to leverage the SUMOylation machinery during infection [178, 179] and two EBV-encoded proteins have previously been suggested to modulate cellular SUMO levels. The latent cycle protein LMP1 has been shown to bind the SUMO-conjugating enzyme UBC9 and increase its activity. This was demonstrated to promote SUMOylation of the interferon regulatory factor 7 (IRF7), reducing its transcription activity, and was suggested to contribute to the establishment of latency. Another study identified the lytic cycle SM protein as a SUMO E3 ligase that promotes the SUMOylation of p53. While the biological significance of this activity is not clear, SUMOylated p53 has been shown to be rapidly exported out of the nucleus. In contrast to LMP1 and SM protein, which are respectively latent and lytic cycle genes, BPLF1 is unique in that it is a component of virions and can be delivered to the cytosol of cells upon infection. Accordingly, we have examined primary B cells during the early stages of infection and observed significant increases in SUMO2/3 foci number. Interestingly, my results show that BPLF1 depleted virus fails to modulate SUMO2/3 foci formation in primary B cells. Furthermore, CENP-A was clearly delocalized from the centromeres of cells exposed to WT EBV and VLPs but not in BPLF1-depleted virus. These findings reflect our detailed analysis in cell lines and support a model whereby BPLF1 inhibits SENP6 during the early phase of B cell infection to increase SUMOylation. These findings agree with previous studies of SENP6 loss-mediate hyperSUMOylation driving neoplasm formation such as diffuse large B-cell lymphoma [128].

A critical question to this work that must be addressed in future studies, is how the interacting domain of BPLF1 (BPLF1$^{765\text{-}1327}$) enters the nucleus to bind SENP6 during early infection? It is known that the N-terminal catalytic portion of BPLF1, which is cleaved via

Caspase-1 (BPLF1$^{1-215}$) activity, freely diffuses into the nucleus due to its small size (< 40 kDa) [61], leaving the putative NLS (BPLF1$^{414-424}$) behind with the remaining peptide. This could be sufficient to explain how BPLF1 reaches SENP6 within the nucleus, but experimental evidence will be needed to draw conclusions. The inquiry on the intracellular movement of BPLF1 in early infection could be addressed through the fusion of a fluorescent protein to BPLF1 within the virus structure to help visually track its movement during early infection via confocal microscopy. This method was attempted in my study using mCerulean as the fusion protein but unfortunately, yielded no visible signal in the subsequent confocal imaging post infection. This was suspected to be due to low BPLF1 presence within the cells, resulting in a weak signal. A solution to the lack of fluorescence signal, would be to find alternative sites to insert the mCerulean gene or to use a brighter fluorophore such as YPet which is roughly 3 fold brighter than mCerulean [180]. Live cell imaging using EBV with fluorescently tagged BPLF1 and SENP6 could provide valuable insight into spaciotemporal effects of BPLF1 on SENP6. In addition, a BPLF1 knockout clone of the VLP (B1050) would provide a more suitable control for future *ex vivo* B cell studies involving the VLPs.

In this study, I did not investigate the effects of BPLF1 on other members of the CCAN such as CENP-E. Since CENP-E has been found to be a prominent mitotic regulator [171], future CENP-E studies could provide greater insight into the effects on the formation and maintenance of the inner kinetochore and effects on CIN. Importantly, the effect that BPLF1 has on Mis18BP1, would also be a prime topic for investigation as Mis18BP1 was found to be an upstream substrate of SENP6. When SENP6 is depleted, hyperSUMOylation and subsequent proteolysis of Mis18bp1, destabilizes the cell's inner kinetochore [126]. It is important to note that the Promyelocytic leukemia protein (PML) is regarded as the model substrate of SENP6 [172]. When SENP6 is depleted, the amount of PML and consequently,

the size and number of PML associated nuclear bodies (NBs) increase. This is driven by SUMO-SIM interactions between PML and the associated components of the nuclear bodies [172]. PML-NBs serve as an innate immune defence against viral infection. Member proteins of the PML-NBs include, but are not limited to, PML, DAXX, ATRX, and sp100. In cell nuclei, DAXX-ATRX has been demonstrated to target and suppress the EBV genome through epigenetic modulations, which aren't clearly understood. There are also studies that have pointed to a more dualistic role, which can serve viral infection, including the γ-Herpesviruses [113, 181, 182]. If BPLF1 suppression of SENP6 activity indeed leads to accumulation of PML-NBs, it would therefore be interesting to investigate the interplay between known EBV encoded PML disruptors such as BNRF1 [88, 183] and EBNA1 [184], and BPLF1 in the context from early infection to latency.

In conclusion, I have identified BPLF1 as a major driver of genomic instability and a modulator of SUMOylation during the early phase of infection. In contrast to preceding studies that focused exclusively on the N-terminal deconjugase domain, I have studied full-length BPLF1 and successfully identified a novel SENP6 interaction domain (765 – 1327 aa) that replicates the wild type effects independently from the deneddylase catalytic domain (1 – 325 aa). Our findings suggest that this domain alone is sufficient for inducing enhanced SUMOylation. Considering these findings in relation to previous studies that identified BPLF1 as a Ubiquitin- and NEDD8-specific deconjugase, it temptingly suggests that BPLF1 has evolved unique domains to modulated different Ubiquitin-like modifiers (Ubl). This line of thought may be especially important when one considers emerging concepts such as crosstalk between Ubl pathways and hybrid chain formation.

5. Materials and methods

5.1. Methods

5.1.1. Ethics statement

All peripheral blood mononuclear cells (PBMCs) used in this study were isolated from buffy coats from anonymous donors. These buffy coats were purchased from the *Institut für Klinische Transfusionsmedizin und Zelltherapie* (IKTZ) in Heidelberg and did not require prior ethical approval.

5.1.2. Cell lines, primary cells, and transfections

Cell lines used in this study were HEK293 cells (ATCC: CRL-1573), HeLa (ATCC: CLL-2), U2OS (ATCC: HTB-96), WI38 primary human embryonic fibroblasts (ATCC: CCL-75), EBV producer cell lines within HEK293 cells, and LCLs that were generated as previously described [140]. The full list of cells used in this study is found in Table 3. The media used to culture HEK293, EBV producer cells, HeLa, and LCLs consisted of RPMI (Gibco™) supplemented with 10 % FCS, and U2OS cells were cultured using DMEM (Gibco™) supplemented with 10 % FCS. Cells were transfected with expression plasmids or viral genome BACs via using Metafectene® or Metafectene® Pro (Biontex).

Table 3: Cell lines used in this study.

Name	Description
DG75	B cell from health donors transformed through infection with EBV lacking BZLF1
HEK293	Human embryonic kindey cell line transformed with sheared Adenovirus 5 DNA [191]
HeLa	Human cervical epithelial cells derived from adenocarcinoma
LCL	B cells from healthy donors were transformed through infection with EBV.
Producer cells	Several EBV and DFEBV producer cell lines were used in this study. Producer cell lines were generated by transfecting HEK293 cells with BAC DNA and selecting with hygromycin (100 µg/mL).
U2OS	Human bone epithelial cell line derived from osteocarcinoma
E.coli DH10B	Plasmid rescue	F– mcrA Δ(mrr-hsdRMS-mcrBC) ϕ80lacZΔM15 ΔlacX74 recA1 endA1 araD139 Δ (ara-leu)7697 galU galK λ– rpsL(StrR) nupG
E.coli DH5α	Cloning and plasmid maintainance	supE44 D(lacZYA-argF)U196 (F80DlacZM15) hsdR17 recA1 endA1 gyrA96 thi-1 relA1
E.coli GS1783	Homologous recombination	W3110 ΔlacU169 gal490 λN:lacZ Δ(N-int) cI857 Δ(cro-bioA)

5.1.3. Recombinant BAC DNA

Recombinant M81 BAC DNA (B110, GenBank accession number: KF373730.1) was generated as previously described [140]. In my study, I generated M81/ΔBPLF1 (B1580) through the *En Passant* method [185] of homologous recombination, replacing nucleotides 179 to the end 9441 of the BPLF1 ORF with an ampicillin resistance cassette. I used PCR to amplify the ampicillin resistance cassette as a linear fragment with 60-bp homology arms that matched flanking regions of the BPLF1 gene. I subsequently generated stable producer clones as per a previously described method [186].

5.1.4. Production of virus

I co-transfected stable producer cells with the BZLF1 (p509), gp110 (pRa), and BRLF1 (p2130) expression plasmids to induce lytic replication for virus production. I also co-transfected the wild-type BPLF1 expression plasmid (B1283), along with the previously listed plasmids, into M81/ΔBPLF1 to produce virus to add the gene for trans-complementation (M81/ΔBPLF1-C) in a similar method as described previously [187]. After 72 hours I collected the virus

supernatants and filtered them through 0.45 μm Millex® syringe filter units. The full list of recombinant virus BACs that were used in my study is found in Table 4.

5.1.5. Recombinant Plasmids

I cloned the full-length BPLF1 (9441 bp) into the pRK5 expression vector using a multi-step process. As the template, I used the M81 EBV strain [140]. I then later added an N-terminal Flag-tag to produce the pRK5-Flag-BPLF1 (1-9441 bp). I proceeded to generate multiple sequential BPLF1 domain deletion mutants described in Figure 12. I performed full plasmid PCR with the Phusion PCR system from Thermo Fisher™, using the pRK5-Flag-BPLF1 expression plasmid as a template. For these reactions, I made use of primers complementary to sequences flanking the regions of the BPLF1 ORF that I intended to delete. After the PCR reaction was complete, I digested the template DNA using DpnI restriction enzyme from Thermo Fisher Scientific™ and transformed DH5α cells with the digestion using heat shock. The resulting recombinant expression plasmids are listed in Table 4.

Table 4: Plasmids used in this study.

Vector/BACmid	Source
pRK5-B95.8.BRLF1	Feederle et al., 2006
pRK5-B95.8.BALF4(=gp110=gB)	Feederle et al., 2006
M81	Tsai et al., 2013
p509-B95.8.BZLF1	Feederle et al, 2006
M81 VLPs	Shumilov et al., 2017
pRK5-CMV.BPLF1	This study
pCMV-BBRF2.His.tag	Adhikary et al.,2007
pCMV-BGLF3.His.tag	Adhikary et al.,2007
pCMV-BGLF4.His.tag	Adhikary et al.,2007
pCMV-BKRF4.His.tag	Adhikary et al.,2007
pCMV-BLRF2.His.tag	Adhikary et al.,2007
pCMV-BNRF1.His.tag	Adhikary et al.,2007
pCMV-BOLF1.His.tag	Adhikary et al.,2007
pCMV-BXLF1.His.tag	Adhikary et al.,2007
M81/ΔZR	Lin et al., 2015
M81/ΔBPLF1(aa60-3147end)	This study
M81/ΔBPLF1-REV(aa60-3147end)	This study
pCDNA-Flag-HA	Adgene
pRK5-CMV.FLAG-BPLF1	This study
pRK5-CMV.FLAG-BPLF1^{C61A}	This study
pRK5-CMV.FLAG-mCerulean	This study
pRK5-CMV.FLAG-BPLF1$^{\Delta 2\text{-}272}$	This study
pRK5-CMV.FLAG-BPLF1$^{\Delta 273\text{-}764}$	This study
pRK5-CMV.FLAG-BPLF1$^{\Delta 765\text{-}1327}$	This study
pRK5-CMV.FLAG-BPLF1$^{\Delta 1328\text{-}1975}$	This study
pRK5-CMV.FLAG-BPLF1$^{\Delta 1976\text{-}2548}$	This study
pRK5-CMV.FLAG-BPLF1$^{\Delta 2549\text{-}3147}$	This study
pRK5-CMV.FLAG-BPLF1$^{765\text{-}1327}$	This study
pRK5-EF1a-FLAG-mCerulean	This study
pRK5-CMV.FLAG-NLS-BPLF1$^{765\text{-}1327}$	This study

5.1.6. Tegument screen for nuclear atypia

The His-tagged tegument protein expression vectors were previously constructed by our lab [188] and were used alongside the full-length BPLF1 that I generated in this study. I transfected HEK293 cells with equimolar amounts of the expression plasmids. After 72 hours

I collected and stained these cells for their respective His or Flag-epitopes in order to identify positively transfected cells along with DAPI for nuclear staining. I used fluorescence microscopy to identify nuclear atypia using nuclear size and multinuclearity as markers.

5.1.7. BPLF1 interactome determination via IP-MS

I transfected HEK293 cells with expression plasmids for Flag-BPLF1 or Flag-HA as a negative control for 48 hours and proceeded to lyse the collected cells in IP lysis buffer (25 mM Tris/HCl pH 7.4, 150 mM NaCl, 1 % NP-40, 1 mM EDTA, 5 % glycerol) that was supplemented with (Halt™ Protease inhibitor and 25 mM NEM). I then purified the Flag-containing proteins using Anti-Pierce DYKDDDDK Magnetic Agarose (Product no. A36798) and a competing Pierce™ 3x DYKDDDDK Peptide (Product no. 36805) for eluting the desired bound Flag tagged protein. The protein samples were loaded onto a one-dimensional SDS-PAGE system, the excised samples had their cysteines reduced by DTT. The samples were further fractionated via the addition of carbamidomethylated and ioacetamide followed by a 4-hour digestion with Trypsin. The resulting peptides were loaded on a cartridge trap column, packed with Acclaim PepMap300 C18, 5µm, 300Å wide pore (Thermo Fisher Scientific™) and separated via a gradient from 3 % to 40 % ACN on a nanoEase MZ Peptide analytical column (300Å, 1.7µm, 75µm x 200 mm, Waters) using a 90 minute MS-method. Eluted peptides were analyzed by an online-coupled Orbitrap Exploris 480 mass spectrometer. Data analysis was performed using MaxQuant with an organism specific database extracted from Uniprot.org under default settings. Identification FDR cut-offs were 0.01 on peptide level and 0.01 on protein level. Match between runs option was enabled to transfer peptide identifications across Raw files based on accurate retention time and m/z. Quantification was done using a label free quantification approach based on the MaxLFQ algorithm. A

minimum of 2 quantified peptides per protein was required for protein quantification. Data have been further processed by in-house compiled R-scripts to plot and filter data.

The Perseus software package (version 1.6.7.0) was used with default settings for further statistical analysis of LFQ data. Adapted from the Perseus recommendations, protein groups with non-zero intensity values in 50 % of the samples of at least one of the conditions were used and imputation with random values drawn from a downshifted (1.8 standard deviation) and narrowed (0.3 standard deviation) intensity distribution of the individual sample.

5.1.8. FACS Sorting of BPLF1-expressing cells

I transfected HEK293 cells with control plasmid expressing Flag-mCerulean or a BPLF1 reporter plasmid, described in Figure 18. After 48 hours I stained the collected cells with 7AAD and then sorted with a FACS Aria Fusion 2 (BD Biosciences™). Gating was performed such that only single cells, 7-AAD negative and mCerulean positive cells were sorted. An 85 µm nozzle and a "4-way purity" sorting mask was used. I then washed the collected cells in PBS, lysed as previously described [189] and analyzed by western blot with mouse α-SUMO2/3 antibody.

5.1.9. Antibodies

In this study, I used primary antibodies against Actin (Santa Cruz sc-8432 1:1000 for immunoblots), BZLF1 (clone BZ.11 1:200 for immunofluorescence), CENP-A (Abcam ab13939 1:500 for immunofluorescence), Centrin-2 (Santa Cruz sc-27793-R 1:1000 for immunofluorescence), CEP170 (Abcam ab72505 1:1000 for immunofluorescence), EBNA2 (clone PE2 1:200 for immunofluorescence), Flag (Sigma-Aldrich F7425 1:40000 for immunofluorescence, Santa Cruz sc-166355 1:1000 for immunofluorescence, and 1:1000 for immunoblots), gp350 (clone OT6 1:300 for immunofluorescence and virus binding assays),

SUMO2/3 (MBL M114-3 1:1000 for immunoblots and 1:500 for immunofluorescence), SENP6 (Santa Cruz 79-M 1:1000 for immunoblots and 4 µg/1 mg cell lysate for immunoprecipitation), and Vinculin (Santa Cruz sc-25336 1:1000 for immunoblots). Secondary antibodies used against mouse were coupled to horseradish peroxidase (Promega, w402b 1:10000 for immunoblots), Alexa488 (Invitrogen A11029 1:300 for immunofluorescence) or Cy5 (Dianova SBA-1031-15 1:300 for immunofluorescence), and secondary antibodies against rabbit were coupled to Alexa647 (Invitrogen A-21245 1:300 for immunofluorescence and virus binding assays) or Alexa488 (Invitrogen A-11008 1:300 for immunofluorescence).

5.1.10. Bioinformatic tools

I analysed and presented all flow cytometry data using FlowJo 10. I planned cloning strategies and analysed sequencing data using Macvector 18.2. The domain structure of BPLF1 shown in Figure 12 was established using homology (BLAST) and structure predictions (RaptorX web server; http://raptorx.uchicago.edu). Protein 3D structures were visualized via PyMol v2.5 [177].

5.1.11. Real-time qPCR

I used quantitative real-time PCR as previously described [187] to quantify viral supernatants. In brief, supernatants were digested with DNAse I (1 U/ml) at 37°C for 1 hour, heat inactivated at 70°C for 10 minutes and treated with proteinase K to release encapsulated viral DNA. Primers and probe specific for the BALF5 gene was used to quantify viral genome copies per mL.

5.1.12. Virus Binding assay to quantify VLPs

I quantified VLP supernatants as previously described [190]. Briefly, I exposed primary B cells to M81 viral supernatant that was previously quantified using qPCR. Using supernatants with increasing concentrations enabled the establishment of a standard curve. In parallel, I exposed primary B cells of the same donor to VLPs of unknown concentration. After 2 hours of binding at 4^{o}C, I washed the cells to remove unbound particles and fixed them with paraformaldehyde (4 %). I then performed immunostainings using α-gp350 (clone 72A1) and subsequently α-mouse IgG-Alexa647. I quantified the number of bound particles as median fluorescence intensity (MFI) values using flow cytometry. I established a standard curve using the MFI values of the known M81 viral supernatant and extrapolated off this standard curve to obtain genome equivalents for the unknown VLP sample.

5.1.13. B cell infection and in vitro transformation experiments.

In order to measure the infectivities of viruses that I used in this study, I exposed 2.5 x 10^5 primary B cells to viral MOIs of 30 for 2 hours. I subsequently washed the cells in PBS and plated them in 96-U-well plates in RPMI supplemented with 20 % FCS. At 3 days post infection (dpi), I collected and fixed the cells in paraformaldehyde (4 %), permeabilized in PBS supplemented with Triton-X (0.05 %), and then performed immunostaining for EBNA2 to determine the percentage of infected cells. I subsequently seeded the cells into a new plate at 30 EBNA2-positive cells per well and analysed these transformed B cells at 30 dpi for abnormalities.

5.1.14. Western Blots

I collected and lysed cell samples in buffer (25 mM Tris-HCl pH 7.6, 50 mM NaCl, 1 mM EDTA, 0.5 % Nonidet P40, 0.1 % SDS, 0.5 % sodium deoxycholate) containing protease inhibitors (Complete Mini Protease Inhibitor Cocktail tablets; Roche) and 10 mM NEM (Sigma). I

measured the protein amounts via Bradford assay to help normalize protein amounts to be loaded onto the gel. Prior to SDS-PAGE, I denatured proteins in Laemmli sample buffer (supplemented with 10 % β-mercaptoethanol) for 10 min at 95°C and then separated the lysate in 7.5 % SDS-Polyacrylamide gels. I subsequently transferred the separated protein onto a nitrocellulose membrane (Amersham Protran 0.45 µm) and then blocked with 5 % milk PBS-T (PBS with 0.1 % Tween 20). I added primary and secondary antibodies diluted in blocking buffer and incubated 1 h at room temperature. After blocking, I washed the membrances with PBS-T to remove unbound antibodies and detected the target proteins using Western Lightning Plus Chemiluminescent Substrate (Perkin Elmer).

5.1.15. Co-Immunoprecipitation

I incubated cell lysates with α-Flag-coupled Magnetic beads or with α-SENP6 antibody/protein-G-coupled Magnetic beads for 1 hour at room temperature. After binding, I separated the bead-antibody-lysate using a magnetic field to immobilize beads and followed by washing 5 times with PBS-T. I then boiled the washed beads for 10 minutes in Laemmli buffer (without β-mercaptoethanol) to elute bound protein complexes. I placed the mixture in a magnet and the clear supernatant was carefully removed and supplemented with β-mercaptoethanol to obtain a final concentration of 1 %. I then briefly boiled and separated the samples via SDS-PAGE.

5.1.16. Immunofluorescence

All cells that I analysed were washed three times and resuspended in PBS (3 % FCS). I subsequently dispensed the washed cells into Shandon cytospin chambers loaded with glass slides (Thermo Scientifics) and centrifuged them at 2,000 r.p.m. using a Thermo Scientific Cytospin 4 Centrifuge for 10 min. I removed and air-dried the slides and fixed with

paraformaldehyde (4 %) for 10 min at room temperature. I proceeded to quench the slides in PBS for 5 min and blocked in 0.1 % Triton-X, 0.2 % BSA, and 2 % FCS in PBS for 1.5 h at RT. Primary and secondary antibodies that I used to probe for targets were diluted in blocking solution. I visualized the stained cells using a camera attached to a DM2500 fluorescence microscope (Leica) or with a confocal microscope (Zeiss LSM700).

5.1.17. Image Analysis

Immunofluorescence data were analysed via Fiji 2 (Image J). For nuclear size, I demarcated nuclear regions using the DAPI signal and measured using the software measure function. For centromere foci analysis, I identified nuclear foci using the find maxima function within the nuclear area with each focus measured for 15 pictures per condition.

5.1.18. Statistical analysis

All statistical data, unless stated otherwise, were analysed using Graphpad Prism 6. The statistical tests used were either paired student t-tests, or One- or Two-way ANOVAs for multiple comparisons using default settings.

6. Bibliography

1. Epstein, M.A., B.G. Achong, and Y.M. Barr, *Virus Particles in Cultured Lymphoblasts from Burkitt's Lymphoma.* The Lancet, 1964. **283**(7335): p. 702-703.
2. Gerber, P., J. Whang-Peng, and J.H. Monroe, *Transformation and chromosome changes induced by Epstein-Barr virus in normal human leukocyte cultures.* Proc Natl Acad Sci U S A, 1969. **63**(3): p. 740-7.
3. Henle, G., W. Henle, and V. Diehl, *Relation of Burkitt's tumor-associated herpes-ytpe virus to infectious mononucleosis.* Proc Natl Acad Sci U S A, 1968. **59**(1): p. 94-101.
4. Cohen, J.I., *Epstein-Barr virus infection.* N Engl J Med, 2000. **343**(7): p. 481-92.
5. Cohen, J.I., et al., *Epstein-Barr virus: an important vaccine target for cancer prevention.* Sci Transl Med, 2011. **3**(107): p. 107fs7.
6. Thorley-Lawson, D.A. and M.J. Allday, *The curious case of the tumour virus: 50 years of Burkitt's lymphoma.* Nat Rev Microbiol, 2008. **6**(12): p. 913-24.
7. Young, L.S. and A.B. Rickinson, *Epstein-Barr virus: 40 years on.* Nat Rev Cancer, 2004. **4**(10): p. 757-68.
8. Roizmann, B., et al., *The family Herpesviridae: an update. The Herpesvirus Study Group of the International Committee on Taxonomy of Viruses.* Arch Virol, 1992. **123**(3-4): p. 425-49.
9. McGeoch, D.J., A. Dolan, and A.C. Ralph, *Toward a comprehensive phylogeny for mammalian and avian herpesviruses.* J Virol, 2000. **74**(22): p. 10401-6.
10. Davison, A.J., *Channel catfish virus: A new type of herpesvirus.* Virology, 1992. **186**(1): p. 9-14.
11. Gerner, C.S., A. Dolan, and D.J. McGeoch, *Phylogenetic relationships in the Lymphocryptovirus genus of the Gammaherpesvirinae.* Virus Res, 2004. **99**(2): p. 187-92.
12. Takada, K., *Cross-linking of cell surface immunoglobulins induces Epstein-Barr virus in Burkitt lymphoma lines.* Int J Cancer, 1984. **33**(1): p. 27-32.
13. Klein, G., *Specific chromosomal translocations and the genesis of B-cell-derived tumors in mice and men.* Cell, 1983. **32**(2): p. 311-315.
14. Leder, P., *Burkitt's lymphoma: a human cancer model. Proceedings of a symposium. Lyon, 6-9 December 1983*. 1985/01/01 ed. IARC Sci Publ. 1985. 1-484.
15. Manolov, G. and Y. Manolova, *Marker band in one chromosome 14 from Burkitt lymphomas.* Nature, 1972. **237**(5349): p. 33-4.
16. Zech, L., et al., *Characteristic chromosomal abnormalities in biopsies and lymphoid-cell lines from patients with Burkitt and non-Burkitt lymphomas.* Int J Cancer, 1976. **17**(1): p. 47-56.
17. Dalla-Favera, R., et al., *Human c-myc onc gene is located on the region of chromosome 8 that is translocated in Burkitt lymphoma cells.* Proc Natl Acad Sci U S A, 1982. **79**(24): p. 7824-7.

18. Taub, R., et al., *Translocation of the c-myc gene into the immunoglobulin heavy chain locus in human Burkitt lymphoma and murine plasmacytoma cells.* Proceedings of the National Academy of Sciences, 1982. **79**(24): p. 7837-7841.

19. Battey, J., et al., *The human c-myc oncogene: Structural consequences of translocation into the igh locus in Burkitt lymphoma.* Cell, 1983. **34**(3): p. 779-787.

20. Kanda, T., M. Yajima, and K. Ikuta, *Epstein-Barr virus strain variation and cancer.* Cancer Sci, 2019. **110**(4): p. 1132-1139.

21. van Tong, H., et al., *Parasite Infection, Carcinogenesis and Human Malignancy.* EBioMedicine, 2017. **15**: p. 12-23.

22. Hodgkin, *On some Morbid Appearances of the Absorbent Glands and Spleen.* Med Chir Trans, 1832. **17**: p. 68-114.

23. Reed, D.M., *On the pathological changes in Hodgkin's disease with special reference to its relation to tuberculosis.* Johns Hopkins Hosp Rep, 1902. **10**: p. 133-198.

24. Sternberg, C., *Ueber eine eigenartige unter dem Bilde der pseudoleukemic verlaufende Tuberkulose des lymphatischen Apparatus.* Ztschr f. Heilk., 1898. **19**: p. 21-90.

25. Kutok, J.L. and F. Wang, *Spectrum of Epstein-Barr virus-associated diseases.* Annu Rev Pathol, 2006. **1**: p. 375-404.

26. Kuppers, R. and K. Rajewsky, *The origin of Hodgkin and Reed/Sternberg cells in Hodgkin's disease.* Annu Rev Immunol, 1998. **16**: p. 471-93.

27. Weniger, M.A. and R. Kuppers, *NF-kappaB deregulation in Hodgkin lymphoma.* Semin Cancer Biol, 2016. **39**: p. 32-9.

28. Caldwell, R.G., et al., *Epstein-Barr Virus LMP2A Drives B Cell Development and Survival in the Absence of Normal B Cell Receptor Signals.* Immunity, 1998. **9**(3): p. 405-411.

29. van Gent, M., et al., *EBV lytic-phase protein BGLF5 contributes to TLR9 downregulation during productive infection.* J Immunol, 2011. **186**(3): p. 1694-702.

30. Bouvard, V., et al., *A review of human carcinogens—Part B: biological agents.* The Lancet Oncology, 2009. **10**(4): p. 321-322.

31. Liu, L., *Fields Virology, 6th Edition.* Clinical Infectious Diseases, 2014. **59**(4): p. 613-613.

32. Iizasa, H., et al., *Role of Viral and Host microRNAs in Immune Regulation of Epstein-Barr Virus-Associated Diseases.* Front Immunol, 2020. **11**: p. 367.

33. Klinke, O., R. Feederle, and H.J. Delecluse, *Genetics of Epstein-Barr virus microRNAs.* Semin Cancer Biol, 2014. **26**: p. 52-9.

34. Cheung, A. and E. Kieff, *Long internal direct repeat in Epstein-Barr virus DNA.* J Virol, 1982. **44**(1): p. 286-94.

35. Wang, F., et al., *Epstein-Barr virus latent membrane protein (LMP1) and nuclear proteins 2 and 3C are effectors of phenotypic changes in B lymphocytes: EBNA-2 and LMP1 cooperatively induce CD23.* J Virol, 1990. **64**(5): p. 2309-18.

36. Tu, C., et al., *Genome-Wide Analysis of 18 Epstein-Barr Viruses Isolated from Primary Nasopharyngeal Carcinoma Biopsy Specimens.* J Virol, 2017. **91**(17).

37. Dambaugh, T., et al., *U2 region of Epstein-Barr virus DNA may encode Epstein-Barr nuclear antigen 2.* Proc Natl Acad Sci U S A, 1984. **81**(23): p. 7632-6.

38. Germi, R., et al., *Three-dimensional structure of the Epstein-Barr virus capsid.* J Gen Virol, 2012. **93**(Pt 8): p. 1769-1773.

39. Johannsen, E., et al., *Proteins of purified Epstein-Barr virus.* Proc Natl Acad Sci U S A, 2004. **101**(46): p. 16286-91.

40. Atkins, S.L., et al., *Small molecule screening identifies inhibitors of the Epstein-Barr virus deubiquitinating enzyme, BPLF1.* Antiviral Res, 2020. **173**: p. 104649.

41. Yuan, J., et al., *Virus and cell RNAs expressed during Epstein-Barr virus replication.* J Virol, 2006. **80**(5): p. 2548-65.

42. Whitehurst, C.B., et al., *Knockout of Epstein-Barr virus BPLF1 retards B-cell transformation and lymphoma formation in humanized mice.* mBio, 2015. **6**(5): p. e01574-15.

43. Schlieker, C., et al., *A deubiquitinating activity is conserved in the large tegument protein of the herpesviridae.* J Virol, 2005. **79**(24): p. 15582-5.

44. He, H.P., et al., *Structure of Epstein-Barr virus tegument protein complex BBRF2-BSRF1 reveals its potential role in viral envelopment.* Nat Commun, 2020. **11**(1): p. 5405.

45. Zaichick, S.V., et al., *The herpesvirus VP1/2 protein is an effector of dynein-mediated capsid transport and neuroinvasion.* Cell Host Microbe, 2013. **13**(2): p. 193-203.

46. Whitehurst, C.B., et al., *The Epstein-Barr virus (EBV) deubiquitinating enzyme BPLF1 reduces EBV ribonucleotide reductase activity.* J Virol, 2009. **83**(9): p. 4345-53.

47. van Gent, M., et al., *Epstein-Barr virus large tegument protein BPLF1 contributes to innate immune evasion through interference with toll-like receptor signaling.* PLoS Pathog, 2014. **10**(2): p. e1003960.

48. Iwasaki, A. and R. Medzhitov, *Regulation of adaptive immunity by the innate immune system.* Science, 2010. **327**(5963): p. 291-5.

49. Mogensen, T.H., *Pathogen recognition and inflammatory signaling in innate immune defenses.* Clin Microbiol Rev, 2009. **22**(2): p. 240-73, Table of Contents.

50. Saito, S., et al., *Epstein-Barr Virus Deubiquitinase Downregulates TRAF6-Mediated NF-k B Signaling during Productive Replication.* Journal of Virology, 2013. **87**: p. 4060-4070.

51. Gupta, S., et al., *Herpesvirus deconjugases inhibit the IFN response by promoting TRIM25 autoubiquitination and functional inactivation of the RIG-I signalosome.* PLoS Pathog, 2018. **14**(1): p. e1006852.

52. Kudoh, A., et al., *Epstein-Barr virus lytic replication elicits ATM checkpoint signal transduction while providing an S-phase-like cellular environment.* J Biol Chem, 2005. **280**(9): p. 8156-63.

53. Li, C.W., B.R. Jheng, and B.S. Chen, *Investigating genetic-and-epigenetic networks, and the cellular mechanisms occurring in Epstein-Barr virus-infected human B lymphocytes via big data mining and genome-wide two-sided NGS data identification.* PLoS One, 2018. **13**(8): p. e0202537.

54. Waters, L.S., et al., *Eukaryotic translesion polymerases and their roles and regulation in DNA damage tolerance.* Microbiol Mol Biol Rev, 2009. **73**(1): p. 134-54.

55. Bienko, M., et al., *Regulation of translesion synthesis DNA polymerase eta by monoubiquitination.* Mol Cell, 2010. **37**(3): p. 396-407.

56. Whitehurst, C.B., et al., *Epstein-Barr virus BPLF1 deubiquitinates PCNA and attenuates polymerase eta recruitment to DNA damage sites.* J Virol, 2012. **86**(15): p. 8097-106.

57. Dyson, O.F., J.S. Pagano, and C.B. Whitehurst, *The Translesion Polymerase Pol eta Is Required for Efficient Epstein-Barr Virus Infectivity and Is Regulated by the Viral Deubiquitinating Enzyme BPLF1.* J Virol, 2017. **91**(19).

58. Gastaldello, S., et al., *Herpes virus deneddylases interrupt the cullin-RING ligase neddylation cycle by inhibiting the binding of CAND1.* J Mol Cell Biol, 2012. **4**(4): p. 242-51.

59. Gastaldello, S., et al., *A deneddylase encoded by Epstein-Barr virus promotes viral DNA replication by regulating the activity of cullin-RING ligases.* Nat Cell Biol, 2010. **12**(4): p. 351-61.

60. Cook, J.G., *Replication licensing and the DNA damage checkpoint.* Front Biosci (Landmark Ed), 2009. **14**: p. 5013-30.

61. Gastaldello, S., et al., *Caspase-1 promotes Epstein-Barr virus replication by targeting the large tegument protein deneddylase to the nucleus of productively infected cells.* PLoS Pathog, 2013. **9**(10): p. e1003664.

62. Lamkanfi, M. and V.M. Dixit, *Inflammasomes and their roles in health and disease.* Annu Rev Cell Dev Biol, 2012. **28**: p. 137-61.

63. Klionsky, D.J. and S.D. Emr, *Autophagy as a regulated pathway of cellular degradation.* Science, 2000. **290**(5497): p. 1717-21.

64. Crotzer, V.L. and J.S. Blum, *Autophagy and adaptive immunity.* Immunology, 2010. **131**(1): p. 9-17.

65. Funderburk, S.F., Q.J. Wang, and Z. Yue, *The Beclin 1-VPS34 complex--at the crossroads of autophagy and beyond.* Trends Cell Biol, 2010. **20**(6): p. 355-62.

66. Kirkin, V. and V.V. Rogov, *A Diversity of Selective Autophagy Receptors Determines the Specificity of the Autophagy Pathway.* Mol Cell, 2019. **76**(2): p. 268-285.

67. Kirkin, V., et al., *A role for ubiquitin in selective autophagy.* Mol Cell, 2009. **34**(3): p. 259-69.

68. Teo, Q.W., S.W. van Leur, and S. Sanyal, *Escaping the Lion's Den: redirecting autophagy for unconventional release and spread of viruses.* FEBS J, 2021. **288**(13): p. 3913-3927.

69. Paludan, C., et al., *Endogenous MHC class II processing of a viral nuclear antigen after autophagy.* Science, 2005. **307**(5709): p. 593-6.

70. Vilmen, G., et al., *BHRF1, a BCL2 viral homolog, disturbs mitochondrial dynamics and stimulates mitophagy to dampen type I IFN induction.* Autophagy, 2020. **17**(6): p. 1296-1315.

71. Yla-Anttila, P., S. Gupta, and M.G. Masucci, *The Epstein-Barr virus deubiquitinase BPLF1 targets SQSTM1/p62 to inhibit selective autophagy.* Autophagy, 2021: p. 1-15.

72. Lemon, S.M., L.M. Hutt, and J.S. Pagano, *Cytofluorometry of lymphocytes infected with Epstein-Barr virus: effect of phosphonoacetic acid on nucleic acid.* J Virol, 1978. **25**(1): p. 138-45.

73. Laichalk, L.L. and D.A. Thorley-Lawson, *Terminal differentiation into plasma cells initiates the replicative cycle of Epstein-Barr virus in vivo.* J Virol, 2005. **79**(2): p. 1296-307.

74. Barouch-Bentov, R., et al., *Hepatitis C Virus Proteins Interact with the Endosomal Sorting Complex Required for Transport (ESCRT) Machinery via Ubiquitination To Facilitate Viral Envelopment.* mBio, 2016. **7**(6).

75. Beattie, E.C., et al., *Regulation of AMPA receptor endocytosis by a signaling mechanism shared with LTD.* Nat Neurosci, 2000. **3**(12): p. 1291-300.

76. Conner, S.D. and S.L. Schmid, *Regulated portals of entry into the cell.* Nature, 2003. **422**(6927): p. 37-44.

77. Kirschner, A.N., et al., *Structure of Epstein-Barr virus glycoprotein 42 suggests a mechanism for triggering receptor-activated virus entry.* Structure, 2009. **17**(2): p. 223-33.

78. Sodeik, B., M.W. Ebersold, and A. Helenius, *Microtubule-mediated transport of incoming herpes simplex virus 1 capsids to the nucleus.* J Cell Biol, 1997. **136**(5): p. 1007-21.

79. Suazo, P.A., et al., *Evasion of early antiviral responses by herpes simplex viruses.* Mediators Inflamm, 2015. **2015**: p. 593757.

80. Fingeroth, J.D., et al., *Epstein-Barr virus receptor of human B lymphocytes is the C3d receptor CR2.* Proceedings of the National Academy of Sciences, 1984. **81**(14): p. 4510-4514.

81. Liu, F., et al., *Mapping the N-terminal residues of Epstein-Barr virus gp42 that bind gH/gL by using fluorescence polarization and cell-based fusion assays.* J Virol, 2010. **84**(19): p. 10375-85.

82. Silva, A.L., et al., *Mutational analyses of Epstein-Barr virus glycoprotein 42 reveal functional domains not involved in receptor binding but required for membrane fusion.* J Virol, 2004. **78**(11): p. 5946-56.

83. Hannah, B.P., et al., *Herpes simplex virus glycoprotein B associates with target membranes via its fusion loops.* J Virol, 2009. **83**(13): p. 6825-36.

84. Nemerow, G.R. and N.R. Cooper, *Early events in the infection of human B lymphocytes by Epstein-Barr virus: The internalization process.* Virology, 1984. **132**(1): p. 186-198.

85. Shannon-Lowe, C. and M. Rowe, *Epstein-Barr virus infection of polarized epithelial cells via the basolateral surface by memory B cell-mediated transfer infection.* PLoS Pathog, 2011. **7**(5): p. e1001338.

86. Tanner, J., et al., *Epstein-Barr virus gp350/220 binding to the B lymphocyte C3d receptor mediates adsorption, capping, and endocytosis.* Cell, 1987. **50**(2): p. 203-13.

87. Shannon-Lowe, C. and M. Rowe, *Epstein Barr virus entry; kissing and conjugation.* Curr Opin Virol, 2014. **4**: p. 78-84.

88. Tsai, K., et al., *Viral reprogramming of the Daxx histone H3.3 chaperone during early Epstein-Barr virus infection.* J Virol, 2014. **88**(24): p. 14350-63.

89. Albanese, M., et al., *Epstein-Barr virus microRNAs reduce immune surveillance by virus-specific CD8+ T cells.* Proc Natl Acad Sci U S A, 2016. **113**(42): p. E6467-E6475.

90. Chen, J., et al., *The KGD motif of Epstein-Barr virus gH/gL is bifunctional, orchestrating infection of B cells and epithelial cells.* mBio, 2012. **3**(1).

91. Chesnokova, L.S., S.L. Nishimura, and L.M. Hutt-Fletcher, *Fusion of epithelial cells by Epstein-Barr virus proteins is triggered by binding of viral glycoproteins gHgL to integrins alphavbeta6 or alphavbeta8.* Proc Natl Acad Sci U S A, 2009. **106**(48): p. 20464-9.

92. Xiao, J., et al., *Characterization of the Epstein-Barr virus glycoprotein BMRF-2.* Virology, 2007. **359**(2): p. 382-96.

93. Tugizov, S.M., R. Herrera, and J.M. Palefsky, *Epstein-Barr virus transcytosis through polarized oral epithelial cells.* J Virol, 2013. **87**(14): p. 8179-94.

94. Shannon-Lowe, C.D., et al., *Resting B cells as a transfer vehicle for Epstein-Barr virus infection of epithelial cells.* Proc Natl Acad Sci U S A, 2006. **103**(18): p. 7065-70.

95. Altmann, M. and W. Hammerschmidt, *Epstein-Barr virus provides a new paradigm: a requirement for the immediate inhibition of apoptosis.* PLoS Biol, 2005. **3**(12): p. e404.

96. Nikitin, P.A., et al., *An ATM/Chk2-mediated DNA damage-responsive signaling pathway suppresses Epstein-Barr virus transformation of primary human B cells.* Cell Host Microbe, 2010. **8**(6): p. 510-22.

97. Kalla, M., et al., *AP-1 homolog BZLF1 of Epstein-Barr virus has two essential functions dependent on the epigenetic state of the viral genome.* Proc Natl Acad Sci U S A, 2010. **107**(2): p. 850-5.

98. Leight, E.R. and B. Sugden, *EBNA-1: a protein pivotal to latent infection by Epstein-Barr virus.* Reviews in Medical Virology, 2000. **10**(2): p. 83-100.

99. Cohen, J.I., *Epstein-Barr virus lymphoproliferative disease associated with acquired immunodeficiency.* Medicine (Baltimore), 1991. **70**(2): p. 137-60.

100. Rastelli, J., et al., *LMP1 signaling can replace CD40 signaling in B cells in vivo and has unique features of inducing class-switch recombination to IgG1.* Blood, 2008. **111**(3): p. 1448-55.

101. Khanna, R., et al., *Activation and adoptive transfer of Epstein-Barr virus-specific cytotoxic T cells in solid organ transplant patients with posttransplant lymphoproliferative disease.* Proc Natl Acad Sci U S A, 1999. **96**(18): p. 10391-6.

102. Hopwood, P. and D.H. Crawford, *The role of EBV in post-transplant malignancies: a review.* J Clin Pathol, 2000. **53**(4): p. 248-54.

103. Ben-Sasson, S.A. and G. Klein, *Activation of the Epstein-Barr virus genome by 5-aza-cytidine in latently infected human lymphoid lines.* Int J Cancer, 1981. **28**(2): p. 131-5.

104. Fahmi, H., et al., *Transforming growth factor beta 1 stimulates expression of the Epstein-Barr virus BZLF1 immediate-early gene product ZEBRA by an indirect mechanism which requires the MAPK kinase pathway.* Journal of Virology, 2000. **74**(13): p. 5810-5818.

105. Luka, J., B. Kallin, and G. Klein, *Induction of the Epstein-Barr virus (EBV) cycle in latently infected cells by n-butyrate.* Virology, 1979. **94**(1): p. 228-31.

106. zur Hausen, H., et al., *Persisting oncogenic herpesvirus induced by the tumour promotor TPA.* Nature, 1978. **272**(5651): p. 373-5.

107. Lai, I.Y., P.J. Farrell, and P. Kellam, *X-box binding protein 1 induces the expression of the lytic cycle transactivator of Kaposi's sarcoma-associated herpesvirus but not Epstein-Barr virus in co-infected primary effusion lymphoma.* J Gen Virol, 2011. **92**(Pt 2): p. 421-31.

108. Liang, X., et al., *Gammaherpesvirus-driven plasma cell differentiation regulates virus reactivation from latently infected B lymphocytes.* PLoS Pathog, 2009. **5**(11): p. e1000677.

109. Miller, G., et al., *Lytic cycle switches of oncogenic human gammaherpesviruses.* Adv Cancer Res, 2007. **97**: p. 81-109.

110. Daikoku, T., et al., *Architecture of replication compartments formed during Epstein-Barr virus lytic replication.* J Virol, 2005. **79**(6): p. 3409-18.

111. Fixman, E.D., G.S. Hayward, and S.D. Hayward, *Replication of Epstein-Barr virus oriLyt: lack of a dedicated virally encoded origin-binding protein and dependence on Zta in cotransfection assays.* J Virol, 1995. **69**(5): p. 2998-3006.

112. Mettenleiter, T.C., *Herpesvirus assembly and egress.* J Virol, 2002. **76**(4): p. 1537-47.

113. Wang, W.H., et al., *Assembly of Epstein-Barr Virus Capsid in Promyelocytic Leukemia Nuclear Bodies.* J Virol, 2015. **89**(17): p. 8922-31.

114. Lv, Y., et al., *Remodeling of host membranes during herpesvirus assembly and egress.* Protein Cell, 2019. **10**(5): p. 315-326.

115. Nanbo, A., T. Noda, and Y. Ohba, *Epstein-Barr Virus Acquires Its Final Envelope on Intracellular Compartments With Golgi Markers.* Front Microbiol, 2018. **9**: p. 454.

116. Nanbo, A., *Epstein-Barr Virus Exploits the Secretory Pathway to Release Virions.* Microorganisms, 2020. **8**(5).

117. Hogue, I.B., et al., *Cellular mechanisms of alpha herpesvirus egress: live cell fluorescence microscopy of pseudorabies virus exocytosis.* PLoS Pathog, 2014. **10**(12): p. e1004535.

118. Shumilov, A., et al., *Epstein-Barr virus particles induce centrosome amplification and chromosomal instability.* Nat Commun, 2017. **8**: p. 14257.

119. Yiu, S.P.T., et al., *Epstein-Barr virus BNRF1 destabilizes SMC5/6 cohesin complexes to evade its restriction of replication compartments.* Cell Rep, 2022. **38**(10): p. 110411.

120. Cancer Genome Atlas Research, N., *Comprehensive molecular characterization of gastric adenocarcinoma.* Nature, 2014. **513**(7517): p. 202-9.

121. Djokic, M., et al., *Post-transplant lymphoproliferative disorder subtypes correlate with different recurring chromosomal abnormalities.* Genes Chromosomes Cancer, 2006. **45**(3): p. 313-8.

122. Finerty, S., et al., *Cytogenetics of malignant epithelial cells and lymphoblastoid cell lines from nasopharyngeal carcinoma.* Br J Cancer, 1978. **37**(2): p. 231-9.

123. Mitelman, F., et al., *A 3q+ marker chromosome in EBV-carrying nasopharyngeal carcinomas.* Int J Cancer, 1983. **32**(6): p. 651-5.

124. Schwanhausser, B., et al., *Global quantification of mammalian gene expression control.* Nature, 2011. **473**(7347): p. 337-42.

125. Yla-Anttila, P., S. Gupta, and M.G. Masucci, *The Epstein-Barr virus deubiquitinase BPLF1 targets SQSTM1/p62 to inhibit selective autophagy.* Autophagy, 2021. **17**(11): p. 3461-3474.

126. Liebelt, F., et al., *The poly-SUMO2/3 protease SENP6 enables assembly of the constitutive centromere-associated network by group deSUMOylation.* Nat Commun, 2019. **10**(1): p. 3987.

127. Mukhopadhyay, D., A. Arnaoutov, and M. Dasso, *The SUMO protease SENP6 is essential for inner kinetochore assembly.* J Cell Biol, 2010. **188**(5): p. 681-92.

128. Schick, M., et al., *Genetic alterations of the SUMO isopeptidase SENP6 drive lymphomagenesis and genetic instability in diffuse large B-cell lymphoma.* Nat Commun, 2022. **13**(1): p. 281.

129. Wagner, K., et al., *The SUMO Isopeptidase SENP6 Functions as a Rheostat of Chromatin Residency in Genome Maintenance and Chromosome Dynamics.* Cell Rep, 2019. **29**(2): p. 480-494 e5.

130. Altschul, S.F., et al., *Basic local alignment search tool.* Journal of Molecular Biology, 1990. **215**(3): p. 403-410.

131. Todd, A.E., C.A. Orengo, and J.M. Thornton, *Evolution of function in protein superfamilies, from a structural perspective.* J Mol Biol, 2001. **307**(4): p. 1113-43.

132. Weinhold, N., et al., *Local function conservation in sequence and structure space.* PLoS Comput Biol, 2008. **4**(7): p. e1000105.

133. Tian, W. and J. Skolnick, *How well is enzyme function conserved as a function of pairwise sequence identity?* J Mol Biol, 2003. **333**(4): p. 863-82.

134. Ma, J., et al., *Protein threading using context-specific alignment potential.* Bioinformatics, 2013. **29**(13): p. i257-65.

135. Ma, J., et al., *A conditional neural fields model for protein threading.* Bioinformatics, 2012. **28**(12): p. i59-66.

136. Peng, J. and J. Xu, *RaptorX: exploiting structure information for protein alignment by statistical inference.* Proteins, 2011. **79 Suppl 10**: p. 161-71.

137. Peng, J. and J. Xu, *A multiple-template approach to protein threading.* Proteins, 2011. **79**(6): p. 1930-9.

138. Peng, J. and J. Xu, *Low-homology protein threading.* Bioinformatics, 2010. **26**(12): p. i294-300.

139. Peng, J. and J. Xu, *Boosting Protein Threading Accuracy.* Res Comput Mol Biol, 2009. **5541**: p. 31-45.

140. Tsai, M.H., et al., *Spontaneous lytic replication and epitheliotropism define an Epstein-Barr virus strain found in carcinomas.* Cell Rep, 2013. **5**(2): p. 458-70.

141. Peng, R., et al., *The Epstein-Barr virus EBNA-LP protein preferentially coactivates EBNA2-mediated stimulation of latent membrane proteins expressed from the viral divergent promoter.* J Virol, 2005. **79**(7): p. 4492-505.

142. Carter, S., et al., *C-terminal modifications regulate MDM2 dissociation and nuclear export of p53.* Nat Cell Biol, 2007. **9**(4): p. 428-35.

143. Gonzalez-Prieto, R., et al., *c-Myc is targeted to the proteasome for degradation in a SUMOylation-dependent manner, regulated by PIAS1, SENP7 and RNF4.* Cell Cycle, 2015. **14**(12): p. 1859-72.

144. Eifler, K. and A.C.O. Vertegaal, *SUMOylation-Mediated Regulation of Cell Cycle Progression and Cancer.* Trends Biochem Sci, 2015. **40**(12): p. 779-793.

145. Muller, S., A. Ledl, and D. Schmidt, *SUMO: a regulator of gene expression and genome integrity.* Oncogene, 2004. **23**(11): p. 1998-2008.

146. Rosemarie, Q. and B. Sugden, *Epstein-Barr Virus: How Its Lytic Phase Contributes to Oncogenesis.* Microorganisms, 2020. **8**(11).

147. Seeler, J.S. and A. Dejean, *SUMO and the robustness of cancer.* Nat Rev Cancer, 2017. **17**(3): p. 184-197.

148. Hoellein, A., et al., *Myc-induced SUMOylation is a therapeutic vulnerability for B-cell lymphoma.* Blood, 2014. **124**(13): p. 2081-90.

149. Borozan, I., et al., *Analysis of Epstein-Barr Virus Genomes and Expression Profiles in Gastric Adenocarcinoma.* J Virol, 2018. **92**(2).

150. Cochet, C., et al., *Expression of the Epstein-Barr virus immediate early gene, BZLF1, in nasopharyngeal carcinoma tumor cells.* Virology, 1993. **197**(1): p. 358-65.

151. Ramayanti, O., et al., *Epstein-Barr virus mRNA profiles and viral DNA methylation status in nasopharyngeal brushings from nasopharyngeal carcinoma patients reflect tumor origin.* Int J Cancer, 2017. **140**(1): p. 149-162.

152. Xue, S.A., et al., *Promiscuous expression of Epstein-Barr virus genes in Burkitt's lymphoma from the central African country Malawi.* Int J Cancer, 2002. **99**(5): p. 635-43.

153. Bristol, J.A., et al., *A cancer-associated Epstein-Barr virus BZLF1 promoter variant enhances lytic infection.* PLoS Pathog, 2018. **14**(7): p. e1007179.

154. Li, J., et al., *The Epstein-Barr virus deubiquitinating enzyme BPLF1 regulates the activity of topoisomerase II during productive infection.* PLoS Pathog, 2021. **17**(9): p. e1009954.

155. Yla-Anttila, P. and M.G. Masucci, *Inhibition of selective autophagy by members of the herpesvirus ubiquitin-deconjugase family.* Biochem J, 2021. **478**(12): p. 2297-2308.

156. Mitra, S., et al., *Genetic screening identifies a SUMO protease dynamically maintaining centromeric chromatin.* Nat Commun, 2020. **11**(1): p. 501.

157. Nowell, P.C., *The clonal evolution of tumor cell populations.* Science, 1976. **194**(4260): p. 23-8.

158. Al-Sohaily, S., et al., *Molecular pathways in colorectal cancer.* J Gastroenterol Hepatol, 2012. **27**(9): p. 1423-31.

159. V. Roschke, A. and I. R. Kirsch, *Targeting Karyotypic Complexity and Chromosomal Instability of Cancer Cells.* Current Drug Targets, 2010. **11**(10): p. 1341-1350.

160. Negrini, S., V.G. Gorgoulis, and T.D. Halazonetis, *Genomic instability--an evolving hallmark of cancer.* Nat Rev Mol Cell Biol, 2010. **11**(3): p. 220-8.

161. Carter, S.L., et al., *Absolute quantification of somatic DNA alterations in human cancer.* Nat Biotechnol, 2012. **30**(5): p. 413-21.

162. Cimini, D., *Merotelic kinetochore orientation, aneuploidy, and cancer.* Biochim Biophys Acta, 2008. **1786**(1): p. 32-40.

163. Bakhoum, S.F., et al., *Chromosomal instability drives metastasis through a cytosolic DNA response.* Nature, 2018. **553**(7689): p. 467-472.

164. Goh, J.Y., et al., *Chromosome 1q21.3 amplification is a trackable biomarker and actionable target for breast cancer recurrence.* Nat Med, 2017. **23**(11): p. 1319-1330.

165. Turajlic, S., et al., *Tracking Cancer Evolution Reveals Constrained Routes to Metastases: TRACERx Renal.* Cell, 2018. **173**(3): p. 581-594 e12.

166. Loh, P.R., et al., *Insights into clonal haematopoiesis from 8,342 mosaic chromosomal alterations.* Nature, 2018. **559**(7714): p. 350-355.

167. Duncan, A.W., *Aneuploidy, polyploidy and ploidy reversal in the liver.* Semin Cell Dev Biol, 2013. **24**(4): p. 347-56.

168. Bielski, C.M., et al., *Genome doubling shapes the evolution and prognosis of advanced cancers.* Nat Genet, 2018. **50**(8): p. 1189-1195.

169. Taylor, A.M., et al., *Genomic and Functional Approaches to Understanding Cancer Aneuploidy.* Cancer Cell, 2018. **33**(4): p. 676-689 e3.

170. van Deursen, J.M., *Rb loss causes cancer by driving mitosis mad.* Cancer Cell, 2007. **11**(1): p. 1-3.

171. Weaver, B.A., et al., *Aneuploidy acts both oncogenically and as a tumor suppressor.* Cancer Cell, 2007. **11**(1): p. 25-36.

172. Hattersley, N., et al., *The SUMO protease SENP6 is a direct regulator of PML nuclear bodies.* Mol Biol Cell, 2011. **22**(1): p. 78-90.

173. Fu, H., et al., *SENP6-mediated M18BP1 deSUMOylation regulates CENP-A centromeric localization.* Cell Res, 2019. **29**(3): p. 254-257.

174. Mukhopadhyay, D., et al., *SUSP1 antagonizes formation of highly SUMO2/3-conjugated species.* J Cell Biol, 2006. **174**(7): p. 939-49.

175. Jumper, J., et al., *Highly accurate protein structure prediction with AlphaFold.* Nature, 2021. **596**(7873): p. 583-589.

176. Varadi, M., et al., *AlphaFold Protein Structure Database: massively expanding the structural coverage of protein-sequence space with high-accuracy models.* Nucleic Acids Res, 2022. **50**(D1): p. D439-D444.

177. Schrodinger, L., *The PyMOL molecular graphics system.* Version, 2010. **1**(5): p. 0.

178. Fan, Y., et al., *SUMOylation in Viral Replication and Antiviral Defense.* Adv Sci (Weinh), 2022. **9**(7): p. e2104126.

179. Wilson, V.G., *Viral Interplay with the Host Sumoylation System.* Adv Exp Med Biol, 2017. **963**: p. 359-388.

180. Nguyen, A.W. and P.S. Daugherty, *Evolutionary optimization of fluorescent proteins for intracellular FRET.* Nat Biotechnol, 2005. **23**(3): p. 355-60.

181. Jan Fada, B., E. Reward, and H. Gu, *The Role of ND10 Nuclear Bodies in Herpesvirus Infection: A Frenemy for the Virus?* Viruses, 2021. **13**(2).

182. Nicewonger, J., et al., *Epstein-Barr Virus (EBV) SM Protein Induces and Recruits Cellular Sp110b To Stabilize mRNAs and Enhance EBV Lytic Gene Expression.* Journal of Virology, 2004. **78**(17): p. 9412-9422.

183. Tsai, K., et al., *EBV tegument protein BNRF1 disrupts DAXX-ATRX to activate viral early gene transcription.* PLoS Pathog, 2011. **7**(11): p. e1002376.

184. Sivachandran, N., F. Sarkari, and L. Frappier, *Epstein-Barr nuclear antigen 1 contributes to nasopharyngeal carcinoma through disruption of PML nuclear bodies.* PLoS Pathog, 2008. **4**(10): p. e1000170.

185. Tischer, B.K., G.A. Smith, and N. Osterrieder, *En passant mutagenesis: a two step markerless red recombination system.* Methods Mol Biol, 2010. **634**: p. 421-30.

186. Zuo, J., et al., *The Epstein-Barr virus-encoded BILF1 protein modulates immune recognition of endogenously processed antigen by targeting major histocompatibility complex class I molecules trafficking on both the exocytic and endocytic pathways.* J Virol, 2011. **85**(4): p. 1604-14.

187. Feederle, R., et al., *Epstein-Barr virus BNRF1 protein allows efficient transfer from the endosomal compartment to the nucleus of primary B lymphocytes.* J Virol, 2006. **80**(19): p. 9435-43.

188. Adhikary, D., et al., *Immunodominance of lytic cycle antigens in Epstein-Barr virus-specific CD4+ T cell preparations for therapy.* PLoS One, 2007. **2**(7): p. e583.

189. Wu, Z.H. and S. Miyamoto, *Analyze the SUMOylation of IKK gamma/NEMO During Genotoxic Stress.* Methods Mol Biol, 2021. **2366**: p. 183-190.

190. van Zyl, D.G., et al., *Immunogenic particles with a broad antigenic spectrum stimulate cytolytic T cells and offer increased protection against EBV infection ex vivo and in mice.* PLoS Pathog, 2018. **14**(12): p. e1007464.

7. List of Figures

8. List of Tables